Max-Planck-Institut
für Meteorologie

MAX-PLANCK-GESELLSCHAFT

International Max Planck Research School
on Earth System Modelling

Long-term stability and adjustment toward equilibrium in a future warm climate

Chao Li

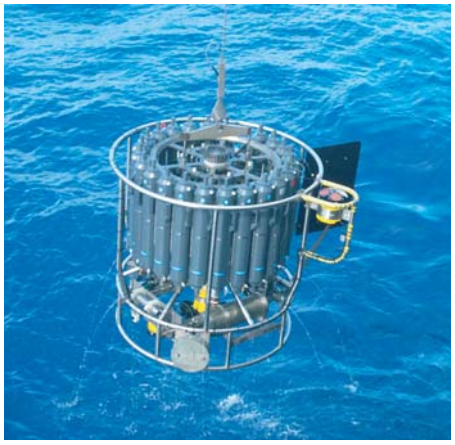

Berichte zur Erdsystemforschung 119/2012

Reports on Earth System Science

Hinweis

Die Berichte zur Erdsystemforschung werden vom Max-Planck-Institut für Meteorologie in Hamburg in unregelmäßiger Abfolge herausgegeben.

Sie enthalten wissenschaftliche und technische Beiträge, inklusive Dissertationen.

Die Beiträge geben nicht notwendigerweise die Auffassung des Instituts wieder.

Die "Berichte zur Erdsystemforschung" führen die vorherigen Reihen "Reports" und "Examensarbeiten" weiter.

Notice

The Reports on Earth System Science are published by the Max Planck Institute for Meteorology in Hamburg. They appear in irregular intervals.

They contain scientific and technical contributions, including Ph. D. theses.

The Reports do not necessarily reflect the opinion of the Institute.

The "Reports on Earth System Science" continue the former "Reports" and "Examensarbeiten" of the Max Planck Institute.

Anschrift / Address

Max-Planck-Institut für Meteorologie
Bundesstrasse 53
20146 Hamburg
Deutschland

Tel.: +49-(0)40-4 11 73-0
Fax: +49-(0)40-4 11 73-298
Web: www.mpimet.mpg.de

Layout:

Bettina Diallo, PR & Grafik

Titelfotos:
vorne:
Christian Klepp - Jochem Marotzke - Christian Klepp
hinten:
Clotilde Dubois - Christian Klepp - Katsumasa Tanaka

Berichte zur Erdsystemforschung 119/2012

Long-term stability and adjustment toward equilibrium in a future warm climate

Chao Li

aus Hubei, China

Hamburg 2012

Reports on Earth System Science 119/2012

ISSN 1614-1199

Chao Li
Max-Planck-Institut für Meteorologie
Bundesstrasse 53
20146 Hamburg

Als Dissertation angenommen
vom Department Geowissenschaften der Universität Hamburg

auf Grund der Gutachten von
Prof. Dr. Jochem Marotzke
und
Dr. Jin-Song von Storch

Hamburg, den 2. Juli 2012
Prof. Dr. Jürgen Oßenbrügge
Leiter des Departments für Geowissenschaften

ISSN 1614-1199

Long-term stability and adjustment toward equilibrium in a future warm climate

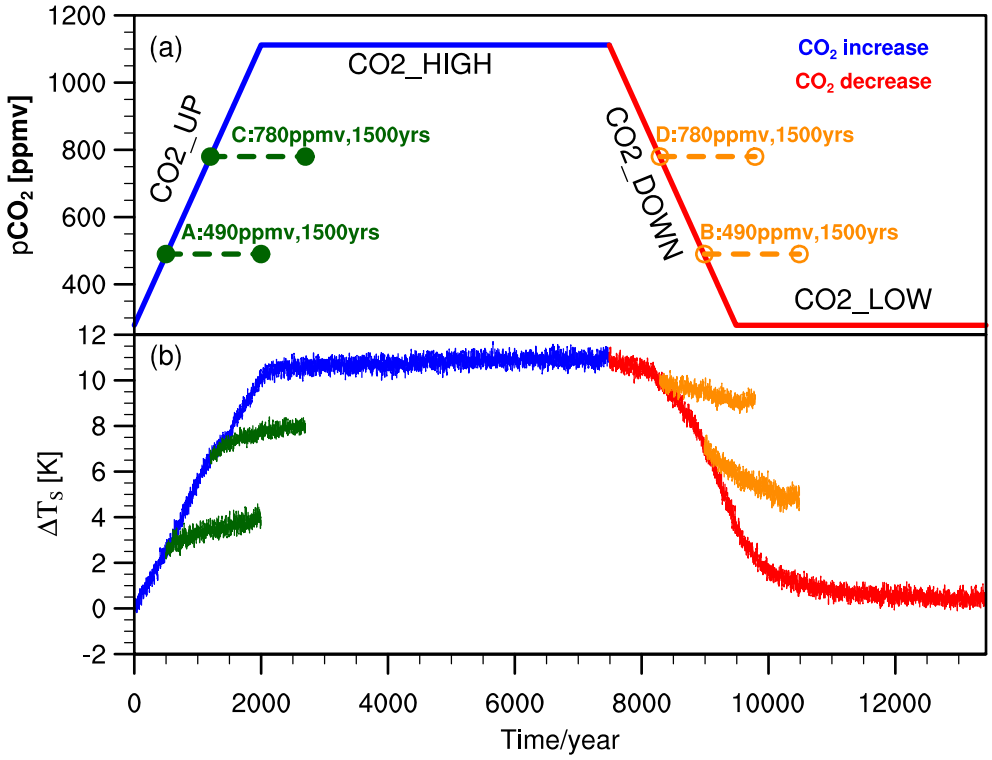

Chao Li

Hamburg 2012

Abstract

This thesis investigates the long-term adjustment of the deep ocean and the long-term stability of sea ice and the Atlantic Meridional Overturning Circulation (AMOC) in several multi-millennia simulations with the coupled climate model ECHAM5/MPIOM.

To understand the long-term adjustment of the deep-ocean warming and its consequence, we integrate ECHAM5/MPIOM to equilibrium with an atmospheric CO_2 concentration that is quadrupled over 140 years and kept constant thereafter. We find that the reduction in deep-ocean circulation and its consequently reduced northward ocean heat transport have very limited effect on the global-mean surface temperature change, but it plays a very important role in determining the geographic pattern of equilibrium surface temperature response and its temporal evolution. The ocean temperature shows a near-uniform warming of around 8.0K at almost all depths, where the deep-ocean warming plays an important role in the thermosteric global sea level change beyond a millennium. We evaluate the effective climate response method described in Gregory et al. (2004) with our simulation, and we show that their method to estimate the equilibrium climate response is accurate to within 10%.

To understand the long-term stability of Arctic and Antarctic sea ice in a future warm climate, an idealized prescribed atmospheric CO_2 concentration is applied to ECHAM5/MPIOM, where the atmospheric CO_2 is increased extremely slowly up to quadrupling over 2000 years, is kept constant for further 5940 years, and is decreased extremely slowly down to pre-industrial level over 2000 years and kept constant for 3940 years thereafter. The Arctic summer sea ice cover retreats linearly with the CO_2 increase, but we see a rapid transition associated with the sudden loss of the Arctic winter sea ice cover. This rapid transition is triggered by atmospheric convection, which can warm the Arctic by trapping the outgoing long-wave radiation and keep the Arctic ice-free in winter. We find no evidence of hysteresis behavior of Arctic winter and summer sea ice cover. It is the surface temperature change that governs the long-term stability of the Arctic sea ice, because a strong halocline in the Arctic Ocean is responsible for isolating the surface

water from the deep water. The Antarctic sea ice cover also shows no evidence of hysteresis behavior in response to the CO_2 forcing. However, the Antarctic sea ice cover shows more strongly lagged response to the CO_2 forcing compared to the Arctic sea ice, and the response of Antarctic sea ice cover lags significantly behind the Southern Hemisphere surface air temperature change. Because in contrast to the Arctic sea ice, the surface temperature change is not the only controlling factor for the Antarctic sea ice change in a warm climate, deep ocean convection and sea ice dynamics also play an important role in determining the Antarctic sea ice long-term stability.

Using the same simulations as in the sea ice hysteresis study, we find no evidence of hysteresis behavior of the AMOC in response to the CO_2 forcing and the anomalous atmospheric freshwater forcing over the North Atlantic deep water formation regions. The AMOC of the "recovery" trajectory is much stronger than that of the "weakening" trajectory. The overshooting recovery of the AMOC is caused by a stronger evaporation over the tropical Atlantic, which leads to anomalously high salinity in the North Atlantic while the CO_2 decreases, resulting in stronger deep convection and a stronger AMOC. However, such a process is not included in the classical water-hosing experiments, which have mostly been used to investigate the AMOC stability in response to a prescribed freshwater forcing over the North Atlantic. Hence, we cannot use the water-hosing experiments to project the long-term stability of the AMOC in a future warm climate.

Contents

Chapter 1

Introduction

1.1 Motivation

It has been widely recognized that the anthropogenic CO_2 emission has caused an increase of global-mean surface temperature by 0.8 K since the early 20th century (Parker et al. 2007). Future CO_2 emission in the 21st century will lead to climate change on both short and long time scales. Many previous studies have focused on the projections of possible 21st century climate change and its consequence (e.g. Meehl et al. 2007; Hansen et al. 2007; Ramanathan and Feng 2008). However, in response to the changes in external forcing, the climate system adjustment processes involve timescales ranging from days in the atmosphere to several millennia in the deep ocean. The long-term adjustment of the deep ocean warming with timescales beyond a millennium and its impact on the surface equilibrium response are not well understood, because rarely have atmosphere-ocean-sea ice general circulation models (AOGCM) been run to equilibrium. The increased CO_2 emissions may have the potential to push components of the Earth system through critical thresholds into qualitatively different states that are not reversible by returning the atmospheric CO_2 concentration to their previous regime. Such possible irreversible shifts caused by the anthropogenic climate change are of particular concern in evaluating the potential societal environmental threat posed by future climate change in a longer term. In this study, we perform several simulations with multi-millennia long-term integrations using the AOGCM ECHAM5/MPIOM and focus on three key topics in order to understand the long-term stability and adjustment of the climate system in a future

warm climate. Topic 1 is the long-term the deep-ocean warming and its impacts on the surface equilibrium response; topic 2 and 3 are about the hysteresis behavior of Arctic and Antarctic sea ice and the Atlantic meridional overturning circulation (AMOC), respectively in response to the atmospheric CO_2 forcing.

Topic 1. Equilibrium climate sensitivity (ECS), which is defined as the global-mean surface warming in response to a doubling of the atmospheric CO_2 concentration after the system has reached a new equilibrium, is a very important factor to understand the Earth's climate in response to external forcing (Cubasch et al. 2001; Randall et al. 2007). However, ECS cannot be measured directly, but it can be estimated from comprehensive climate models. To reduce the computational cost of an AOGCM integrated to equilibrium, different methods have been developed to estimate the ECS. The classical "Charney" ECS is obtained using an atmospheric general circulation model (AGCM) coupled with a slab ocean model (SOM). The SOM is a simple non-dynamic model of the upper ocean with prescribed ocean heat transport convergence. This simplified configuration makes it possible to estimate the ECS with only several decades of integration. But the disadvantage is that any change in the ocean heat transport cannot be represented. Another method is the effective climate sensitivity described in (Gregory et al. 2004), who estimated the ECS based on the transient climate response obtained with an AOGCM. However, some slow feedbacks owing to the deep ocean adjustment with their own intrinsic timescale could influence the ECS on long timescales. But rarely have AOGCMs been run to equilibrium and the validity of these methods with high forcing is not well established (Knutti and Hegerl 2008). Hence, both methods should be evaluated with an AOGCM for long-term projections for CO_2 levels beyond CO_2 doubling, because the feedbacks might be quite different in such a system.

Topic 2. A possible irreversible shift of the Arctic sea ice state caused by anthropogenic climate change is subject to an ongoing scientific debate, especially since a strong retreat of Arctic summer sea ice has already been observed in recent decades (Vinnikov et al. 1999; Lindsay and Zhang 2005; Serreze and Francis 2006). By using a single-column model, Eisenman and Wettlaufer (2009) find a smooth transition from a perennially ice-covered state to a seasonally ice-free state during a gradual increase in forcing, but found a rapid transition of the remaining winter sea ice for further increased forcing. Since the large-scale processes

are highly parameterized in such simplified conceptual mathematical models, the transient scenarios of the sea ice strongly depend on the choice of the parameterization (as reviewed by Eisenman 2012). Hence, it is important to study the transient behavior of sea ice by using an AOGCM, although testing for hysteresis is extremely challenging in AOGCMs due to the computational constrains.

Topic 3. Multiple equilibria and a rapid transition between different states of the Atlantic meridional overturning circulation (AMOC) have been widely reproduced in climate models at different complexity levels (e.g. Stommel 1961; Rooth 1982; Bryan 1986; Marotzke et al. 1988; Manabe and Stouffer 1988; Stocker and Wright 1991; Marotzke and Willebrand 1991; Rahmstorf and Willebrand 1995; Ganopolski and Rahmstorf 2001; Hawkins et al. 2011). Moreover, the Atlantic paleoclimate records have attributed paleoclimate shifts to the AMOC transitions(e.g. Broecker et al. 1985; Bond et al. 1997; Marotzke 2000; Alley et al. 2003; Rahmstorf 2002; McManus et al. 2004; Ellison et al. 2006). A future warmer climate caused by the anthropogenic CO_2 emission is likely to increase the freshwater input to the North Atlantic. In turn, a gradual weakening in the strength of the AMOC is projected by AOGCMs, although there is considerable uncertainty in the magnitude of the change (Dixon et al. 1999; Mikolajewicz and Voss 2000; Gregory et al. 2005; Meehl et al. 2007). Although much work has been done to project the AMOC change in a future warm climate, the previous studies with AOGCMs mentioned here only investigated the transient behavior of the AMOC with "ramping-up" the atmospheric CO_2 forcing. To understand the hysteresis behavior or the reversibility of the AMOC in a future warm climate, water-hosing experiments have been carried out (Stouffer et al. 2006; Hawkins et al. 2011). However, in contrast to the water-hosing experiments, the substantially changed precipitation and changes in the evaporation and the precipitation patterns caused by the surface warming might also influence the salinity in the North Atlantic, thus influencing the long-term stability of AMOC. Therefore, it is important to study the hysteresis behavior of AMOC in response to the atmospheric CO_2 forcing rather than in response to the prescribed freshwater forcing using an AOGCM.

1.2 Thesis objective

In this thesis, we aim at answering the following research questions brought up in the previous section.

1. Deep-ocean heat uptake and equilibrium climate response

In the first research topic, we tackle the following research questions:

- What is the equilibrium surface-temperature response to atmospheric CO_2 quadrupling in ECHAM5/MPIOM? Does the equilibrium surface-temperature response in ECHAM5/MPIOM confirm of the result in ECHAM5/SOM?
- What is the final equilibrium of the ocean temperature in response to atmospheric CO_2 quadrupling in ECHAM5/MPIOM? Does the ocean warming in ECHAM5/MPIOM confirm of the result in a upwelling-diffusion model or a multi-box ocean model?
- Does the effective climate response method described in Gregory et al. (2004) give an accurate estimation of the equilibrium climate response?

2. Sea ice in a future warm climate

In the second topic, we tackle the following research questions:

- Does the Arctic sea ice show hysteresis behavior in a future warm climate? Which processes govern the long-term stability of Arctic sea ice?
- Is there any rapid transition during the retreat of Arctic sea ice?
- Does the Antarctic sea ice show hysteresis behavior in a future warm climate? Which processes govern the long-term stability of Antarctic sea ice?

3. AMOC in a future warm climate

In the final research topic, we tackle the following research questions:

- Does the AMOC show hysteresis behavior in response the atmospheric CO_2 forcing?
- Which processes govern the long-term stability and reversibility of AMOC in a future warm climate?

1.3 Outline of the thesis

This thesis contains three major chapters, which are written in the style of journal publications. Thus, each major chapter contains its own abstract, introduction and conclusion, and can be read independently on their own. Chapter 2 has already been published, chapter 3 has already been submitted, while the chapter 4 is in preparation for submission.

- In **Chapter 2**, we investigate the long-term adjustment of the deep ocean and its impact on the surface equilibrium response by integrating coupled climate model ECHAM5/MPIOM to equilibrium under atmospheric CO_2 quadrupling. The final equilibrium in ECHAM5/MPIOM is then compared with a simulation of ECHAM5/SOM. The effective climate response method described in Gregory et al. (2004) is evaluated with our simulation. This work has been published in *Climate Dynamics*[1].

- In **Chapter 3**, we examine the hysteresis behavior of Arctic and Antarctic sea ice in response to the atmospheric CO_2 forcing in ECHAM5/MPIOM by extremely slowly increasing and decreasing the CO_2 over 2000 years. We analyse the large-scale Arctic energy budget and the Antarctic ocean circulation change to better understand the mechanism governing the long-term stability of Arctic and Antarctic sea ice area. This chapter has been submitted to *Journal of Climate*[2].

- In **Chapter 4**, we examine the hysteresis behavior of AMOC in response to atmospheric CO_2 forcing using the same simulations as in chapter 3. We diagnose the freshwater budget in the Atlantic basin to understand the processes governing the long-term stability of AMOC in a warm climate. This chapter is in preparation for submission to *Nature Geoscience*[3].

We close this thesis with a summary of the main findings in **Chapter 5**.

[1] Chao Li, Jin-Song von Storch and Jochem Marotzke, 2012: Deep-ocean heat uptake and equilibrium climate response, *Climate Dyanmics*, DOI: 10.1007/s00382-012-1350-z.

[2] Chao Li, Dirk Notz, Steffen Tietsche and Jochem Marotzke, 2012: The transient versus the equilibrium response of sea ice to global warming, *Journal of Climate*, Submitted.

[3] Chao Li, Jin-Song von Storch and Jochem Marotzke, 2012: Proccesses governing the stability of Atlantic meridional overturning circulation in a future warm climate, *Nature Geoscience*, in preparation.

Chapter 2

Deep-ocean heat uptake and equilibrium climate response

We integrate ECHAM5/MPIOM to equilibrium under atmospheric CO_2 quadrupling. The equilibrium global-mean surface-temperature change is 10.8 K. The surface equilibrates within about 1200 years, the deep ocean within 5000 years. The impact of the deep ocean on the equilibrium surface-temperature response is illustrated by the difference between ECHAM5/MPIOM and ECHAM5 coupled with slab ocean model (ECHAM5/SOM). The equilibrium global-mean surface temperature response is 11.1 K in ECHAM5/SOM and is thus 0.3 K higher than in ECHAM5/MPIOM. ECHAM5/MPIOM shows less warming over the northern-hemisphere mid and high latitudes, but larger warming over the tropical ocean and especially over the southern-hemisphere high latitudes. ECHAM5/MPIOM shows similar polar amplification in both the Arctic and the Antarctic, in contrast to ECHAM5/SOM, which shows stronger polar amplification in the northern hemisphere. The southern polar warming in ECHAM5/MPIOM is greatly delayed by Antarctic deep-ocean warming due to convective and isopycnal mixing. The equilibrium ocean temperature warming under CO_2 quadrupling is around 8.0 K and is near-uniform with depth. The global-mean steric sea-level rise is 5.8 m in equilibrium; of this, 2.3 m are due to the deep-ocean warming after the surface temperature has almost equilibrated. This result suggests that the surface temperature change is a poor predictor for steric sea-level change in the long term. The effective climate response method described in Gregory et al. (2004) is evaluated with our simulation, which shows that their method to estimate the equilibrium climate response is accurate to within 10%.

2.1 Introduction

In response to changes in external forcing, the climate system adjustment processes involve timescales ranging from days in the atmosphere to several millennia in the deep ocean. The long-term adjustment with timescales above a millennium is not well understood, because rarely have atmosphere-ocean global circulation models (AOGCM) been run to equilibrium. To gain a more comprehensive understanding of the long-term adjustment of the deep ocean and its impact on the surface equilibrium response, we integrate a coupled climate model, ECHAM5/MPIOM, to equilibrium under atmospheric CO_2 quadrupling. The final equilibrium in ECHAM5/MPIOM is then compared with a simulation of ECHAM5 coupled to a slab ocean model (ECHAM5/SOM).

Equilibrium climate sensitivity (ECS), as defined by the Intergovernmental Panel of Climate Change (IPCC) assessments (e.g. Cubasch et al. 2001; Randall et al. 2007), is the equilibrium annual and global mean surface temperature response to atmospheric CO_2 doubling from a pre-industrial level. In this study, to avoid confusion, we define the equilibrium climate response (ECR) as the equilibrium annual and global mean surface temperature response to atmospheric CO_2 quadrupling. To reduce the computational cost of an AOGCM integrated to equilibrium, different methods have been developed to estimate the ECR or ECS. In one of the methods, the ECR is obtained using an AGCM coupled with a slab ocean model (SOM) and the thermodynamic part of the sea-ice component. The SOM is a simple non-dynamic model of the upper ocean with prescribed ocean heat transport convergence. This simplified configuration makes it possible to estimate the ECR with only several decades of integration. But the disadvantage is that any change in the ocean heat transport cannot be represented. Another method estimates the ECR from the transient climate response in an AOGCM. Gregory et al. (2004) show that, when the net downward TOA (top of the atmosphere) radiative heat flux N is plotted against the surface temperature change ΔT with a fixed forcing of the Hadley Center slab climate model version 3 (HadSM3), a straight line gives a good fit. Hence, they suggest that a linear regression between N and ΔT gives a good estimate of the ECR and the radiative forcing. However, the feedback strength is time-dependent, which is associated with difference in cloud feedback arising from inter-hemispheric tem-

perature differences due to the slower warming rate of the Southern Ocean (Senior and Mitchell 2000), and in a more complex climate model, some feedbacks will change with the climate state (Boer and Yu 2003; Gregory and Webb 2008). Therefore, the assumptions of a linear feedback is valid only for perturbations of a few degrees, and the method of Gregory et al. (2004) should be evaluated with an AOGCM.

Williams et al. (2008) and Winton et al. (2010) show that the spatial warming pattern changes as the climate evolves toward equilibrium because of the ocean heat uptake. Apart from the impacts on the spatial pattern of climate change, the ocean heat uptake also influences the temporal aspects of climate change from decades to multi-millennia. The large upper-ocean heat uptake changes the climate transient response on decadal timescales, and the small deep-ocean heat uptake (DOHU) may influence the ECR on timescales from centuries to millennia due to its impact on some slow feedbacks of the climate system (Knutti and Hegerl 2008). However, the long-term effects of DOHU are poorly understood, because it requires thousands of years of simulation to achieve a steady state of an AOGCM.

Beside the warming processes on the earth surface, the ocean warming is also very important in sea level change and ocean biogeochemical processes. Levitus et al. (2005) showed that roughly 80% of the earth radiation imbalance due to the anthropogenic greenhouse gases has gone into heating the ocean. In response to this external forcing, the heat content of the world ocean above 3000 m depth has increased by nearly 2×10^{23} joules, which corresponded to a warming rate of $0.3\,\mathrm{W\,m^{-2}}$ in the last half of the 20th century (Levitus et al. 2000). By using different historical data, the ocean heat uptake of the top 700 m ocean is estimated as $0.41\,\mathrm{W\,m^{-2}}$ (Levitus et al. 2009) and $0.64\,\mathrm{W\,m^{-2}}$ (Lyman et al. 2010); von Schuckmann and Traon (2011) found $0.55\,\mathrm{W\,m^{-2}}$ for the top 1500 m of the ocean. The ocean heat uptake below 2000 m is estimated as $0.07\,\mathrm{W\,m^{-2}}$. At present, the upper-ocean warming is larger than the deep-ocean warming, because the upper ocean is ventilated much more efficiently. However, will the deep ocean also experience less warming than the upper ocean in the final equilibrium? And how does the deep-ocean warming contribute to the global sea level change in the long term? A long integration with an AOGCM is required to answer these questions.

Very rarely have coupled AOGCMs been integrated over more than 1000 years with atmospheric CO_2 doubling or quadrupling. The first long run with a coupled AOGCM was described by Stouffer and Manabe (1999) and Stouffer and Manabe (2003). By using a flux-adjusted coupled AOGCM with coarse resolution, they performed a 15000-year pre-industrial control run and a 4000-year integration with atmospheric CO_2 doubling. In their experiments, the Atlantic meridional overturning circulation (AMOC) recovered to the pre-industrial control level, implying that the ocean heat transport showed little change. By using an AOGCM with flux-adjustment, ECHAM3/LSG, Voss and Mikolajewicz (2001) performed two 850-year integrations with atmospheric CO_2 doubling and quadrupling. They mainly focused on describing the long-term climate adjustment processes and their timescales. Gregory et al. (2004) analyzed a 1200-year integration with atmospheric CO_2 quadrupling by using the non-flux-adjusted Hadley Center Coupled Model, version 3 (HadCM3), but the ocean was still warming up at the end of the run. Recently, by using the low-resolution version of the non-flux-adjusted Community Climate System Model, version 3 (CCSM3), Danabasoglu and Gent (2009) analyzed a 3000-year long integration with atmospheric CO_2 doubling, but the total ocean heat content still had a small trend. They concluded that the equilibrium climate sensitivity to CO_2 doubling determined by a SOM is similar to that in an AOGCM, because the AMOC and northward ocean heat transport did not change much in response to CO_2 doubling in CCSM3. In our long integration, however, the AMOC is weaker by 46% in the final equilibrium, which gives us an opportunity to study the impact of a deep-ocean circulation change on the surface equilibrium.

In order to gain a more comprehensive understanding of the deep ocean's role on climate response to atmospheric CO_2 forcing, we integrate ECHAM5/MPIOM to equilibrium under atmospheric CO_2 quadrupling. We study the slow deep-ocean warming, the change in deep-ocean circulation, and their impact on the surface equilibrium response. Section 2.2 is a brief introduction of the models and experiment design. Section 2.3 shows the long-term adjustment toward equilibrium. Section 2.4 compares the final equilibrium in the ECHAM5/MPIOM with that in ECHAM5/SOM; section 2.5 discusses the effective climate response; and section 2.6 gives our conclusions.

2.2 Models and experimental design

The coupled climate model applied in this study is a coarse-resolution version of ECHAM5/MPIOM. The spectral atmospheric model ECHAM5 is run at T31 resolution ($\sim 3.75°$) with 19 levels (Roeckner et al. 2003, 2006). The Max-Planck-Institute Ocean Model (MPIOM) is used at a resolution of roughly 3° near the equator with 40 levels. Technical details of MPIOM and the embedded sea ice model can be found in (Marsland et al. 2003) and (Jungclaus et al. 2006). Here, we summarize the main features. MPIOM is a z-coordinate global GCM based on the primitive equations for a hydrostatic Boussinesq fluid with a free surface. The spatial arrangements of scalar and vector variables are formulated on an orthogonal curvilinear C-grid (Arakawa and Lamb 1977). The coordinate poles are located on central Greenland and Antarctica, thus avoiding the pole-singularity problem. The model uses an along-isopycnal diffusion following Redi (1982) and Griffies (1998), and isopycnal tracer transport by unresolved eddies is parameterized following Gent et al. (1995). For the vertical eddy viscosity and diffusion the Richardson-number dependent scheme of Pacanowski and Philander (1981) is applied. Since the Pacanowski-Philander (PP) scheme in its classical form underestimates the turbulent mixing close to the surface, an additional wind mixing parameterization is included. In the presence of static instability, convective overturning is parameterized by greatly enhanced vertical diffusion. A bottom boundary layer slope convection scheme allows for an improved representation of the flow of statically unstable dense water over sills. The embedded sea ice module is a Hibler-type dynamic-thermodynamic sea ice model with viscous-plastic rheology and snow (Hibler 1979). Thermodynamic growth of sea ice is described by the zero-layer formulation of Semtner (1976). Ocean and atmosphere are coupled daily using the OASIS3 coupler (Valcke et al. 2003); no flux adjustments are applied. A higher-resolution version of the model (Jungclaus et al. 2006) has been used for the scenario simulations of the IPCC assessment report 4 (AR4).

To make our model run at hot climate states, we employ two modifications of ECHAM5. The first is an adjustment of the prescribed and fixed ozone concentration based on the observed climatology in standard ECHAM5. To avoid the artificially large ozone concentration in the upper troposphere that would follow an increase in tropopause height, the ozone contributing to a concentra-

tion above 0.15 ppmv below the tropopause is moved into the uppermost level in ECHAM5. Second, a positive definite optical thickness in the longwave radiative transport model is ensured, to avoid unphysical negative optical thicknesses for gases and aerosols. Both modifications were introduced for the simulation of the Paleocene-Eocene Thermal Maximum by Heinemann et al. (2012). Without the ozone adaptation, we find an unstoppable global warming after 5000 years of integration in ECHAM5/MPIOM, and the global surface temperature is 4.0 K higher than the experiment which is used in this study. Both modifications hardly affect the pre-industrial control simulation.

The SOM assumes a fixed mixed-layer depth (default value is 50 m). The SST is determined by the energy balance between net surface heat fluxes and a Q-flux that approximates the ocean heat transport convergence. In the SOM, the Q-flux values are diagnosed from an ECHAM5 control run and represent seasonal deep water exchange and horizontal ocean heat transport. Hence, the ocean heat transport in ECHAM5/SOM should not change in response to atmospheric CO_2. However, the Q-flux term is only applied in the ice-free regions; in the ice-covered region the surface heat flux is calculated differently by the simple sea-ice model. This can lead to an unrealistic change of the surface heat flux during the loss of Antarctic sea-ice, and thus change the implied ocean heat transport in the Southern Hemisphere.

Our first integration with ECHAM5/MPIOM is a 1600-year pre-industrial control run (CNTR) with constant atmospheric CO_2 at 278 ppmv. CNTR is close to a steady-state climate at the end of the simulation. The last 100 years of data are used as the CNTR reference in this study. A second integration starts from the end of CNTR; the atmospheric CO_2 concentration is increased by 1% per year until it reaches CO_2 quadrupling at year 140, and is held constant thereafter. The experiment is continued for further 5940 years until the whole system has reached the final equilibrium. To evaluate the signal of climate change at any time in these integrations, the CNTR is subtracted. In our third integration, ECHAM5 is coupled to a 50m slab ocean model (SOM). We first run a 110-year atmosphere-only spin-up under preindustrial boundary conditions and 278 ppmv pCO2; the ocean advective heat flux is diagnosed from the last 50 years of this spin-up. Then we run the model for another 50 years as the pre-industrial control run of ECHAM5/SOM. Thereafter, we increase pCO2 by 1% per year until

it reaches $2\times CO_2$ at year 70 and $4\times CO_2$ at year 140, and it held constant thereafter. The experiment is continued for further 660 years; we use averages over the last 100 years for our analysis.

In this study, we performed idealized experiments with prescribed atmospheric CO_2 concentrations that are kept constant over long periods of time. The long-term change of the atmospheric CO_2 concentration due the carbon cycle processes in the earth system has not been included. Moreover, the coupled climate model used here has neither dynamic glaciers nor dynamic vegetation; as one consequence, we cannot explore the impact of ice-sheet melting on the AMOC and other climate components. Our idealized experimental strategy allows us, however, to explore the true equilibrium response of a climate model to enhanced CO_2 concentration.

2.3 Multi-millennium adjustment toward equilibrium

2.3.1 Adjustment stages

The equilibrium global-mean surface temperature response to atmospheric CO_2 quadrupling is 10.8 K (Fig. 2.1a). After year 140, the time of CO_2 quadrupling, the globally averaged surface air temperature has increased by approximately 5.5 K. In the following millennium with atmospheric CO_2 constant at 1112 ppmv, the globally averaged surface temperature increases by an additional 5.3 K. There is still a very weak trend after the first 1200 years integration; the surface air temperature increases by 0.4 K in 3400 years. This weak trend mainly comes from the Southern Ocean and the Antarctic continent (Fig. 2d) where the surface warming is closely connected to the deep-ocean heat uptake in the Southern Ocean (Gregory 2000). In the ocean, the globally averaged equilibrium surface temperature response to CO_2 quadrupling is 10.0 K (Fig. 2.1b), 92% of the globally averaged surface temperature change.

The net TOA downward radiative flux (N) reaches its maximum of 3.5 $\mathrm{W\,m^{-2}}$ at year 140 when the atmospheric CO_2 concentration has just quadrupled (Fig. 2.1c). In the following millennium, N decreases but is still 0.7 $\mathrm{W\,m^{-2}}$ at year 1200 when the surface temperature change almost becomes stationary; N goes to zero when the system reaches the final equilibrium. The DOHU is non-zero at year

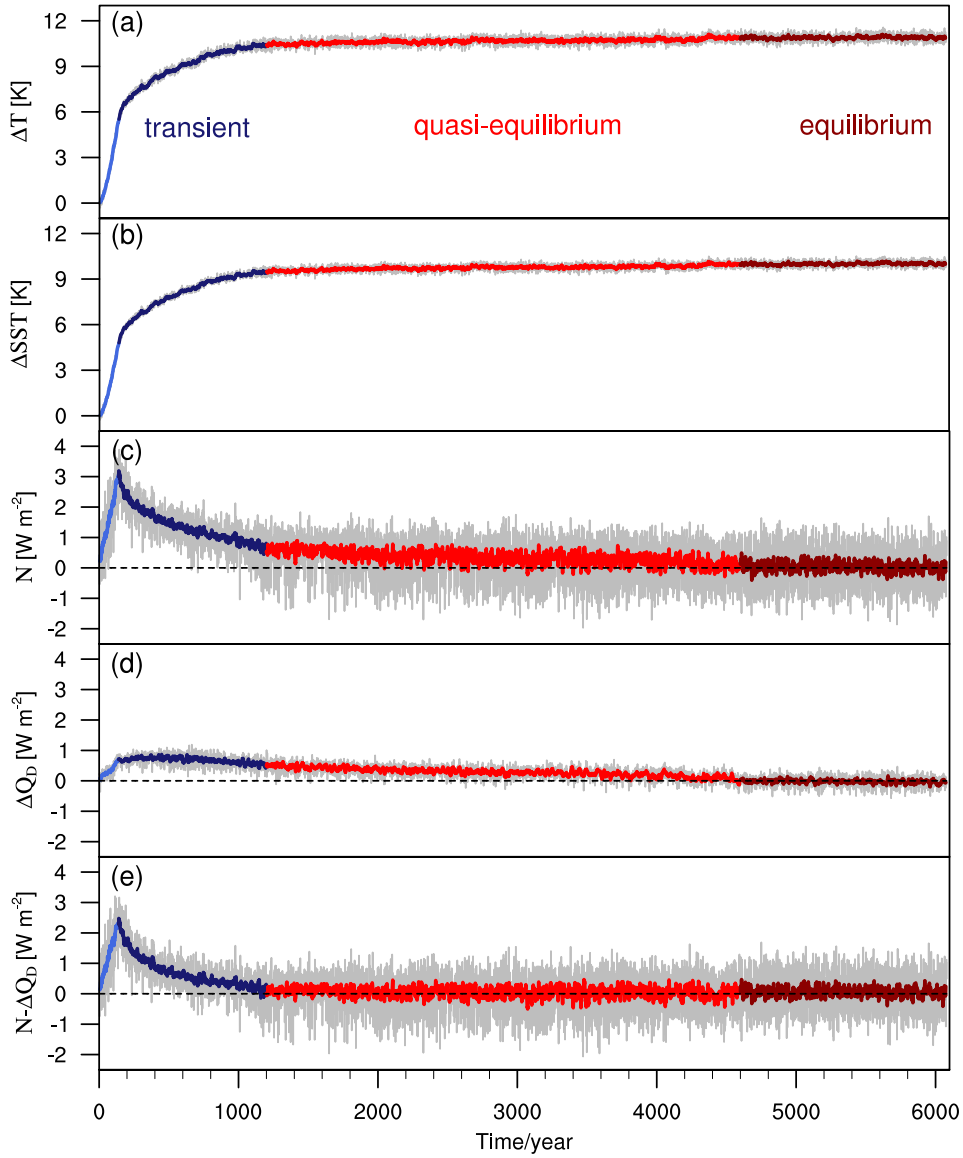

Fig. 2.1: Time series of, (a) globally averaged surface temperature change (ΔT, Unit: K), (b) sea surface temperature change (ΔSST, Unit: K), (c) globally averaged net TOA downward radiative flux (N, Unit: $\mathrm{W\,m^{-2}}$), (d) globally averaged deep-ocean heat uptake below 1525 m (ΔQ_D, Unit: $\mathrm{W\,m^{-2}}$), (e) difference between (c) and (d) (N-ΔQ_D, Unit: $\mathrm{W\,m^{-2}}$), by using ECHAM5/MPIOM with CO_2 quadrupling in 140yr. All time series are relative to the reference period from CNTR. The gray line represents annual-mean data for the entire experiment, the other colors represent an 11-year running mean.

1200, but it goes to zero when the deep-ocean reaches equilibrium (Fig. 2.1d). Hence, the surface temperature change reaches equilibrium when N is balanced by the ocean heat transfer across 1500m, rather than when the net TOA radiative flux goes to zero.

According to the adjustments of the global-mean surface temperature, of the radiative flux into the whole system, and of the heat flux into the deep ocean (Fig. 2.1), the time after CO_2 quadrupling can be divided into three periods: the transient period (yr140-1200), the quasi-equilibrium period (yr1200-4600) and the equilibrium period (yr4600-6080). In the transient period, the surface temperature and the upper ocean temperature are non-stationary, the whole system is adjusting. In the quasi-equilibrium period, the surface temperature and the upper ocean temperature (above 1500m) are nearly stationary, but the deep ocean is still warming. In the equilibrium period, the surface, the upper ocean, and the deep-ocean temperature change are stationary, and the whole system has reached its final equilibrium under atmospheric CO_2 quadrupling.

2.3.2 Patterns of surface temperature change

We now compare the patterns of surface temperature change that have occurred by the beginning of the transient period, the end of the transient period, and the end of the equilibrium period (Fig. 2.2a). By the beginning of the transient period, we see the familiar pattern of greater warming over land than over the ocean, large warming in the Arctic, and less warming over the North Atlantic and the Southern Ocean (e.g. Meehl et al. 2007). By the end of the transient period, the surface temperature has almost reached equilibrium, except over the Southern Ocean and Antarctica (Fig. 2.2ab,c) where the surface temperature still rises during the quasi-equilibrium period. The slow surface warming over these domains is related to the DOHU (Gregory 2000). The greater warming in southern high latitudes during the quasi-equilibrium period (Fig. 2.2ac) implies that in equilibrium, our AOGCM shows similar polar amplification in both the Arctic and Antarctic domains. The southern polar warming is greatly delayed by the Southern Ocean deep-ocean warming, implying that shorter simulations only show polar amplification in the Northern Hemisphere (e.g. Manabe and Stouffer 1980; Holland and Bitz 2003).

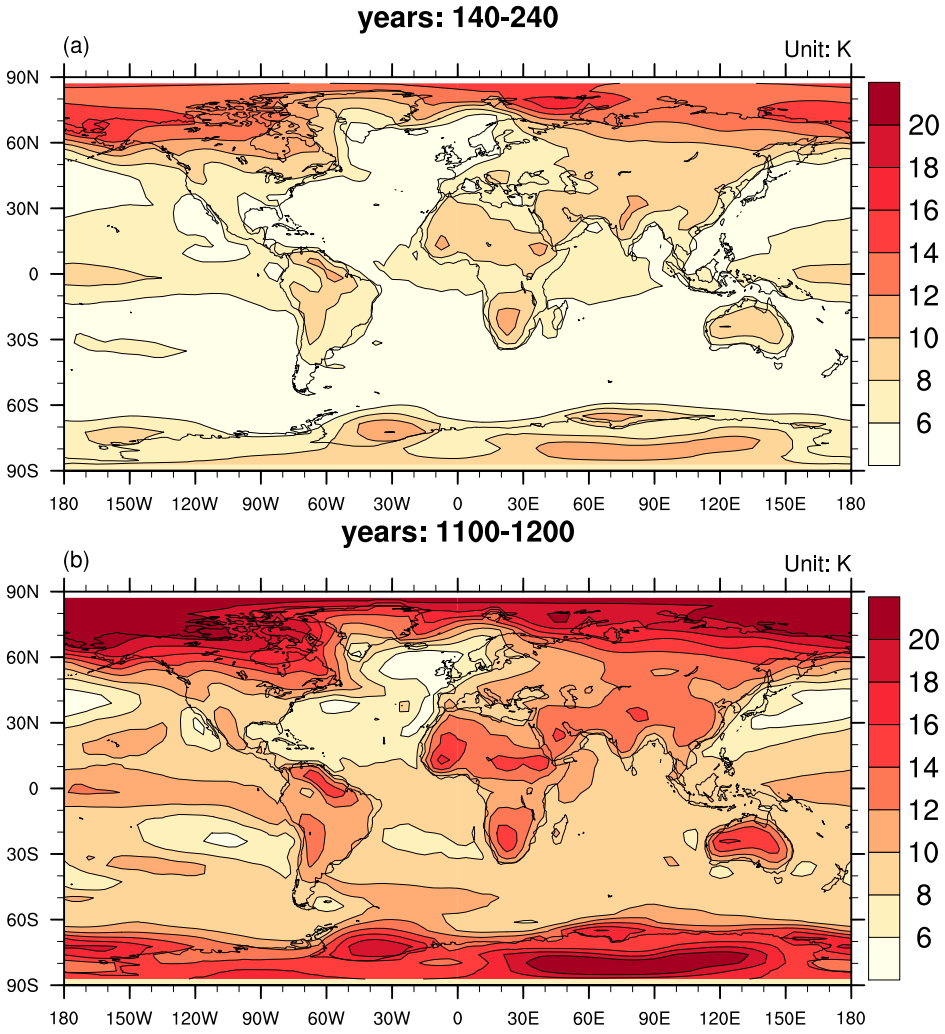

(a) Fig. 2(1)

Fig. 2.2: Geographic distribution of the surface air temperature change of ECHAM5/MPIOM in response to CO_2 quadrupling, (a) by the beginning of the transient period (i.e., the average from the 140th year to the 240th year), (b) the end of the transient period (i.e., the average from the 1100th year to the 1200th year), (c) the end of the equilibrium period (i.e., the average from the 5980th year to the 6080th year). (d) is the difference between (c) and (b). Unit: K.

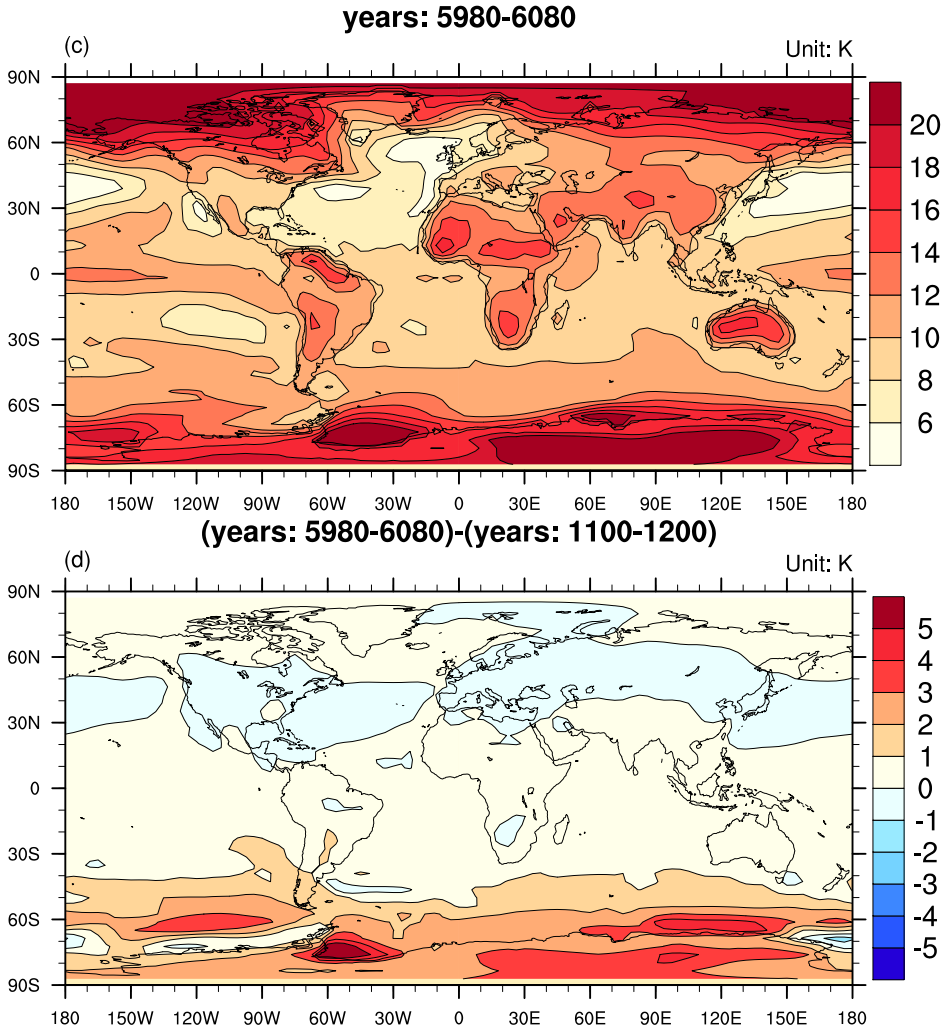

(b) Fig. 2(2)

Fig. 2.2: Continued

2.3.3 Ocean temperature and sea level change

The upper ocean (above 1500 m) and the deep ocean (below 1500 m) adjust to equilibrium on two different time scales (Fig. 2.3). The upper ocean reaches equilibrium by the end of the transient period, just as the surface (Fig. 2.1a). During the CO_2 increase period, the response of the deep ocean is very weak, and the warming trend increases in the following centuries. The deep ocean is still far away from the new equilibrium when the upper ocean is already stable, implying that the deep ocean still takes up heat from the upper ocean when the surface temperature change is almost stationary. The whole system reaches the final equilibrium after about 4600 years when the deep ocean stops warming.

At equilibrium, we find a near-uniform warming of around 8.0 K at almost all levels of the ocean (Fig. 2.4). The maximum warming, which is about 10.0 K, is located between 1000 m and 2000 m depth. In order to estimate the ocean equilibrium response to atmospheric CO_2 forcing, previous studies have mainly used upwelling-diffusion energy-balance climate models (Hoffert et al. 1980; Gornitz et al. 1982; Harvey and Schneider 1985; Wigley and Raper 1987, 1992; Raper et al. 2001; Marčelja 2010). These models have suggested small warming in the deep ocean but large warming in the surface. Therefore, the ocean heat content change is mainly determined by the temperature change occurring in the upper 1000 m (Marčelja 2010). In contrast, Harvey and Schneider (1985) used a three-layer ocean box model coupled to a global-mean energy balance model and found uniform ocean warming under an increase of the solar constant. Our AOGCM results confirm the results of the globally averaged ocean box model but are inconsistent with the results of the upwelling-diffusion energy-balance ocean models. It is conceivable that the results of upwelling-diffusion models can be brought into agreement with our results by including a time-dependent bottom temperature. This strategy was pursued by Harvey and Schneider (1985) (Section 5), who, however, did not nearly increase their bottom temperature enough to be consistent with our results.

Since the deep ocean and the upper ocean show a nearly identical temperature change in the final equilibrium, the deep-ocean temperature change also plays an important role for the long-term globally averaged sea level change. Notice that our model cannot represent a possible sea level rise due to an additional fresh-

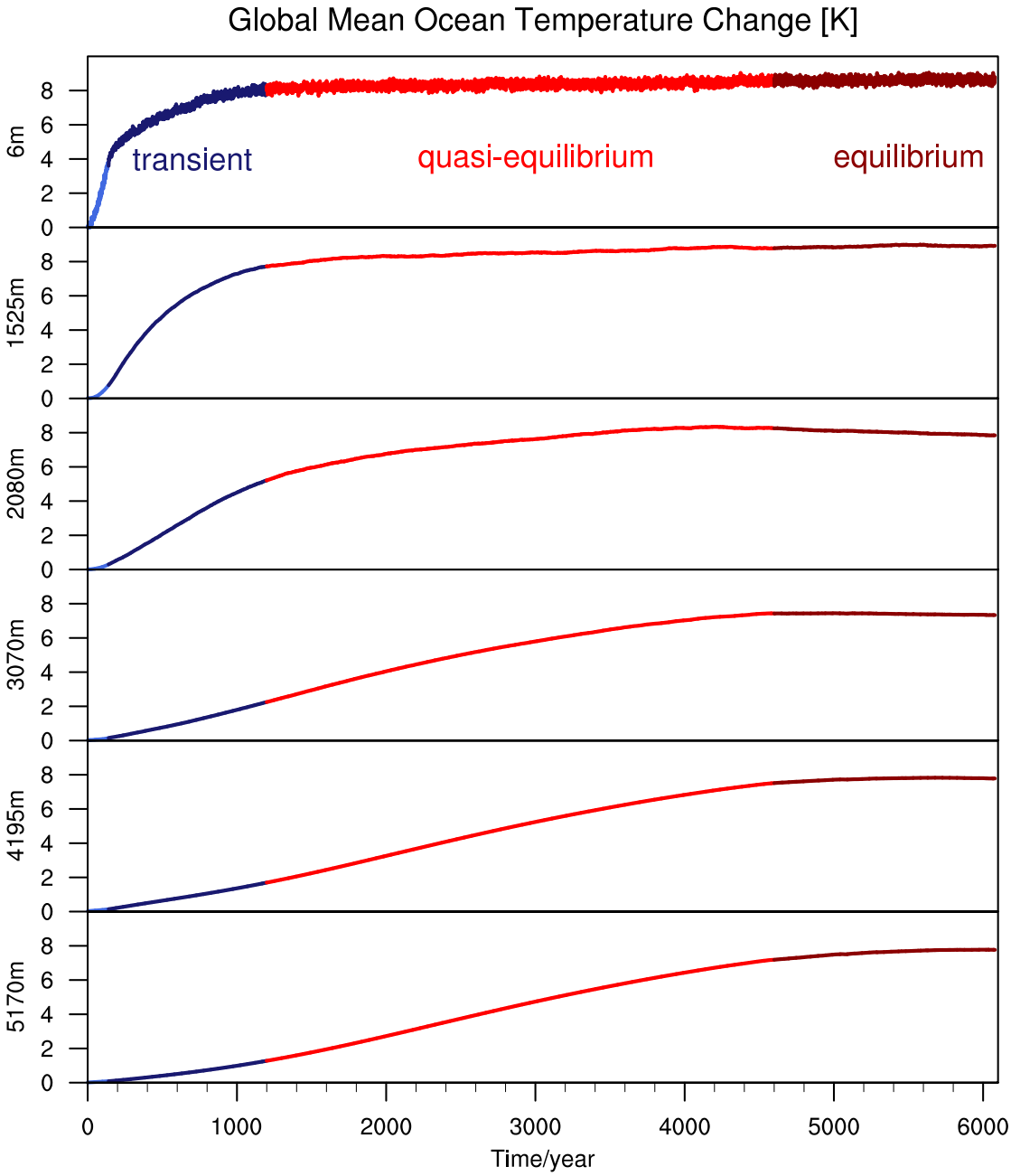

Fig. 2.3: Time series of annual-mean, globally averaged ocean temperature change with CO_2 quadrupling in ECHAM5/MPIOM. The time series are relative to the reference period from CNTR. Unit: K.

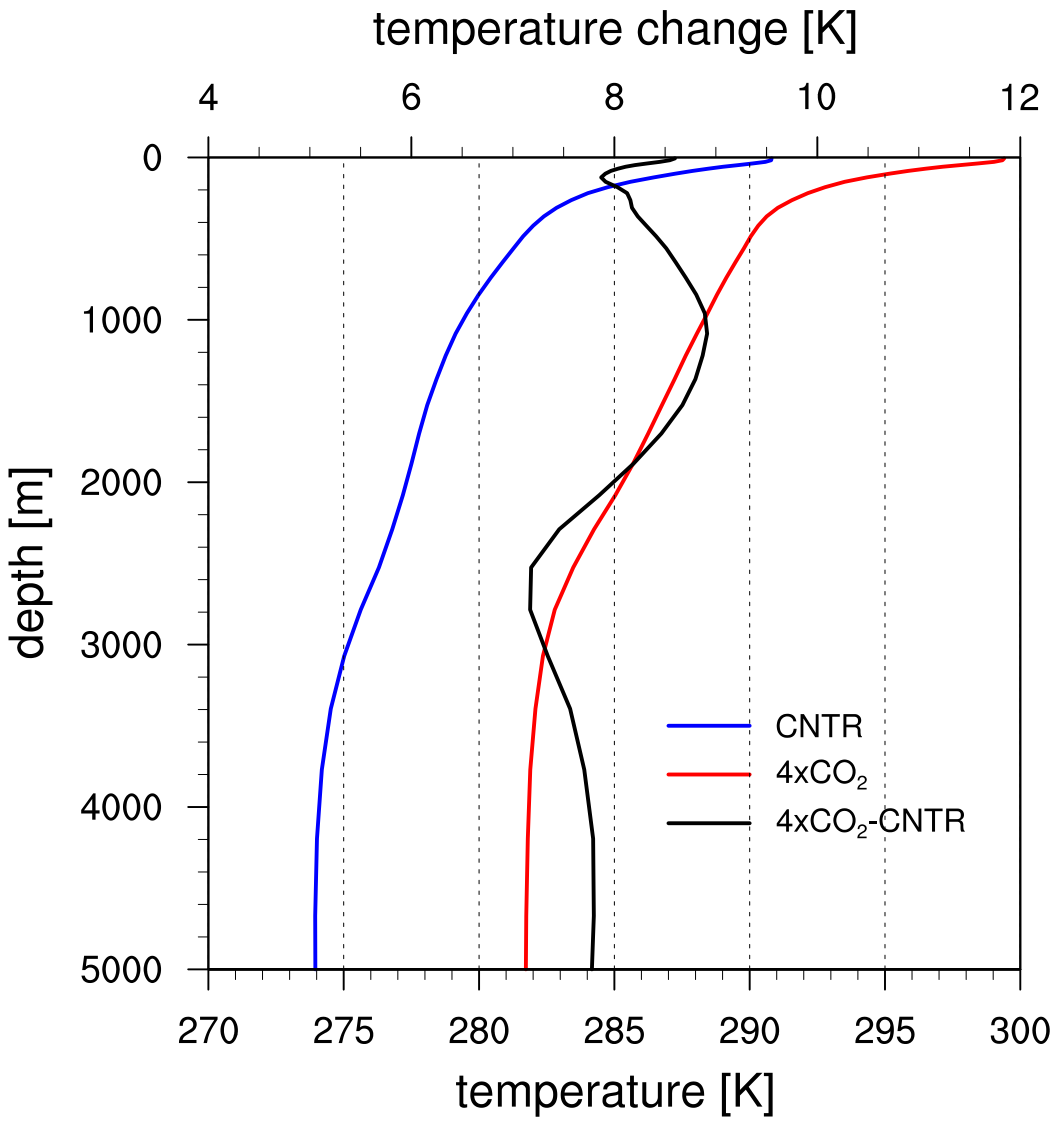

Fig. 2.4: Globally averaged ocean temperature profiles. The blue line represents the pre-industrial control run, the red line represents the final 100-year mean of the $4 \times CO_2$ run, and the black line represents the difference between the final 100 years of $4 \times CO_2$ relative to CNTR. Unit: K.

water input caused by melting land ice. But following Landerer et al. (2007), we calculate the steric sea level change (ζ_S), thermosteric (ζ_S^{thermo}) and halosteric (ζ_S^{halo}) sea level changes contributed by each model depth layer from

$$\zeta_S(K) = \frac{1}{A}\int_A \frac{\rho(S_C,T_C,p)-\rho(S_{EX},T_{EX},p)}{\rho(S_C,T_C,p)}\Delta Z dxdy, \tag{2.1}$$

$$\zeta_S^{thermo}(K) = \frac{1}{A}\int_A \frac{\rho(S_C,T_C,p)-\rho(S_C,T_{EX},p)}{\rho(S_C,T_C,p)}\Delta Z dxdy, \tag{2.2}$$

$$\zeta_S^{halo}(K) = \frac{1}{A}\int_A \frac{\rho(S_C,T_C,p)-\rho(S_{EX},T_C,p)}{\rho(S_C,T_C,p)}\Delta Z dxdy, \tag{2.3}$$

where the subscripts EX and C refer to the atmospheric CO_2 quadrupling experiment and to the control run, ΔZ is the thickness of each model layer, A is the ocean area at each model level, and the in-situ density ρ is a time-dependent, nonlinear function of salinity, temperature and pressure (Gill 1982). ζ_S, ζ_S^{thermo} and ζ_S^{halo} are calculated as a function of model level K. The thermosteric (ζ_S^{thermo}) and halosteric (ζ_S^{halo}) sea level changes are calculated to evaluate the individual contribution of temperature and salinity to the steric anomalies in reference to the temperature and salinity fields of the control run. The total globally averaged sea level change is cumulatively summed up over the whole ocean depth, the contribution from the upper ocean is cumulatively summed up over the top 1500m, and the contribution from the deep ocean is cumulatively summed up over the depth below 1500m (Fig. 2.5a). Global-mean sea level rises by 5.8 m with the 10.8 K surface warming in the steady state of the $4\times CO_2$ run, roughly 0.5 m per 1.0 K increase of the surface temperature. This number is much larger than in the upwelling-diffusion ocean model of Marčelja (2010), who only found a sea level rise of 0.125 m for a 1.0 K surface temperature rise. During our transient period, the global sea level change is mainly caused by the upper-ocean warming. However, during the quasi-equilibrium period the sea level change due to the upper-ocean warming is stationary while the sea level change due to deep-ocean warming is still ongoing (Fig. 2.5). In the final equilibrium, the global sea level change induced by the deep-ocean warming is 3.4 m while the upper ocean contributes 2.4 m.

Starting at the sea surface, the thermosteric and halosteric contribution from each level are cumulatively summed up to a depth of 5000 m for the last 100

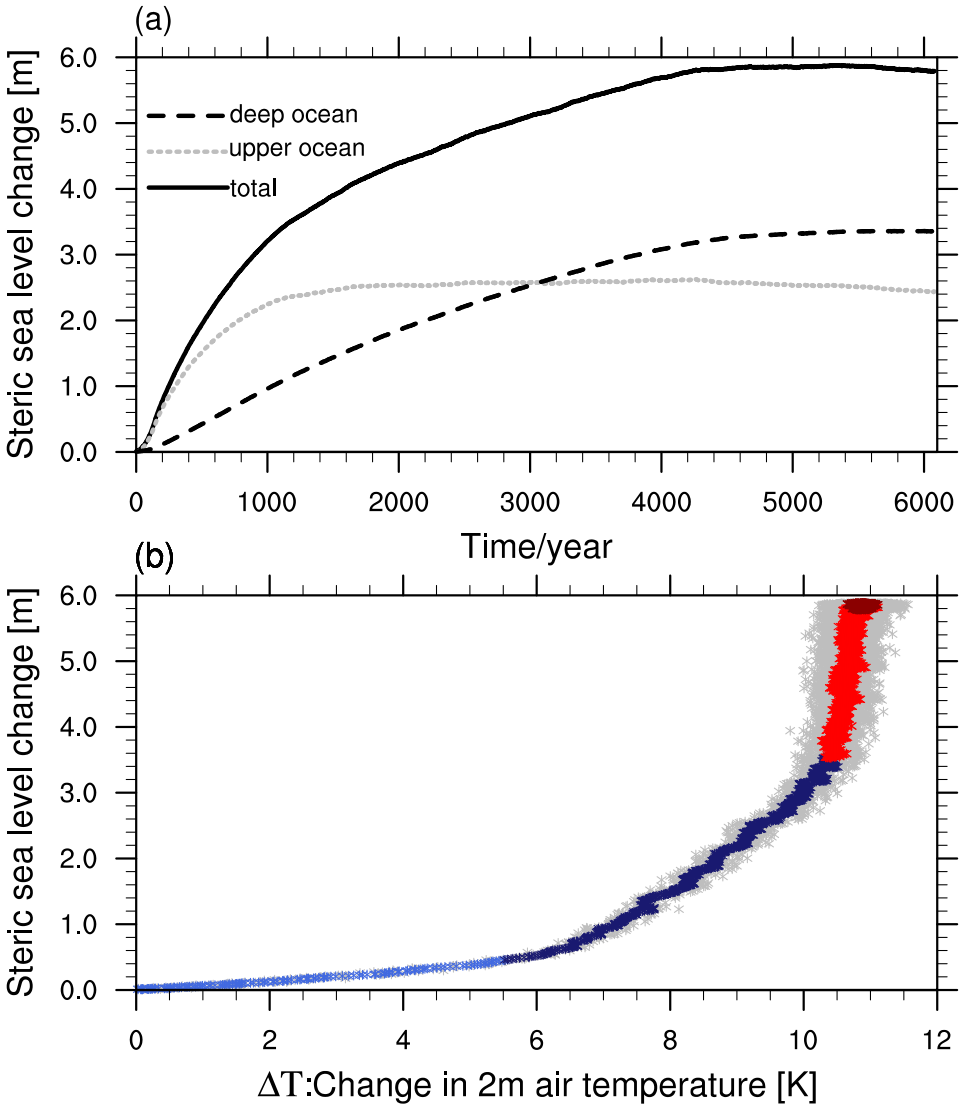

Fig. 2.5: (a) Time series of the annual-mean, globally averaged steric sea-level change (black solid line), and its contribution from the upper ocean (gray dotted line) and the deep ocean (black dashed line). The separation between upper and deep ocean is at 1500 m. Unit: m. (b) Globally averaged steric sea-level change (Unit: m) as a function of globally averaged surface temperature change(ΔT) (Unit: K). The gray crosses represent annual-mean data for the entire experiment, the other color crosses represent data from an 11-year running mean. The light blue crosses represent the CO_2 increase period (1-140yr), the dark blue crosses represent the transient period (140-1200yr), the red crosses represent the quasi-equilibrium period (1200-4600yr), and the firebrick crosses represent the final equilibrium period (4600-6080yr). The change is with respect to the reference period from CNTR.

years of the final equilibrium period (Fig. 2.6). Generally, the thermosteric sea level change plays a dominant role for the global-mean sea level change while the halosteric change is less important; the salinity anomalies may, however, have a significant influence on regional sea level change (e.g. Landerer et al. 2007).Figure 2.6 also shows that the thermosteric signal has its largest contribution within the upper 4000m, not only in the upper 1000m.

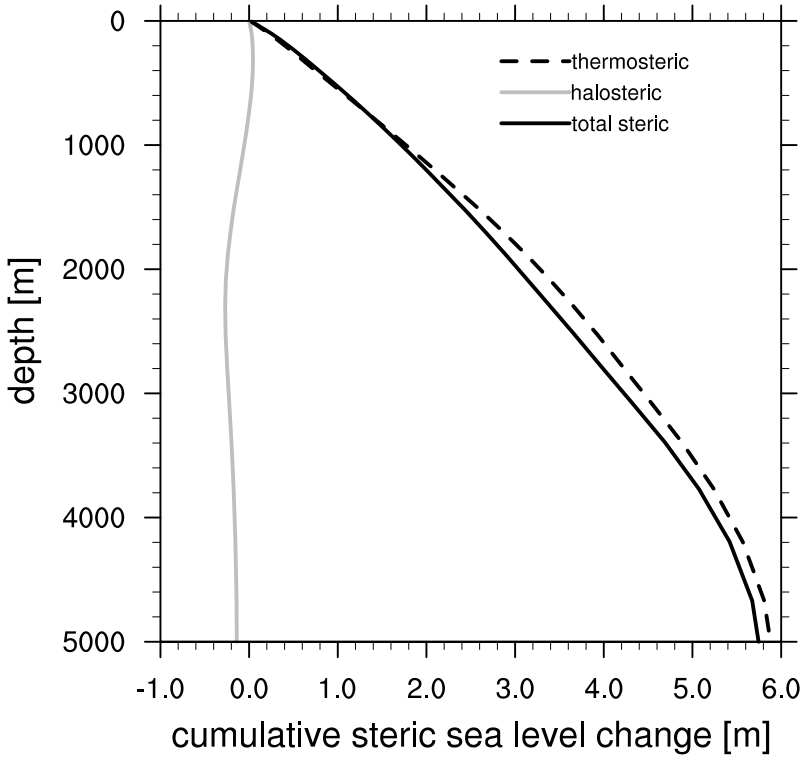

Fig. 2.6: Cumulative sum of thermosteric sea-level change (dashed line), halosteric sea-level change (grey line) and total steric sea-level change (black line) for the global ocean in the last 100 years of the equilibrium period. Starting at the surface, the steric anomaly from each depth layer is added up. Unit: m.

Future sea-level rise has also been estimated using empirical approaches (Rahmstorf 2007; Vermeer and Rahmstorf 2009). The general assumption of the empirical approach is that the relationship between sea level change and surface temperature change or radiative forcing will hold in the future and for a much greater range of warming than occurred during the period from which it was calibrated. Based on this assumption, the future sea level change can be calculated

directly from the climate model projections of global warming. Our AOGCM result shows that the globally averaged sea level changes by 0.45 m and the surface temperature increases by 5.5 K during the first 140 years when the atmospheric CO_2 increases by $1\%\,\mathrm{yr}^{-1}$, and the globally averaged sea level rises by 3.05 m and surface temperature increases by 4.9 K during the transient period. During the quasi-equilibrium period, the globally averaged sea level still rises by 2.3 m while the surface temperature is almost stationary (Fig. 2.5b). The relationship between sea level rise and the surface temperature will not hold because the ocean temperatures at different depths respond on different timescales. During the short-term transient response, we may use the empirical approaches and 1-D upwelling-diffusion ocean models to estimate steric sea level change, but for the long-term equilibrium response, we cannot use these two methods because they both underestimate the contribution of the deep-ocean warming to the steric sea level change.

2.3.4 Change in Atlantic meridional overturning circulation

As in most previous global warming studies, the Atlantic meridional overturning circulation (AMOC) weakens, but does not collapse in our experiment (Fig. 2.7). We define an Atlantic meridional overturning circulation index (MOI) as the annual-mean zonally integrated streamfunction in Sverdrups ($1\,\mathrm{Sv}{\equiv}10^6\,\mathrm{m}^3\,\mathrm{s}^{-1}$) at the depth of 1000 m in the Atlantic at 30 °N. The MOI weakens from 18.5 Sv to about 7.5 Sv (decline by 62.2%) during the first 140 years while CO_2 is increasing (Fig. 2.7c). Thereafter, the MOI slowly recovers and reaches 10 Sv in the new equilibrium. The increase of the AMOC with stationary $4{\times}CO_2$ forcing is due to the salt advection feedback as found by Latif et al. (2000). In a warmer climate, the enhanced evaporation in the tropical Atlantic leads to increased salinity there; this saline water is eventually advected into the deep-water formation regions in the North Atlantic, decreases the upper ocean stability there, and thus strengthens the AMOC. But in contrast to other AOGCM long-term integrations (Voss and Mikolajewicz 2001; Stouffer and Manabe 2003), the AMOC in our experiment does not recover to the pre-industrial control value. The MOI is about 46.0% weaker than in CNTR, and the AMOC upper cell is shallower, which indicates that the North Atlantic Deep Water does not penetrate as deep

as in CNTR, and the bottom cell becomes thicker and weaker.

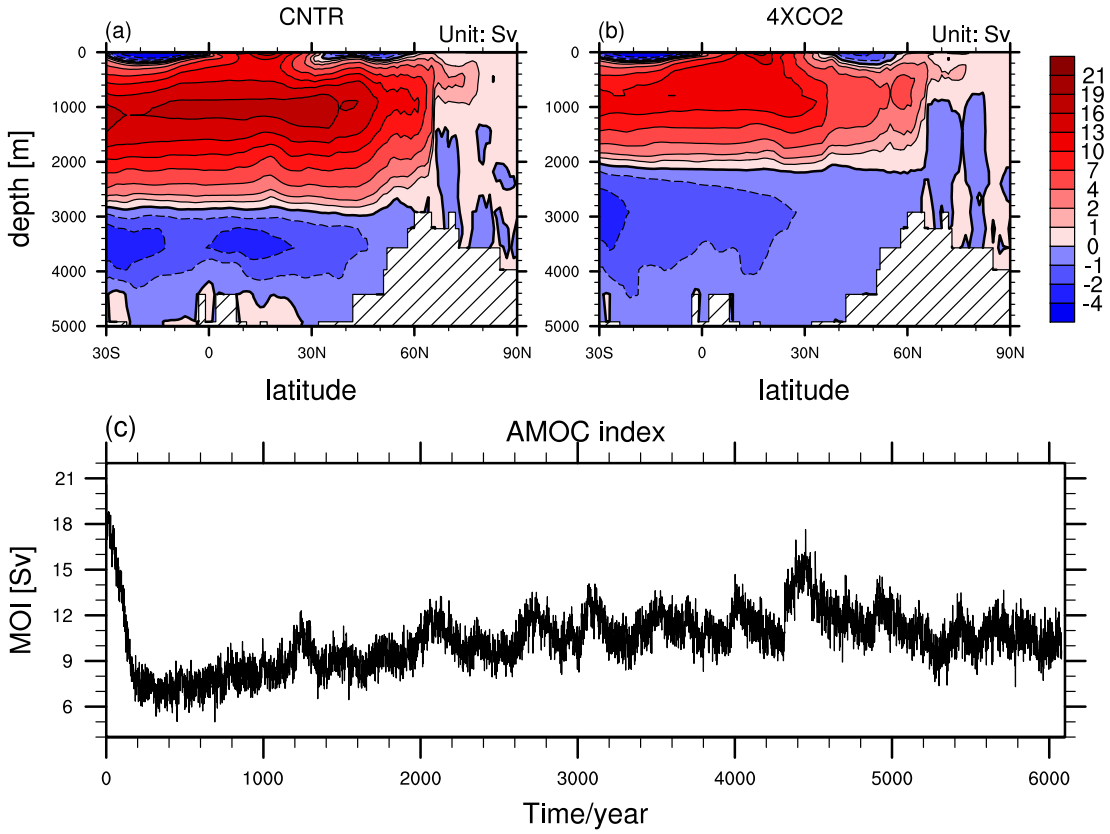

Fig. 2.7: Latitude-depth distribution of the meridional streamfunction in the Atlantic, (a) for the pre-industrial control run, and (b) for the equilibrium of CO_2 quadrupling. (c) Time series of the Atlantic meridional circulation index (MOI). The MOI is defined as the annual mean zonally integrated streamfunction at the depth of 1000m in the Atlantic at 30°N. Unit: Sv.

2.4 Equilibrium climate response in ECHAM5/SOM

In ECHAM5/MPIOM the AMOC declines by 46% in the $4\times CO_2$ case; this weakening in AMOC reduces the northward ocean heat transport by 0.57 PW across 30 °N (decline by about 35% relative to the pre-industrial mean value, Fig. 2.8a). By contrast, the implied ocean heat transport with CO_2 quadrupling is almost the same as in CNTR in ECHAM5/SOM, except in the southern-hemisphere high latitudes where we find an unrealistic decline by 0.29 PW (Fig. 2.8b). The implied ocean heat transport should be constant by construction but is not really

because of a contribution from changes in sea-ice. To investigate whether the surface equilibrium response is affected by the change in ocean heat transport, we compare the ECR in both ECHAM5/MPIOM and ECHAM5/SOM.

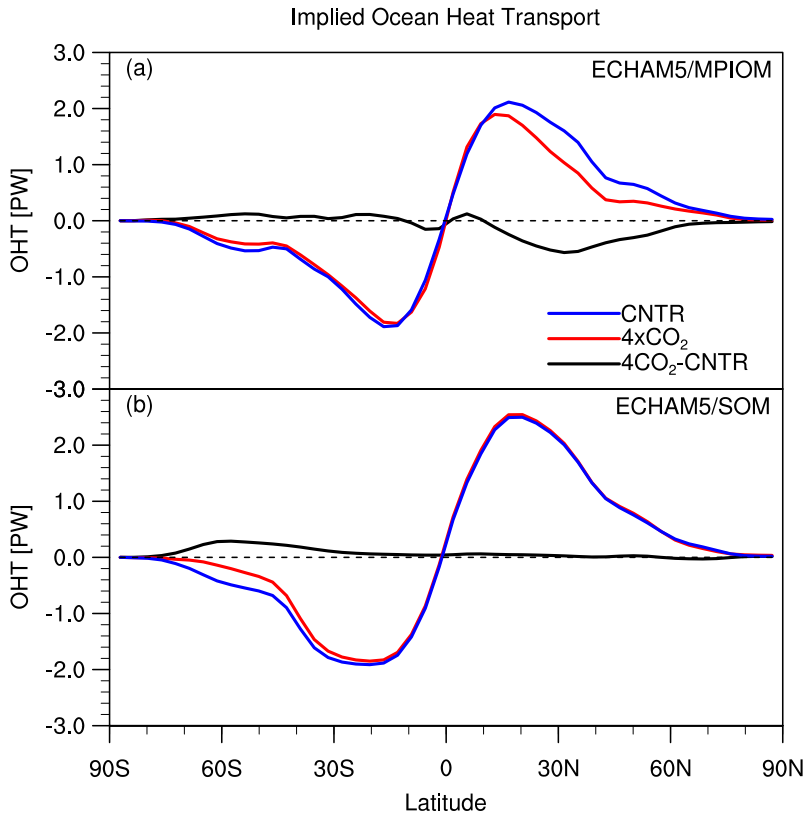

Fig. 2.8: Implied ocean heat transport simulated by (a) ECHAM5/MPIOM and (b) ECHAM5/SOM as a function of latitude for the $4\times CO_2$ (red lines), control runs (blue lines) and the difference between $4\times CO_2$ and control runs (black line). The heat transports are computed for the last 100 years of each run. Unit: 1.0 PW$= 1.0\times10^{15}$ W.

In ECHAM5/SOM, the globally averaged surface temperature is 287.6 K in the pre-industrial control run and is 0.9 K higher than that in ECHAM5/MPIOM; SST is also 0.9 K higher. The ECR is 11.1 K in ECHAM5/SOM and is 0.3 K higher than in ECHAM5/MPIOM. The change in SST is identical in both models, which suggests that the slight overestimation in ECHAM5/SOM is mainly caused by the response over the continent (Table 2.1). The equilibrium climate sensitivity of ECHAM5/SOM with atmospheric CO_2 doubling from 278 ppmv to 556 ppmv amounts to 3.7 K, which is in the climate sensitivity range from 2.1 to 4.4 K

reported in the IPCC AR4 (Randall et al. 2007). The second atmospheric CO_2 doubling from $2\times CO_2$ to $4\times CO_2$ leads to an additional warming of 7.4 K (Fig. 2.9). Hence, the climate sensitivity of the second CO_2 doubling is much larger than for the first CO_2 doubling. Heinemann et al. (2012), who investigated a range of CO_2 increases with the same model but in a Paleocene configuration, found that the larger climate sensitivity of the second doubling of atmospheric CO_2 is mainly caused by a larger negative longwave cloud radiative forcing, leading to a warming of 4.6 K compared to 2.3 K for the first doubling. The larger surface albedo change and a larger reduction of the shortwave cloud radiative forcing together cause a warming of 1.9 K compared to 0.7 K for the first doubling.

Table 2.1: Globally averaged surface temperature in ECHAM5/MPIOM and ECHAM5/SOM, unit: K

	Global		Ocean	
	CNTR	4xCO_2	CNTR	4xCO_2
ECHAM5/MPIOM	286.7	297.5(+10.8)	288.9	298.9(+10.0)
ECHAm5/SOM	287.6	298.7(+11.1)	289.8	299.8(+10.0)

$*$ The numbers in parentheses in the last columns give the equilibrium surface temperature change in ECHAM5/MPIOM and in ECHAM5/SOM, relative to their pre-industrial control runs.

While the global-mean surface temperature response to CO_2 quadrupling is very similar in ECHAM5/SOM and ECHAM5/MPIOM; the geographic distribution of the surface temperature change shows some marked differences between ECHAM5/SOM and ECHAM5/MPIOM (Fig. 2.10). ECHAM5/SOM shows a clearly asymmetric temperature change between Northern and Southern Hemispheres; the increase of the surface temperature in the Northern Hemisphere is much larger than that in the Southern Hemisphere (Fig. 2.10a). In the difference (ECHAM5/MPIOM minus ECHAM5/SOM), the maximum negative anomalies of over 5.0 K occur south of Greenland, corresponding to the typical deep convection site in the Labrador Sea. The negative anomalies extend eastward into most of the Eurasian continent. In the Southern Hemisphere, the surface warming in

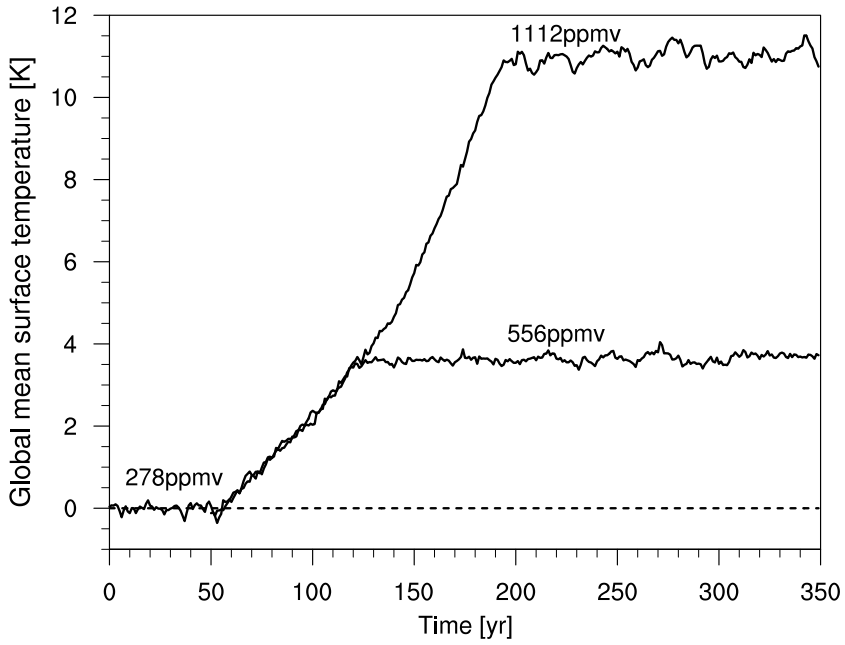

Fig. 2.9: Time series of global-mean surface temperature change of ECHAM5/SOM. All time series are relative to the pre-industrial control run of ECHAM5/SOM. Unit: K.

ECHAM5/MPIOM is larger than that in ECHAM5/SOM. The maximum positive anomalies of over 5.0 K occur over the Southern Ocean and the Antarctic continent. Generally speaking, this anomaly pattern between ECHAM5/MPIOM and ECHAM5/SOM is very similar to the bipolar seesaw response due to the AMOC reduction in the multi-model ensemble simulation of the water-hosing experiments (Fig.14 in Stouffer et al. 2006), although there are differences in the amplitude in specific regions. The reduction in AMOC reduces the warming in the Northern Hemisphere but enhances the warming in the Southern Hemisphere, because of the associated reduction of the northward heat transport out of the Southern Hemisphere.

However, different from the AMOC-induced bipolar seesaw pattern, we find in ECHAM5/MPIOM stronger warming of 3.0 K in the tropical Pacific and weaker warming in the western boundary regions in the North Pacific. In the tropical Pacific, the reduction of vertical heat transport, which is caused by the weakening of vertical mixing associated with the upper-ocean warming, enhances the surface warming found in the tropical Pacific. The tropical Pacific warming looks very similar to an El Nino-like response pattern and can influence the global climate

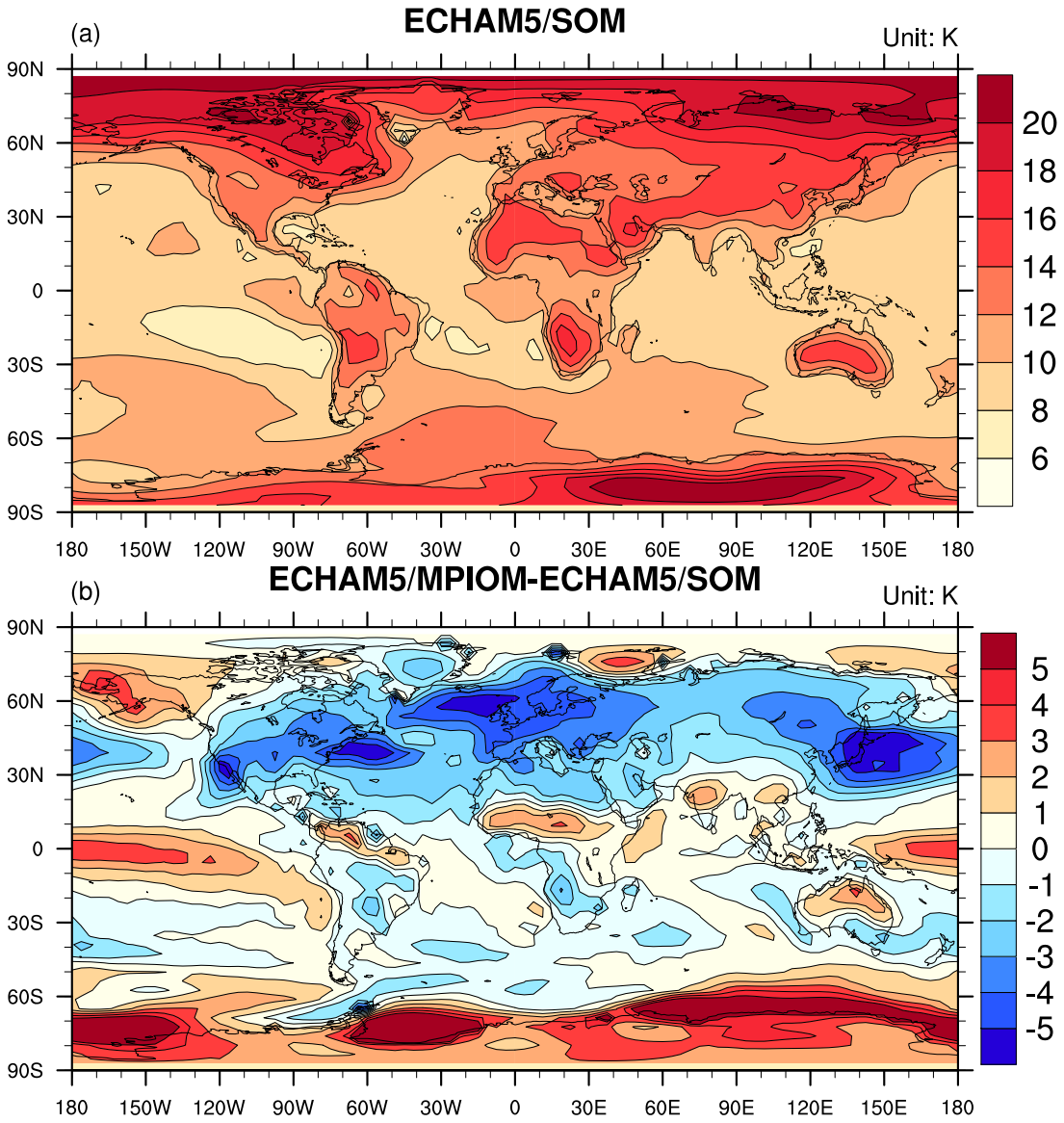

Fig. 2.10: Geographic distribution of the surface temperature change relative to the pre-industrial control run in response to CO_2 quadrupling in ECHAM5/SOM, and the difference of the geographic warming pattern between ECHAM5/MPIOM and ECHAM5/SOM. Unit: K.

through large-scale air-sea interaction. The tropical Pacific warming can cause the easterly trade winds to weaken and can thus weaken the Pacific western boundary current. Hence, the warming in western boundary current is reduced due to the reduction of the northward ocean heat transport. The ECHAM5/SOM cannot produce the enhanced tropical Pacific warming because the change in ocean circulation is not included in SOM. We also find much stronger warming over the Southern Hemisphere in the anomaly pattern between ECHAM5/MPIOM and ECHAM5/SOM, compared to the AMOC-induced bipolar seesaw pattern. The strong deep-ocean warming found in ECHAM5/MPIOM (details in section 3b,c) can also enhance the surface warming because the Southern Ocean is very well mixed.

2.5 Effective climate response

Extending the experiment to equilibrium enables us to test the method for estimating the effective climate response as described by Gregory et al. (2004). Here, we use the phrase "effective climate response" instead of "effective climate sensitivity" to discriminate the long integration for CO_2 quadrupling from that for CO_2 doubling.

Following Gregory (2000) and Held et al. (2010), we use a two-layer horizontal-mean ocean model; the separation between the upper ocean and the deep ocean is at 1500 m. We consider the following equations:

$$N = F - \alpha \Delta T \approx \Delta Q_S, \tag{2.4}$$

$$C_U \frac{dT_U}{dt} = \Delta Q_S - \Delta Q_D = F - \alpha \Delta T - \Delta Q_D, \tag{2.5}$$

$$C_D \frac{dT_D}{dt} = \Delta Q_D, \tag{2.6}$$

where N is the rate of increase in the heat stored in the climate system; because the ocean has a vastly larger heat capacity than the atmosphere, N approximately equals the total ocean heat uptake (ΔQ_S), and it also equals the net downward radiative flux at the top of the atmosphere (TOA). F is the radiative forcing, α is the climate response parameter, and ΔT is the global mean surface temperature change. ΔQ_D is the deep-ocean heat uptake (DOHU) defined as the tendency

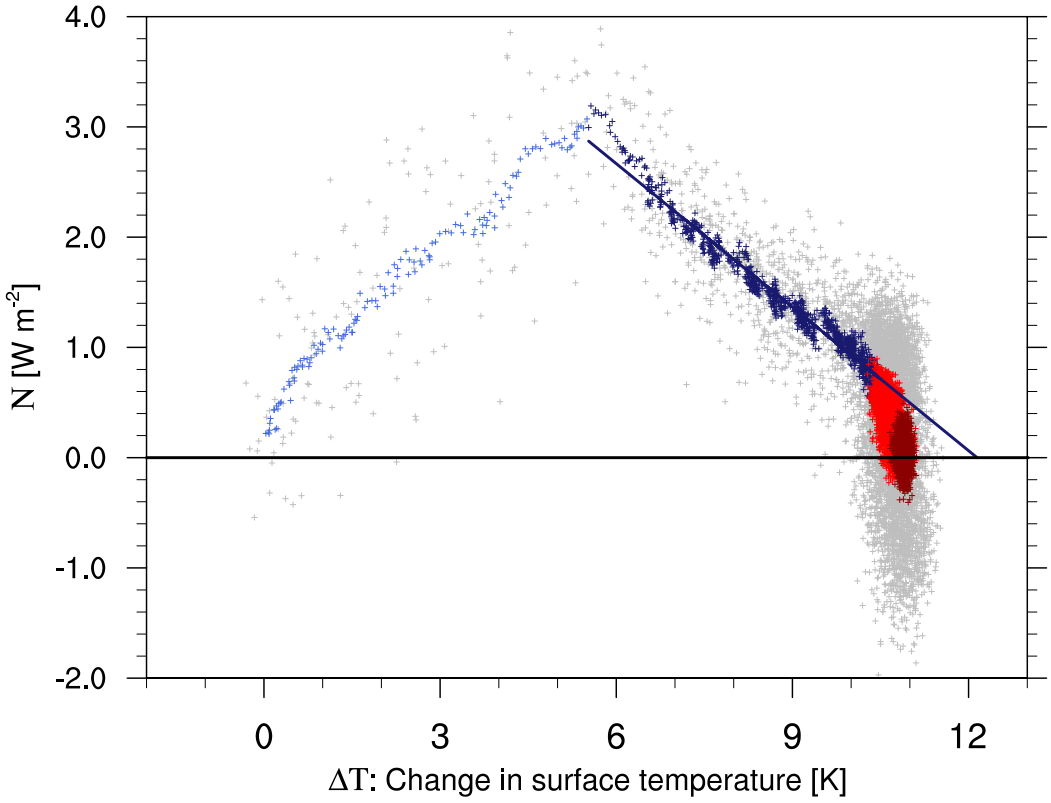

Fig. 2.11: Globally averaged TOA net downward radiative flux (N) (Unit: $\mathrm{W\,m^{-2}}$) as a function of globally averaged surface temperature change(ΔT) (Unit: K). The gray crosses represent annual-mean data for the entire experiment, the other color crosses represent data from an 11-year running mean and relative to CNTR. The light blue crosses represent the CO_2 increase period (1-140yr), the dark blue crosses represent the transient period (140-1200yr), the red crosses represent the quasi-equilibrium period (1200-4600yr), and the firebrick crosses represent the final equilibrium period (4600-6080yr). The dark blue line is a regression for the whole transient period.

of total ocean heat content below 1500m. The unit of DOHU is $\mathrm{W\,m^{-2}}$ because we divide the total ocean heat content by the surface area of the Earth. ΔT_U and ΔT_D are the ocean mean temperatures in the upper and the deep ocean, respectively. C_U and C_D are the heat capacities of the ocean layers. We assume that the heat exchange is proportional to the difference between the temperature in the two layers,

$$\Delta Q_D = \lambda(\Delta T_U - \Delta T_D), \tag{2.7}$$

where λ is the deep-ocean heat uptake efficiency.

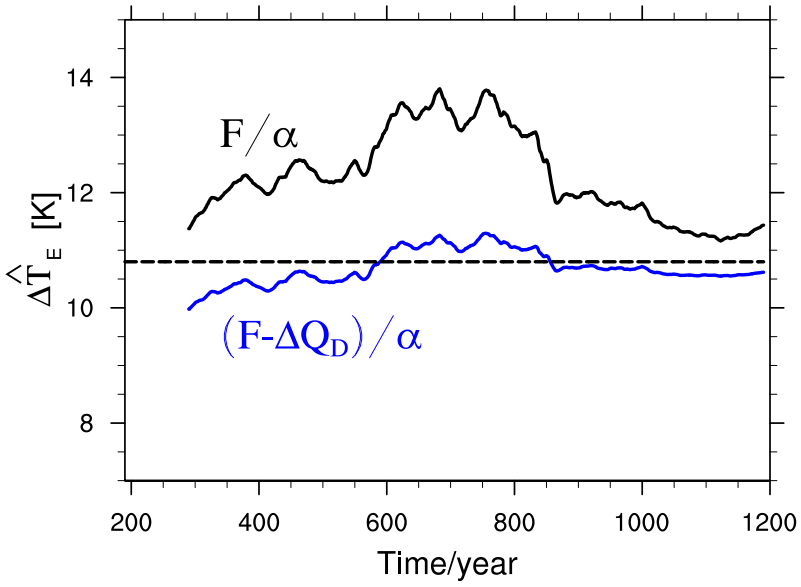

Fig. 2.12: Effective climate response. The black solid line represents the estimate following the method described by Gregory et al. (2004), the blue solid line represents the estimate including the deep-ocean heat uptake (ΔQ_D), and the dashed black line represents the ECR of ECHAM5/MPIOM, which is 10.8 K. A 300-year moving-window linear regression has been used. Unit: K.

By using the data of the transient period, we perform a linear regression between N and ΔT, which gives us an estimate of both the radiative forcing F and the climate response parameter α. We find that the effective climate response ($\Delta T_E = F/\alpha$, while N=0) is 12.2 K, which is 1.4 K higher than the ECR of ECHAM5/MPIOM; the radiative forcing F is $5.26\,\mathrm{W\,m^{-2}}$, and the climate response parameter α is $0.43\,\mathrm{W\,m^{-2}\,K^{-1}}$. The fundamental assumption of this effec-

tive climate response method is that the radiative forcing F and climate response parameter α are time-independent. However, Figure 2.11 shows that the TOA net downward radiative flux decreases by $2.3\,\mathrm{W\,m^{-2}}$ with 4.9 K surface warming in the transient period (blue crosses), compared to a decrease by $0.7\,\mathrm{W\,m^{-2}}$ with 0.4 K surface warming in the quasi-equilibrium period (red crosses). The change in the slope of the data suggests that the climate response parameter α is time-dependent. However, while the steeper slope for the quasi-equilibrium period in Fig. 2.11 implies that the linear fit overestimates the equilibrium climate response; the error we commit is, at 1.4 K, which is relatively small.

Our results suggest that the change in the climate response parameter α also plays an important role in the adjustment of the TOA radiative flux in the quasi-equilibrium period. According to (4), α can be diagnosed from $\alpha = (\mathrm{F\text{-}N})/\Delta T$. At the end of the transient period, there is still $0.7\,\mathrm{W\,m^{-2}}$ radiative flux imbalance at TOA; the climate response parameter change contributes $0.52\,\mathrm{W\,m^{-2}}$ ($\Delta\alpha \cdot \triangle\overline{T}$ =0.05×10.4=$0.52\,\mathrm{W\,m^{-2}}$, where $\Delta\alpha$ is the climate response parameter change in the quasi-equilibrium period) to balance the radiative flux, whereas the surface temperature change (0.4K warming in the quasi-equilibrium period) only contributes $0.17\,\mathrm{W\,m^{-2}}$ ($\alpha \cdot \triangle T'$ =0.43×0.4=$0.17\,\mathrm{W\,m^{-2}}$, where $\triangle T'$ is the surface temperature change in the quasi-equilibrium period). This slow increase in α may be caused by the slow warming over the Southern Ocean and the Antarctic continent (Fig. 2.2a). By using the Hadley Centre coupled climate model with flux adjustment, Senior and Mitchell (2000) demonstrated that the time-dependence of the climate feedback parameter can be caused by cloud feedback arising from the inter-hemispheric temperature difference due to the slower warming of the Southern Ocean. Further investigations are still needed to quantify the impact of Southern-Ocean warming on the surface climate feedbacks in our experiment.

We can reduce the estimation error of the ECR still further by considering the upper and the deep ocean separately, noting that an alternative expression for the ECR can be derived from equations 2.4-2.6, assuming $N = \Delta Q_D$ instead of N=0,

$$\Delta\hat{T}'_E = (F - \Delta Q_D)/\alpha. \tag{2.8}$$

By using the data of the whole transient period (140yr-1200yr), the ECR estimated by equation 2.8 is 10.7 K, which is very close to the ECR of 10.8 K in ECHAM5/MPIOM. To further clarify whether both methods work over the whole transient period, we use the same linear-regression technique with a sliding 300-year-window. The results suggest that the ECR estimated with the two-layer ocean model is much closer to the result from the ECHAM5/MPIOM simulation than the original method of Gregory et al. (2004) (Fig. 2.12). The overestimate by 10% of the ECR method of Gregory et al. (2004) arises from ignoring the impact of DOHU on the surface climate response parameter.

2.6 Summary and conclusions

Using the coupled atmosphere-ocean-sea ice general circulation model ECHAM5 /MPIOM, we perform a multi-millennium climate simulation by gradually increasing the CO_2 concentration by 1% yr^{-1} and keeping it constant after 140 years. The integration is continued until the whole system reaches equilibrium in year 6080. To our knowledge, we have achieved the first steady state simulation with CO_2 quadrupling by using a modern non-flux-adjusted AOGCM. The final equilibrium in the ECHAM5/MPIOM is compared with the corresponding simulation in ECHAM5/SOM (ECHAM5 coupled to a slab ocean model). We summarize our research as follows.

(1) The equilibrium surface-temperature change from CO_2 quadrupling in ECHAM5/MPIOM is 10.8 K in the global mean and 10.0 K over the ocean.

(2) The ocean temperature shows a near-uniform warming of around 8 K at almost all levels of the ocean; this result confirms globally averaged multi-box ocean model simulation (e.g. Harvey and Schneider 1985), but does not support the globally averaged upwelling-diffusion ocean model simulations (e.g. Harvey and Schneider 1985; Raper et al. 2001; Marčelja 2010)).

(3) We find that deep-ocean warming plays an important role for the thermosteric global sea level change. The globally averaged sea level still rises by 2.3 m due to the deep-ocean warming while the surface temperature is

stationary. In the long term, surface temperature change is hence a poor predictor for steric sea-level change.

(4) The equilibrium climate response in ECHAM5/SOM is 11.1 K, which is only 0.3 K higher than that in ECHAM5/MPIOM. This suggests that the change in AMOC and the reduced northward ocean heat transport have very limited effect on the global-mean surface temperature change, although the AMOC weakens in equilibrium by 46%. However, the deep-ocean adjustment plays a very important role in determining the geographic pattern of equilibrium surface temperature response and its time evolution. The change in ocean heat transport damps the warming over the northern hemisphere mid and high latitudes, but enhances the warming over the tropical ocean and especially over the Southern-Hemisphere high latitudes. The pattern of the AMOC-induced surface temperature change in our experiments is similar to the multi-model ensemble simulation of water-hosing experiments (Stouffer et al. 2006), although there are differences in the amplitude in specific regions. In contrast to ECHAM5/SOM, which shows an asymmetric polar warming amplification, ECHAM5/MPIOM shows polar amplification in both the Arctic and Antarctic domains. The southern polar warming is greatly delayed by the Antarctic deep-ocean warming.

(5) The equilibrium climate sensitivity in ECHAM5/MPIOM to CO_2 doubling amounts to 3.7 K, which is considerably less than half the ECR to CO_2 quadrupling (11. K). The climate sensitivity to the second CO_2 doubling (from 556 ppmv to 1112 ppmv) is much larger than to the first CO_2 doubling (from 278 ppmv to 556 ppmv) because of a larger negative longwave cloud radiative forcing, a larger surface albedo change, and a larger reduction of the shortwave cloud radiative forcing (Heinemann et al. 2012).

(6) The method to determine the effective climate response from transient simulation (Gregory et al. 2004) overestimates the ECR by only 10%. The error is due to ignoring the impact of deep-ocean heat uptake on the estimated value of the surface climate feedback parameter.

Chapter 3

Sea ice in a future warm climate

— The transient versus the equilibrium response of sea ice to global warming

To examine the long-term stability of Arctic and Antarctic sea ice, idealized simulations are carried out with ECHAM5/MPIOM. Atmospheric CO_2 concentration is increased over 2000 years from pre-industrial levels to quadrupling, is then kept constant for 5940 years, is afterwards decreased over 2000 years to pre-industrial levels, and finally again kept constant for 3940 years.

Despite these very slow changes, the response of sea ice significantly lags behind the CO_2 concentration change. This lag, which is caused by the thermal inertia of the ocean, implies that the equilibrium response of sea ice to increasing CO_2 concentration is substantially underestimated by transient simulations. The response of sea ice to CO_2 concentration change is not truly hysteretic and in principle reversible.

We find no lag in the evolution of Arctic sea ice relative to changes in annual-mean northern-hemisphere surface temperature. The summer sea-ice cover changes linearly with respect to both CO_2 concentration and temperature, while the Arctic winter sea-ice cover shows a rapid transition to a very low sea-ice coverage for a warming of about 8 K. This rapid transition of winter sea ice is triggered by a sudden onset of atmospheric convection, which traps outgoing long-wave radiation.

The Antarctic sea-ice cover retreats continuously without any rapid transition

during the warming. Compared to Arctic sea ice, Antarctic sea ice shows a much more strongly lagged response to changes in CO_2 concentration. It even shows a lagged response to surface temperature change, which is caused by a different response of ocean deep convection during the warming and the cooling periods.

3.1 Introduction

Simple models suggest that sea ice might exhibit multiple equilibria due to the ice–albedo feedback (e.g., Budyko 1969; Sellers 1969; North 1990). A possible irreversible shift of the sea-ice state caused by anthropogenic climate change is of particular concern in evaluating the potential societal and environmental threat posed by future climate change, especially given the strong retreat of Arctic summer sea ice that has been observed in recent decades (e.g. Vinnikov et al. 1999; Lindsay and Zhang 2005; Serreze and Francis 2006). The present study explores the long-term stability and the possibility of hysteresis behavior of Arctic and Antarctic sea ice, by performing long-term integrations with a state-of-the-art coupled atmosphere-ocean-sea ice general circulation model (AOGCM).

If the climate is altered, a transition may occur between climate states that is not reversible by returning the climate to its previous regime (this irreversibility is termed 'hysteresis behavior'). Recently, Armour et al. (2011) and Ridley et al. (2012) investigated the reversibility of sea ice retreat in AOGCM integrations with "ramp-up and ramp-down" atmospheric CO_2 concentration. Both studies found no evidence of irreversible behavior or multiple ice-cover states of the Arctic and Antarctic Oceans in a future warm climate. However, in their studies the atmospheric CO_2 concentration was changed relatively quickly, by 1% per year in Armour et al. (2011) and by 2% per year in Ridley et al. (2012). Hence, the sea-ice covered states in these experiments are still transient, because the forcing is changed too fast to ensure a quasi-equilibrium system. For example, Ridley et al. (2008) found earlier that the Arctic sea ice had not reached a new equilibrium even after 600 years of stabilization after an atmospheric CO_2 quadrupling. This long timescale implies that slow oceanic adjustments may lead to differences between increasing and decreasing surface temperature trajectories if atmospheric CO_2 concentration is changed rapidly; these differences might be mistaken as indicating hysteresis. True hysteresis is, however, only presented if in a study with

a given input forcing that is alternately increased and decreased, (a) the system shows different trajectories for the increase and the decrease of the forcing, and (b) if the resulting multiple internal states for the same external forcing do not disappear as the forcing changes more slowly. Because of these requirements, it is a challenge to examine true hysteresis behavior in an AOGCM due to the computational constraints. In the present study, we examine the possible hysteresis behavior of sea ice in response to changes in atmospheric CO_2 forcing using our state-of-the-art AOGCM ECHAM5/MPIOM. In contrast to the experiments of Armour et al. (2011) and Ridley et al. (2012), we perform experiments in which both the increase and the decrease of the atmospheric CO_2 forcing occur very slowly over 2000 years, hoping to ensure a quasi-equilibrium system. In addition, four experiments are carried out to clarify whether indeed the warming and the cooling trajectories change the CO_2 concentration slowly enough to maintain quasi-equilibrium.

This experimental design also allows us to examine if and why for slowly varying forcing the transition between two sea-ice states can be rapid. Addressing this question in a single-column model, Eisenman and Wettlaufer (2009) found a smooth transition from a perennially ice-covered state to a seasonally ice-free state during a gradual increase in forcing, but found a sudden loss of the remaining winter sea ice for further increased forcing. Since the large-scale processes are highly parameterized in such conceptual models, the transition scenarios of the sea ice strongly depend on the choice of the parameterizations (as reviewed by Eisenman 2012). Hence, it is important to study the transition behavior of sea ice by using an AOGCM. Using the 21st century climate projections from the Coupled Model Intercomparison Project Phase 3 (CMIP3) model runs, several studies have indirectly assessed possible Arctic sea ice bifurcation thresholds in AOGCMs. Some studies indicated that the complete loss of Arctic summer sea ice would occur in a continuous fashion (e.g. Winton 2006, 2008; Ridley et al. 2008). On the other hand, some AOGCMs exhibited abrupt reductions in summer minimum Arctic sea ice cover (Holland et al. 2006); however, further analysis revealed that this abrupt reduction of Arctic summer sea ice might largely be a consequence of increased inter-annual variability of sea ice extent due to the slow shift in ice-thickness distribution (Holland et al. 2008; Notz 2009). Tietsche et al. (2011) found that the sea ice extent recovered within about 2 years when they re-

moved all of the Arctic sea ice at various times during a simulation of 21st century climate with ECHAM5/MPIOM (the same model is used in the present study). In the present study, we directly assess possible threshold behavior of summer and winter sea ice in both Arctic and Antarctic with the most rigorous experimental strategy to date: we increase and decrease the atmospheric CO_2 concentration very slowly over 2000 years. Thus, the increase and decrease have been closer to quasi-equilibrium than in any other previous numerical experiments.

The remainder of the paper is organized as follows: in section 2, we give a brief introduction of the model and experimental design. Section 3 shows the changes in surface temperature in response to changes in atmospheric CO_2 concentration. In section 4, we investigate the possibility of hysteresis in Arctic sea ice; section 5 discusses the possibility of hysteresis in Antarctic sea ice; and we close the paper with conclusions in section 6.

3.2 Model and experimental design

The AOGCM applied in this study is a coarse-resolution version of ECHAM5/ MPIOM. The spectral atmospheric model ECHAM5 is run at T31 resolution ($\sim 3.75°$) with 19 levels (Roeckner et al. 2003, 2006). The Max-Planck-Institute Ocean Model (MPIOM) is used with a curvilinear grid that has a horizontal resolution of roughly 3° near the equator and a horizontal resolution of 50-200 km in the Arctic ocean, with 40 vertical levels. Details of MPIOM and the embedded sea ice model can be found in (Marsland et al. 2003) and (Jungclaus et al. 2006). The embedded sea ice model is a dynamic-thermodynamic sea ice model with viscous-plastic rheology and snow (Hibler 1979). Thermodynamic growth of sea ice is described by the zero-layer formulation of Semtner (1976). Ocean and atmosphere are coupled daily using the OASIS3 coupler (Valcke et al. 2003). The same model setup has been used to investigate the long-term adjustment of the deep-ocean heat uptake and equilibrium climate response to the atmospheric CO_2 forcing (Li et al. 2012). A higher-resolution version of the model (Jungclaus et al. 2006) has been used for the scenario simulations assessed in the IPCC Assessment Report 4 (AR4).

We perform the following experiments: the first integration is a 1600-year pre-industrial control run (CNTR) with a constant atmospheric CO_2 concentration of

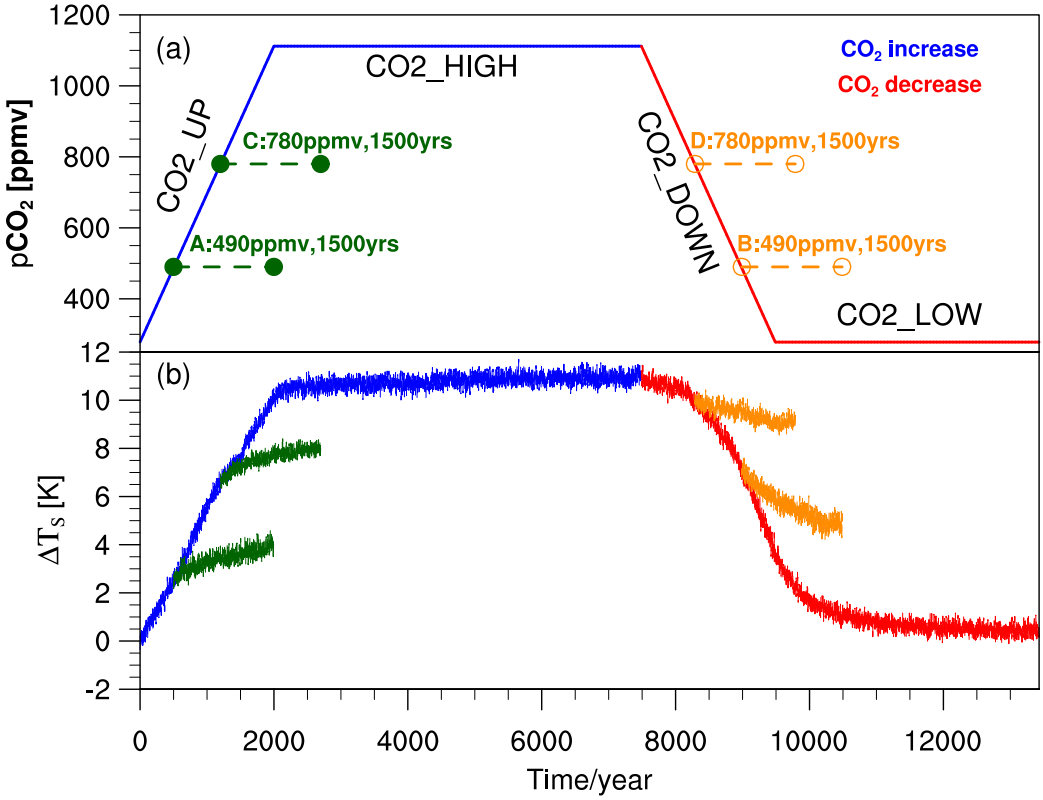

Fig. 3.1: Time series of (a) the prescribed atmospheric CO_2 concentration, and (b) global annual-mean surface temperature change. Increasing CO_2 concentration (blue) results in a warming trajectory and decreasing CO_2 concentration (red) results in a cooling trajectory. CO2_UP is the period when the CO_2 concentration is increased from 278 ppmv to 1112 ppmv over 2000 years; CO2_HIGH is the period when the CO_2 concentration is stabilized at 1112 ppmv over 5940 years; CO2_DOWN is the period when the CO_2 concentration is decreased from 1112 ppmv to 278 ppmv over 2000 years; and CO2_LOW is the period when the CO_2 concentration is stabilized at 278 ppmv over 3940 years. The dark green experiments start from the CO2_UP with CO_2 concentration fixed at 490 ppmv and 780 ppmv for 1500 years. The dark orange experiments start from CO2_DOWN with CO_2 concentration fixed at 490 ppmv and 780 ppmv for 1500 years. Temperature anomalies are with respect to the CNTR.

278 ppmv. CNTR is close to a steady-state climate at the end of the simulation. The last 100 years are used as the CNTR reference in this study. A second integration starts from the end of CNTR; the atmospheric CO_2 concentration is linearly increased from its pre-industrial level to quadrupling over 2000 years (CO2_UP in Fig. 3.1a), and is held constant thereafter for a further 5940 years until the whole system has reached equilibrium (CO2_HIGH in Fig. 3.1a). A third integration starts from the end of CO2_HIGH; the atmospheric CO_2 concentration is linearly decreased from quadrupling to its pre-industrial level over 2000 years (CO2_DOWN in Fig. 3.1a), and is held constant thereafter for further 3940 years until the whole system has reached equilibrium (CO2_LOW Fig. 3.1a). We change the atmospheric CO_2 concentration very slowly, hoping to keep the system close to a quasi-equilibrium. To examine whether the quasi-equilibrium is really maintained, four additional simulations with a constant atmospheric CO_2 concentration at 490 ppmv and 780 ppmv are carried out for 1500 years during both CO2_UP and CO2_DOWN (A, B, C, D in Fig. 3.1a). Overall, almost 20,000 years of simulations are completed in this study.

3.3 Response of the surface temperature to atmospheric CO_2 forcing

As the atmospheric CO_2 concentration increases in CO2_UP, the global-mean surface temperature continuously increases, resulting in a total warming of 9.9 K (Fig. 3.1b). The Northern Hemisphere (NH) mean surface temperature increases by 10.2 K, and the Southern Hemisphere (SH) mean surface temperature increases by 9.6 K. The mean surface temperature is almost stationary while keeping CO_2 concentration fixed at 1112 ppmv in CO2_HIGH. As the atmospheric CO_2 concentration decreases in CO2_DOWN, the global-mean and hemisphere-mean surface temperature decrease again. However, for the same amount of the atmospheric CO_2 concentration the cooling trajectory has much higher temperature than the warming trajectory (Fig. 3.2). As the atmospheric CO_2 concentration reaches its pre-industrial level in CO2_DOWN, the global-mean surface temperature is 3.3 K warmer than that in CNTR. After keeping the CO_2 concentration at the pre-industrial for several millennia (CO2_LOW), the global-mean and hemispheric-

mean temperatures eventually return to their pre-industrial state. Such convergence of the temperature for CO2_UP and CO2_DOWN also occurs at intermediate CO_2 concentration: keeping the atmospheric CO_2 concentration fixed at 490 ppmv and 780 ppmv for 1500 years, the surface temperature of the cooling trajectory and the surface temperature of the warming trajectory slowly approach each other (Fig. 3.2a,b,c). Hence, the offset between the cooling trajectory and the warming trajectory simply implies a lagged response of the climate system, despite the very slow change in CO_2 concentration that we apply. This suggests that the change of the atmospheric CO_2 concentration in our experiments is not slow enough to ensure the maintenance of a quasi-equilibrium system.

3.4 Possibility of hysteresis in Arctic sea ice

3.4.1 Arctic sea-ice area

As the atmospheric CO_2 concentration increases in CO2_UP, Arctic summer sea-ice area decreases continuously; sea ice disappears completely as the CO_2 concentration reaches 620 ppmv (Fig. 3.3a). Once the CO_2 concentration decreases again in CO2_DOWN, the summer sea ice starts to recover after the CO_2 concentration is reduced to 400 ppmv. As the CO_2 concentration again reaches its pre-industrial level, the Arctic summer sea-ice area is about $3.0\times10^6\,km^2$, which is only half of that in CNTR. For the atmospheric CO_2 concentration between 400 ppmv and 620 ppmv, we find a summer ice-covered state in the CO_2 concentration increase trajectory and a summer ice-free state in the CO_2 concentration decrease trajectory (Fig. 3.3a), suggestive of multiple equilibria of Arctic summer sea ice cover in response to the atmospheric CO_2 forcing. However, with CO_2 concentration fixed at 490 ppmv, the summer sea ice in the simulation with increasing CO_2 concentration eventually disappears to meet the summer ice-free state, which hence is the steady state for such CO_2 concentration (Fig. 3.3a and Fig. 3.4a). This result can be interpreted such that the Arctic summer sea-ice cover shows quasi-hysteretic behaviour in response to CO_2 concentration changes on policy-relevant time scales; however, there is no true hysteresis, which would imply two separate steady states at the same CO_2 concentration. The quasi-hysteretic behavior only occurs because of a lagged response of the sea-ice cover

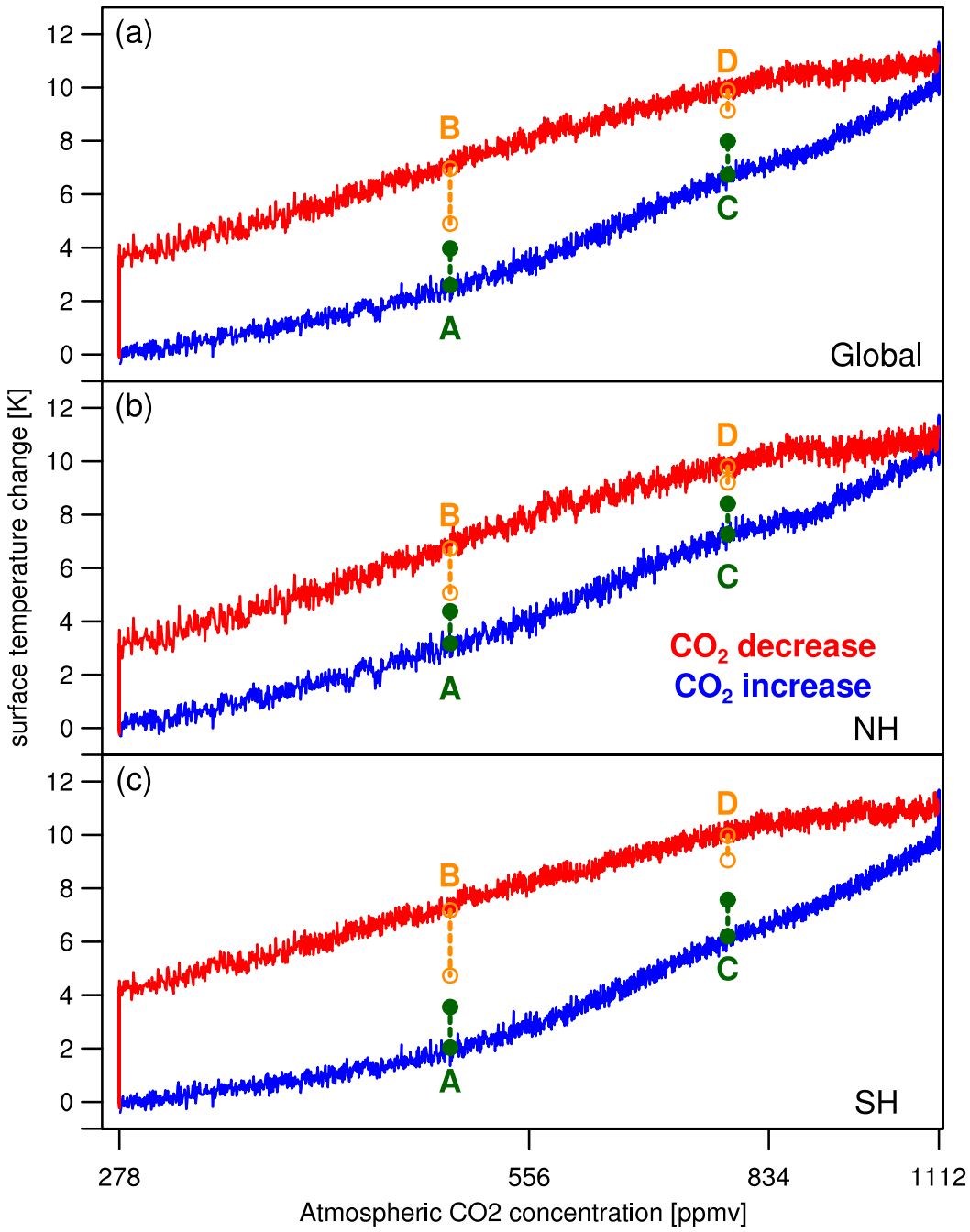

Fig. 3.2: (a) Global-averaged, (b) NH-averaged and (c) SH-averaged annual-mean surface temperature anomalies as a function of the atmospheric CO_2 concentration in the ECHAM5/MPIOM simulations. The use of blue, red, dark green and dark orange is as described in Fig. 3.1. Temperature anomalies are with respect to the CNTR, and CO_2 concentration is plotted on a logarithmic scale.

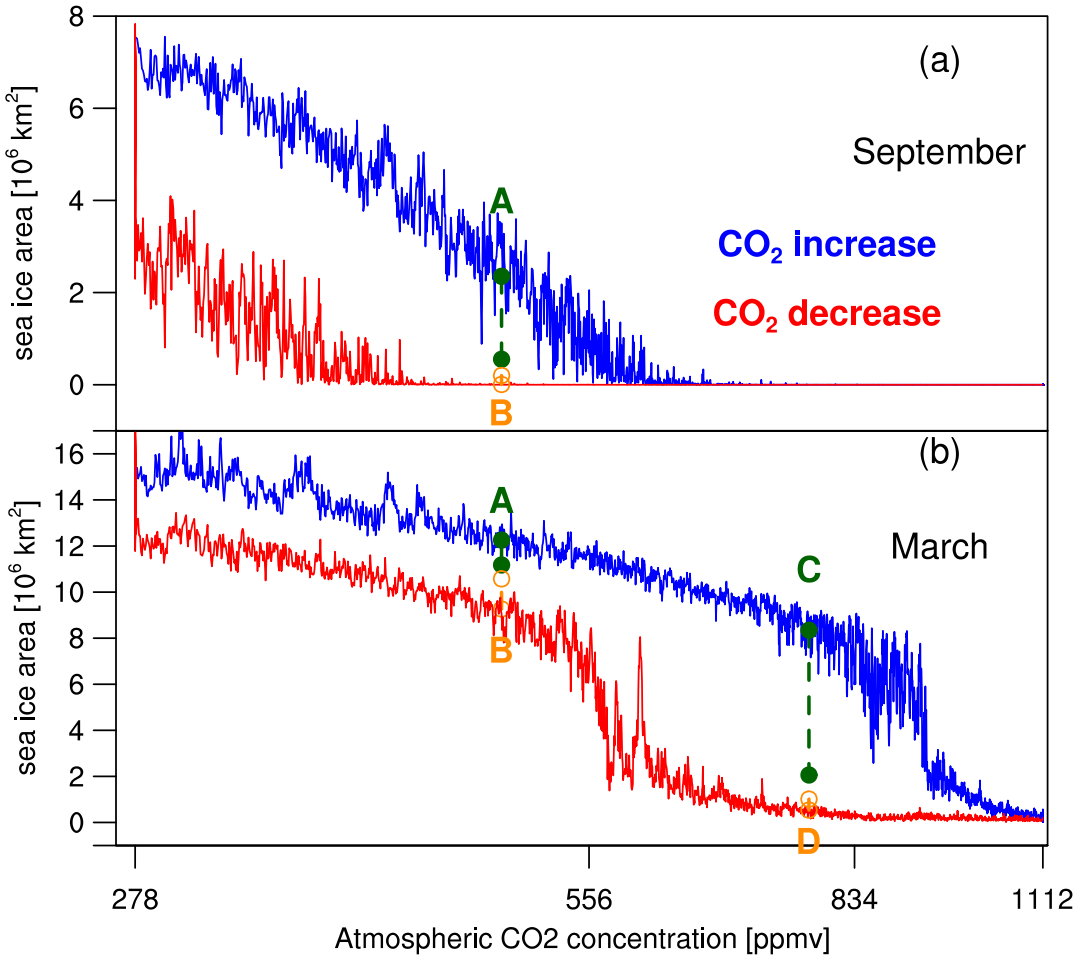

Fig. 3.3: Arctic sea-ice area as a function of the atmospheric CO_2 concentration. (a) Arctic sea-ice area in September and (b) Arctic sea-ice area in March. The use of blue, red, dark green and dark orange is as described in Fig. 3.2. CO_2 concentration is plotted on a logarithmic scale.

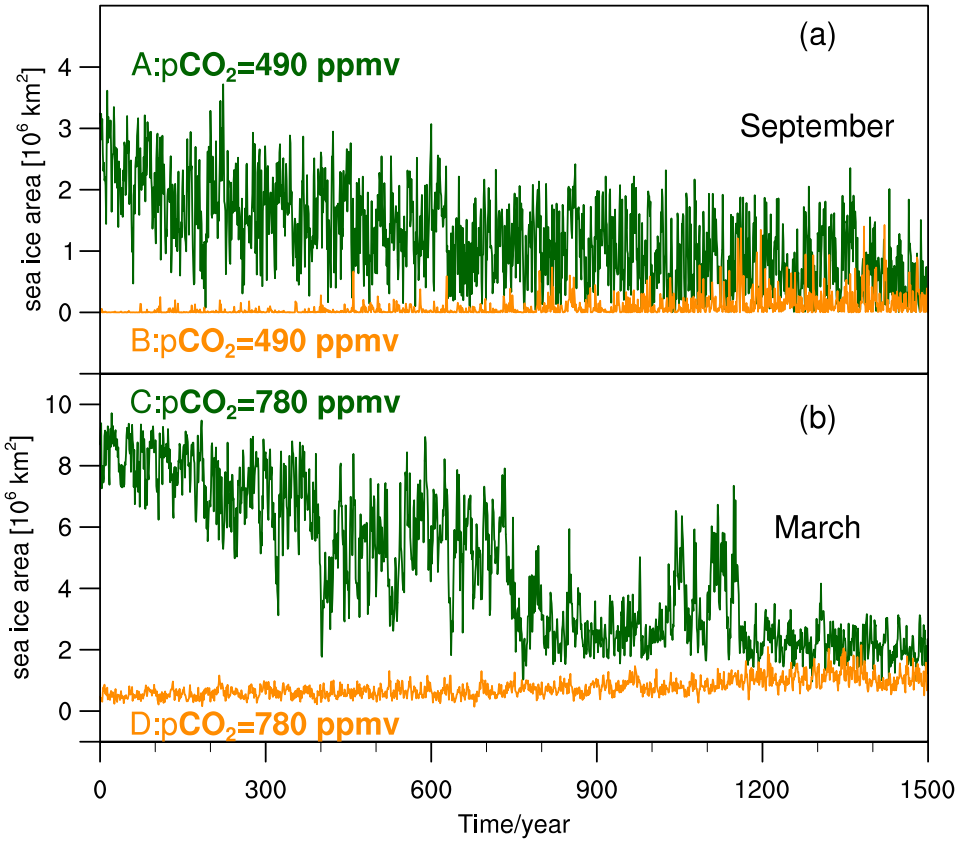

Fig. 3.4: Time series of Arctic sea-ice area (a) in September with keeping the atmospheric CO_2 concentration fixed at 490 ppmv, and (b) in March with keeping the atmospheric CO_2 concentration fixed at 780 ppmv (Bottom panel). The dark green respects experiments started from CO2_UP. The dark orange respects experiments started from CO2_DOWN.

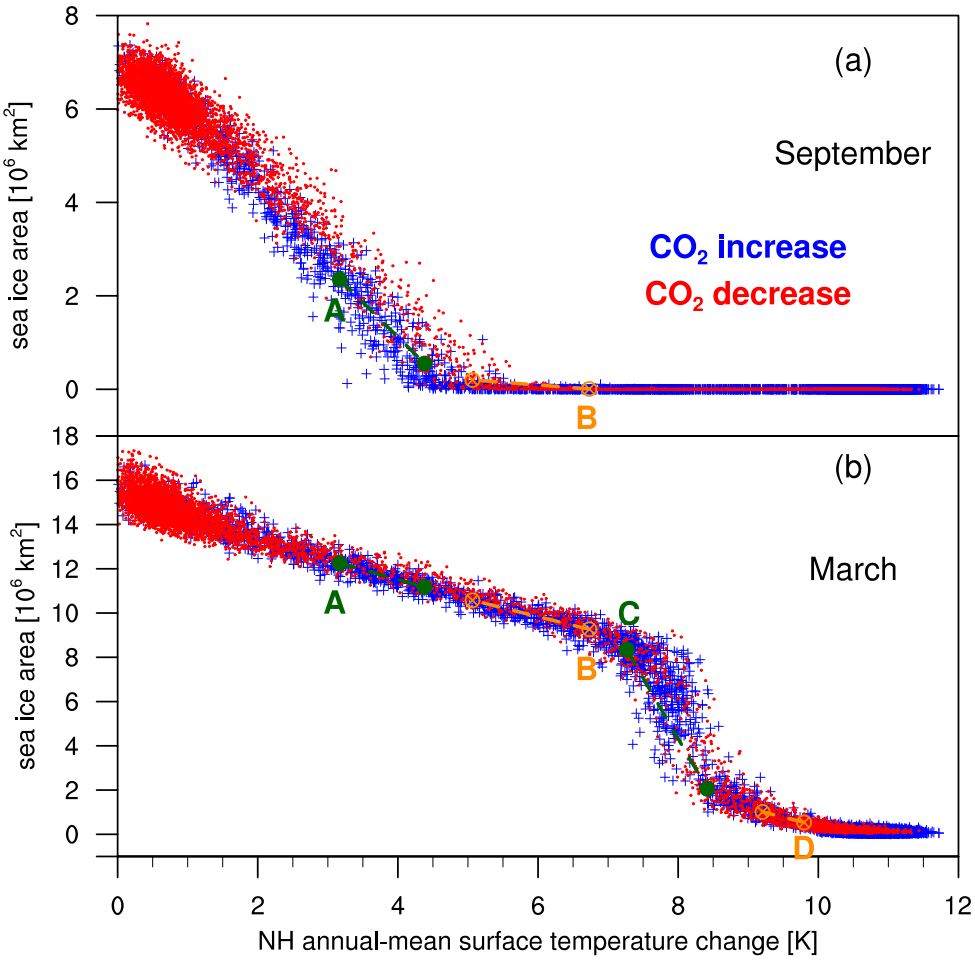

Fig. 3.5: Arctic sea-ice area as a function of NH-averaged annual-mean surface temperature change. (a) Arctic sea-ice area in September and (b) Arctic sea-ice area in March. The use of blue, red, dark green and dark orange is as described in Fig. 3.2. All surface temperature changes are given relative to the simulated CNTR NH annual-mean surface temperature of 287.2 K (14.1 °C).

to the change in CO_2 concentration, caused by some slow adjustment processes in the system.

This non-hysteretic behavior is also underlined by the changes in Arctic sea-ice cover as a function of NH annual-mean surface temperature change. Here, Arctic summer sea-ice area recovers for decreasing CO_2 concentration along a trajectory that is indistinguishable from that with increasing CO_2 concentration. From this we can conclude that Arctic sea ice reacts rapidly to changes in surface temperature, which in turn only slowly adjusts to the transient CO_2 forcing. Before we discuss the dominating impact of the surface temperature on Arctic sea ice in more detail, we will now turn to the response of Arctic winter sea ice.

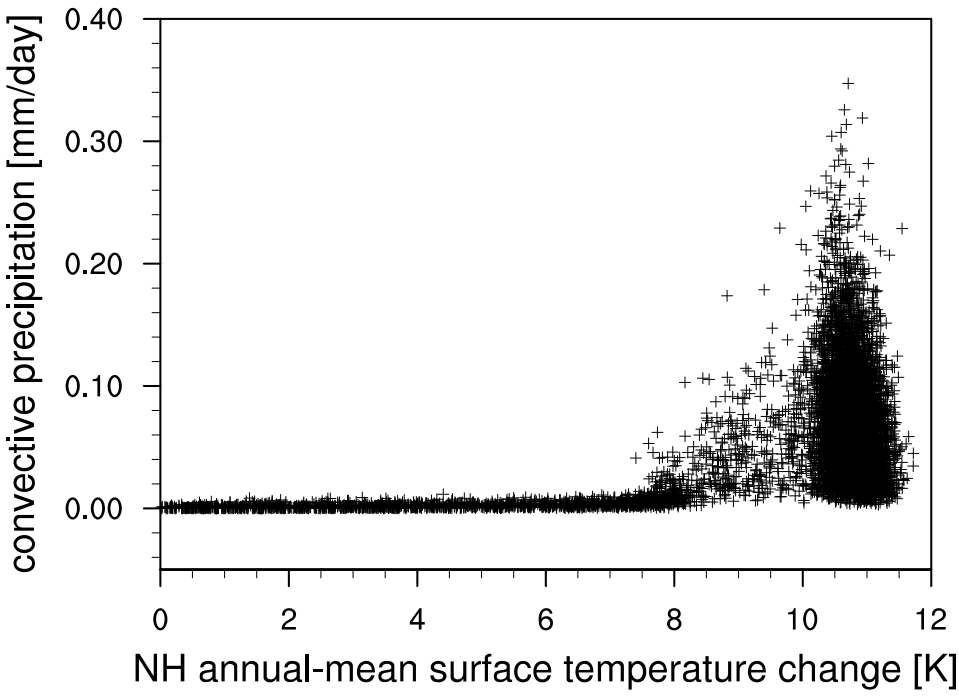

Fig. 3.6: Convective precipitation in March averaged over Arctic Ocean basin as a function of NH annual-mean surface temperature change. Temperature change is with respect to the CNTR. All surface temperature changes are given relative to the simulated CNTR NH annual-mean surface temperature of 287.2 K (14.1 °C).

Here, in contrast to the smooth summer sea-ice decline, we find a rapid transition from a winter ice-covered state to an ice-free state when the NH-averaged annual-mean surface temperature increases by about 8 K (Fig. 3.5b) to reach 295.2 K (22.1 °C), while the annual-mean surface temperature north of 60° N

reaches about 275.3 K (2.2 °C). Analyzing the sudden decrease further, we find a sudden increase in the convective precipitation over the Arctic Ocean domain in March when the rapid reduction of Arctic winter sea-ice area happens (Fig. 3.6). This suggests that atmospheric convection is suddenly triggered by the increased heat and moisture fluxes from the ocean surface once the NH-averaged annual-mean surface temperature increases by about 8 K. Abbot and Tziperman (2008) suggested that this atmospheric convection produces optically thick convective clouds and increases high-latitude moisture levels, both of which trap outgoing longwave radiation and therefore result in further warming and sea-ice loss. This convective cloud feedback, as estimated here from convective precipitation, can play an essential role in the elimination of the Arctic winter sea ice cover (Abbot et al. 2009) and is likely to be the main cause of the rapid transition that we find here. A similar behavior of a rapid decrease in Arctic winter sea-ice conver was also found in CMIP5 RCP8.5 (Representative Concentration Pathways 8.5) senario simulations with the Max Planck Institute Meteorology's Earth System Model (MPI-ESM) (Notz et al. 2012, submitted manuscript).

As the atmospheric CO_2 concentration is reduced in CO2_DOWN to about 650 ppmv, the winter sea-ice area rapidly recovers to about 8×10^6 km^2, which is approximately equal to the area of the Arctic Ocean basin. With the atmospheric CO_2 concentration in the range of 650 ppmv to 950 ppmv, we find a winter ice-covered state in CO2_UP and a winter ice-free state in CO2_DOWN (Fig. 3.3b). To verify whether the Arctic winter sea ice cover exhibits multiple equilibria, we examine two additional 1500-year long simulations in which CO_2 concentration is kept fixed at 780 ppmv during both CO2_UP and CO2_DOWN (points C and D in Fig. 3.3b). We then find that in CO2_UP the winter ice-covered state evolves toward the winter ice-free state after 1200 years (Fig. 3.3b and Fig 3.4b). The winter ice-free state in CO2_DOWN is almost stationary over 1500 years. This suggests that the winter ice-free state is the steady state for this CO_2 concentration; the winter ice-covered state is only transient. Hence, as for Arctic summer sea ice, the apparent hysteresis behavior shown in Fig. 3.3c is not a real hysteresis, but simply a result of the lagged response of the system. This is also apparent from the response of the Arctic winter sea ice as a function of NH-mean surface temperature: Arctic winter sea-ice recovers with decreasing CO_2 concentration along a trajectory that is indistinguishable from that with increasing CO_2

concentration (Fig. 3.5b). Both in the warming and the cooling trajectories, the rapid transition of the winter sea-ice cover occurs when the NH-mean surface temperature is about 8 K higher than in the pre-industrial climate.

As we will see later, in the Antarctic there is a clear difference in the sea-ice area as a function of surface temperature change between the cooling and the warming trajectories, indicating a less pronounced impact of surface temperature on the sea-ice state there. To examine why surface temperature is so dominant in defining the sea-ice state in the Arctic, we must examine the oceanic near-surface conditions. In the Arctic Ocean, the strong halocline is responsible for maintaining water column stability, thus isolating the surface water and hence the sea ice from the deep water in the Arctic. While we increase the atmospheric CO_2 forcing, a warming and freshening of the surface water strengthens the Arctic halocline and inhibits the penetration of heat into the deep ocean (Aagaard et al. 1981; Akitomo 1999). As we decrease the CO_2 concentration in CO2_DOWN, we find no evidence that the Arctic halocline is destroyed by strong deep convection. The upper and the intermediate water masses remain decoupled, owing to the protection given by the strong halocline. In addition, the thermodynamic forcing is more relevant for the change in Arctic sea-ice cover, because the sea ice movement there is constrained by the surrounding land masses (e.g., Eisenman 2010; Notz and Marotzke 2012). Consequently, surface temperature change is the controlling factor (directly or indirectly) for the Arctic sea-ice area. The Arctic sea-ice area shows a lagged response to the atmospheric CO_2 concentration, because the surface temperature change lags the atmospheric CO_2 concentration due to the ocean thermal inertia.

The fact that both Arctic summer and winter sea-ice covers show no true hysteresis behavior suggests that the evolution of the Arctic ice cover is in principle reversible. However, the Arctic remains ice-free for a very long time as we decrease the atmospheric CO_2 concentration. The Arctic summer and winter ice-free states in the CO2_DOWN are steady state; in contrast, the Arctic summer and winter ice-covered states in CO2_UP are only transient. As we will discuss next, some slow adjustment processes eliminate the Arctic sea ice cover already at relatively low atmospheric CO_2 concentration. Hence the Arctic sea ice state as simulated by, for example, the transient simulations of CMIP3 only presents an upper bound for the amount of Arctic sea ice that can exist at any given CO_2

concentration.

3.4.2 Mechanism of the lagged response in the Arctic sea-ice decline

In our experiments, we quadruple the atmospheric CO_2 concentration over 2000 years, but the reduction of Arctic summer and winter sea-ice area still shows a lagged response. Which slow climatic adjustment eliminates the Arctic sea-ice cover as we keep the CO_2 concentration fixed at 490 ppmv and 780 ppmv? To answer this question, we examine the changes in the annual cycles of sea-ice volume, heat flux, upper-100 m ocean heat content, and vertically integrated water vapor content over the Arctic Ocean domain of experiment A (pCO_2=490 ppmv) and experiment C (pCO_2=780 ppmv). For changes in the heat flux, we consider five terms: the net shortwave radiative flux difference (i.e., the last 100-year mean minus the first 100-year mean) at the top of the atmosphere (ΔF_{SW}), the cloud-longwave radiative forcing difference (ΔF_{CRF}), which is the difference between full-sky net longwave radiative flux and the clear-sky net longwave radiative flux at the top of the atmosphere, the atmospheric heat transport difference (ΔF_A), the net surface heat flux difference (ΔF_{SF}), and the oceanic heat transport difference (ΔF_O).

In experiment A, where we keep the atmospheric CO_2 concentration at 490 ppmv for 1500 years, the sea ice volume decreases in all seasons; the summer sea-ice cover eventually disappears (Fig. 3.7a). The energy budget analysis shows that during summer the short-wave radiation over the Arctic increases due to a positive ice–albedo feedback. The atmospheric heat transport increases simultaneously (Fig. 3.7c). This increased heat flux and heat transport enhances the surface warming, thus promoting the Arctic summer sea-ice loss, which allows the Arctic ocean to absorb more solar radiation (Fig. 3.7c), increasing the heat storage of the Arctic Ocean (Fig. 3.8a). In the following autumn and winter, the Arctic Ocean releases more heat to the atmosphere (Fig. 3.7c), which delays the sea-ice formation and reduces the sea-ice area and thickness. Meanwhile, the warming of the Arctic Ocean enhances the evaporation and increases the water vapour content over the Arctic Ocean region (Fig. 3.8a). This, in turn, traps more outgoing long-wave radiative flux and therefore prevents the sea-ice formation in winter,

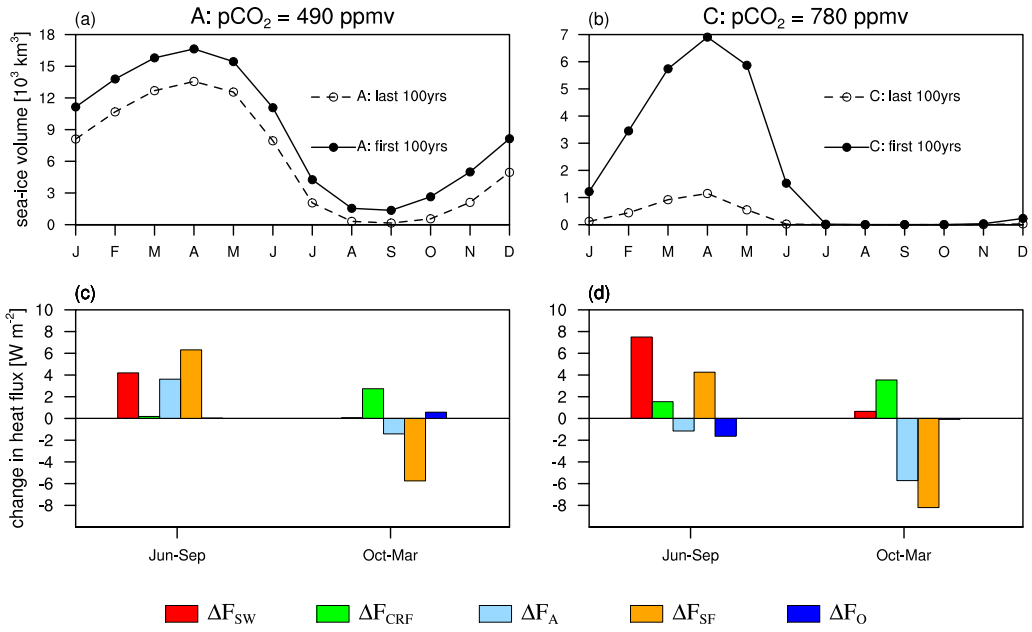

Fig. 3.7: Mean annual cycle of Arctic sea ice volume (a,b) and mean energy budget anomalies for the Arctic Ocean domain (c,d), (a) and (c) are from experiment A (pCO_2=490 ppmv), (b) and (d) are from experiment C (pCO_2=780 ppmv). The solid line in (a) and (c) represents the first 100-year mean, and the dashed line reprents the last 100-year mean of each experiment. ΔF_{SW} (red) is accumulated short wave radiative flux difference at the top-of-atmosphere. ΔF_{CRF} (green) is accumulated cloud-longwave radiative heat flux difference at the top-of-atmosphere. ΔF_A (light blue) is the accumulated atmospheric heat transport difference. ΔF_{SF} (orange) is accumulated net surface heat flux difference. ΔF_O (blue) is the accumulated oceanic heat transport difference. The difference represents the last 100-year mean minus the first 100-year mean of each experiment. Positive sign in (c) and (d) means downward heat flux.

which further promotes the summer sea ice loss in the following year.

In experiment C, where we keep the atmospheric CO_2 concentration at 780 ppmv for 1500 years, the Arctic sea ice volume decreases from a maximum of $7\times10^3\,km^3$ in April to less than $1\times10^3\,km^3$ in all seasons (Fig. 3.7b). Here, the ice–albedo feedback is not active in late summer because the Arctic is ice free from July to November in this experiment. However, the shortwave radiative flux increases by nearly $10\,W\,m^{-2}$ due to the ice–albedo feedback in late spring and early summer when the Arctic is still ice covered (Fig. 3.7d). This increased shortwave radiative flux allows the Arctic ocean to gain more heat in spring and summer (Fig. 3.7d), increasing the heat storage of the Arctic ocean (Fig. 3.8b). On the one hand, a warmer Arctic Ocean releases more sensible and latent heat to the atmosphere in the winter, causing a higher surface temperature and preventing sea ice formation; on the other hand, a warmer Arctic Ocean also increases water vapour over the Arctic region (Fig. 3.8b), trapping more outgoing long-wave radiative flux and further reducing the Arctic winter sea ice. We find no significant changes of oceanic heat transport in either experiment A or C, which suggests that the oceanic heat transport plays a minor role in reducing the sea ice with constant CO_2 forcing. A decreased atmospheric heat transport into the Arctic region is caused by the warming of the atmosphere over the Arctic due the the local ocean heating (Fig. 3.7d).

Hence, the slow reduction of the Arctic summer and winter sea ice cover is mainly caused by the ice–albedo feedback, the slowness of the Arctic Ocean warming, and the corresponding local air-sea interactions. The atmospheric and oceanic heat transports play a minor role in reducing the sea ice with constant CO_2 concentration. Although the ice–albedo feedback is only active during the sunlit periods, the impact of the corresponding shortwave radiative flux change can be extended into the winter sea-ice cover, since the Arctic Ocean stores heat during sunlit periods and releases heat during autumn and winter. The ability of the Arctic Ocean to store the excess heat over the course of winter is the key determinant for the evolution and stability of the Arctic sea-ice cover (Serreze and Francis 2006; Tietsche et al. 2011). However, the Arctic Ocean warming is a slow process, because it is very difficult for the Arctic Ocean to carry the absorbed extra heat in summer through winter so as to perpetuate the feedbacks because of the increased heat loss from an ocean in the following autumn and winter with

a decreased sea-ice cover (Tietsche et al. 2011). Hence, the reduction of Arctic summer and winter sea-ice cover can be strongly delayed by the slowness of the Arctic Ocean warming.

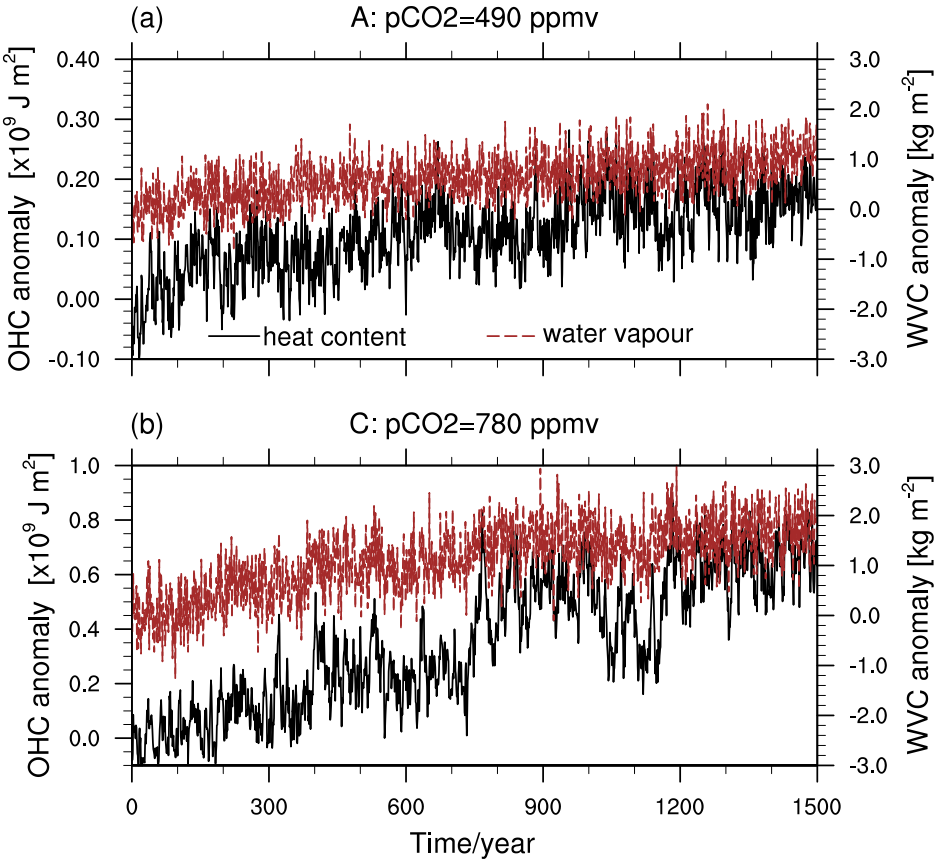

Fig. 3.8: Time series of annual-mean ocean heat content difference of the upper 100m of Arctic Ocean (black solid line), and annual-mean vertically integrated water vapour content difference over Arctic Ocean (brown dash line). (a) is from experiment A (pCO_2=490 ppmv), (b) is from experiment C (pCO_2=780 ppmv). The difference is with respect to the first 100 years mean of the corresponding experiments.

3.5 Possibility of hysteresis in Antarctic sea ice

The Antarctic sea-ice cover behaves very differently from the Arctic sea-ice cover in response to the atmospheric CO_2 forcing. Both the Antarctic summer and winter sea-ice area decreases continuously during the warming in CO2_UP (Fig. 3.9a,b); we do not find any rapid transition. The Antarctic needs longer time and also needs higher atmospheric CO_2 concentration to become ice-free, compared to the Arctic. The Antarctic reaches the summer ice-free state after almost 1200 model years when the atmospheric CO_2 concentration is increased to 770 ppmv in CO2_UP; it reaches the winter ice-free state after almost 2000 years when the atmospheric CO_2 concentration is increased to 1112 ppmv in CO2_UP. The Antarctic remains ice-free even if the atmospheric CO_2 concentration is reduced to the pre-industrial level at the end of CO2_DOWN. While keeping the atmospheric CO_2 concentration at 278 ppmv for several millennia in CO2_LOW, the Antarctic sea ice cover recovers slowly to the pre-industrial level. In contrast to the Arctic sea-ice area, the Antarctic sea-ice area with decreasing CO_2 concentration does not recover along the trajectory of increasing CO_2 concentration as a function of SH annual-mean surface temperature change (Fig. 3.10a,b), which suggests the possibility of multiple equilibria of Antarctic sea-ice cover in response to the atmospheric CO_2 forcing.

However, examining the equilibrium response of Antarctic sea ice with experiments A and C, the Antarctic summer sea-ice cover almost disappears to meet the summer ice-free state, which hence is the steady state for this CO_2 concentration (Fig. 3.9a and Fig. 3.11c). The Antarctic winter sea-ice area from experiments A and B also tend to meet (Fig. 3.9b and Fig. 3.11a,b). This suggests that the Antarctic sea-ice covered state in the CO_2 increase trajectory is still transient. Similar to the Arctic sea-ice area, the reduction of the Antarctic sea ice is delayed in its response to the increase of the atmospheric CO_2 concentration. In experiment C, the Antarctic winter sea-ice area is decreasing; winter sea-ice area in experiment D shows very strong century-timescale variability starting after 700 years of integration (Fig. 3.11b). Hence, similar to the Arctic sea ice, the Antarctic winter and summer sea-ice cover shows no true hysteresis behavior in response to changing atmospheric CO_2 concentration.

The lagged response in the Antarctic sea-ice cover relative to SH surface tem-

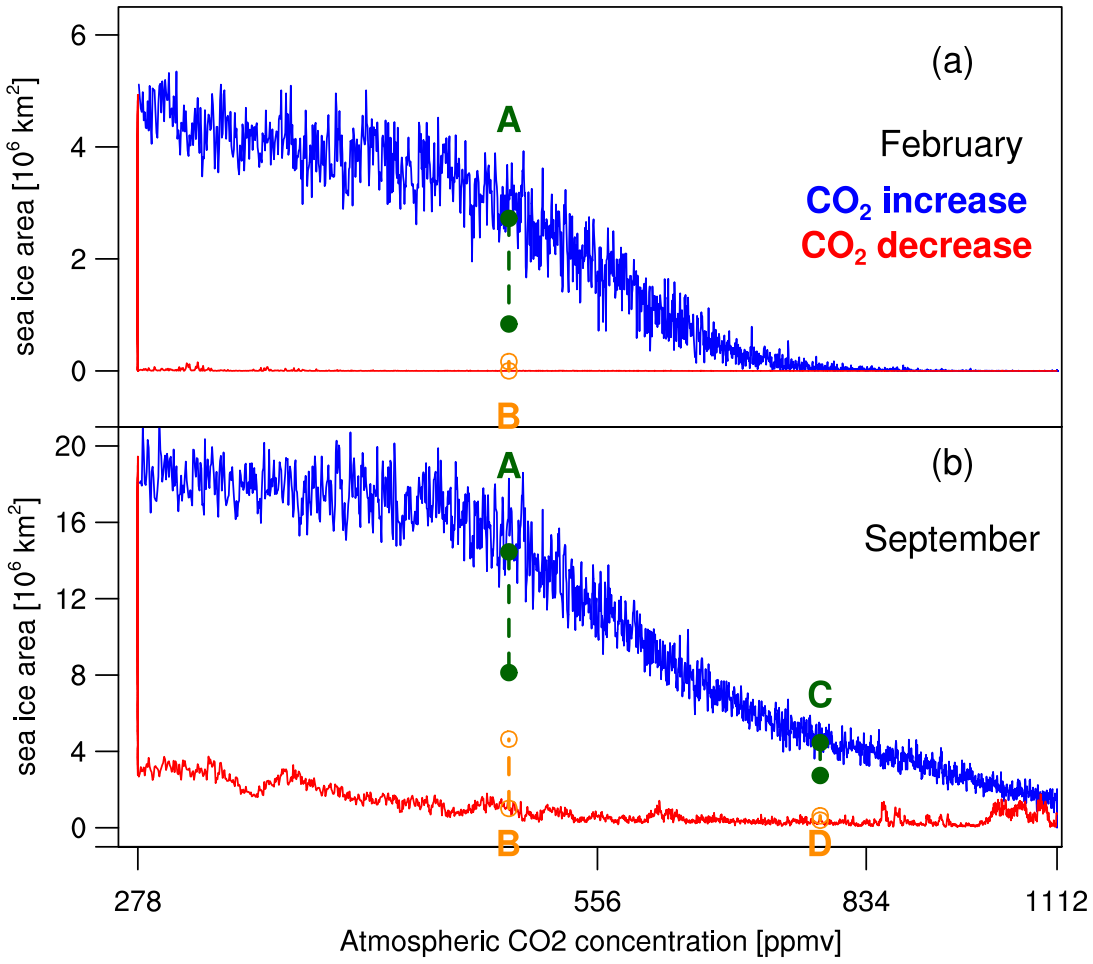

Fig. 3.9: Antarctic sea-ice area as a function of the atmospheric CO_2 concentration. (a) Antarctic sea-ice area in September and (b) Antarctic sea-ice area in February. The use of blue, red, dark green and dark orange is as described in Fig. 3.2. CO_2 concentration is plotted on a logarithmic scale.

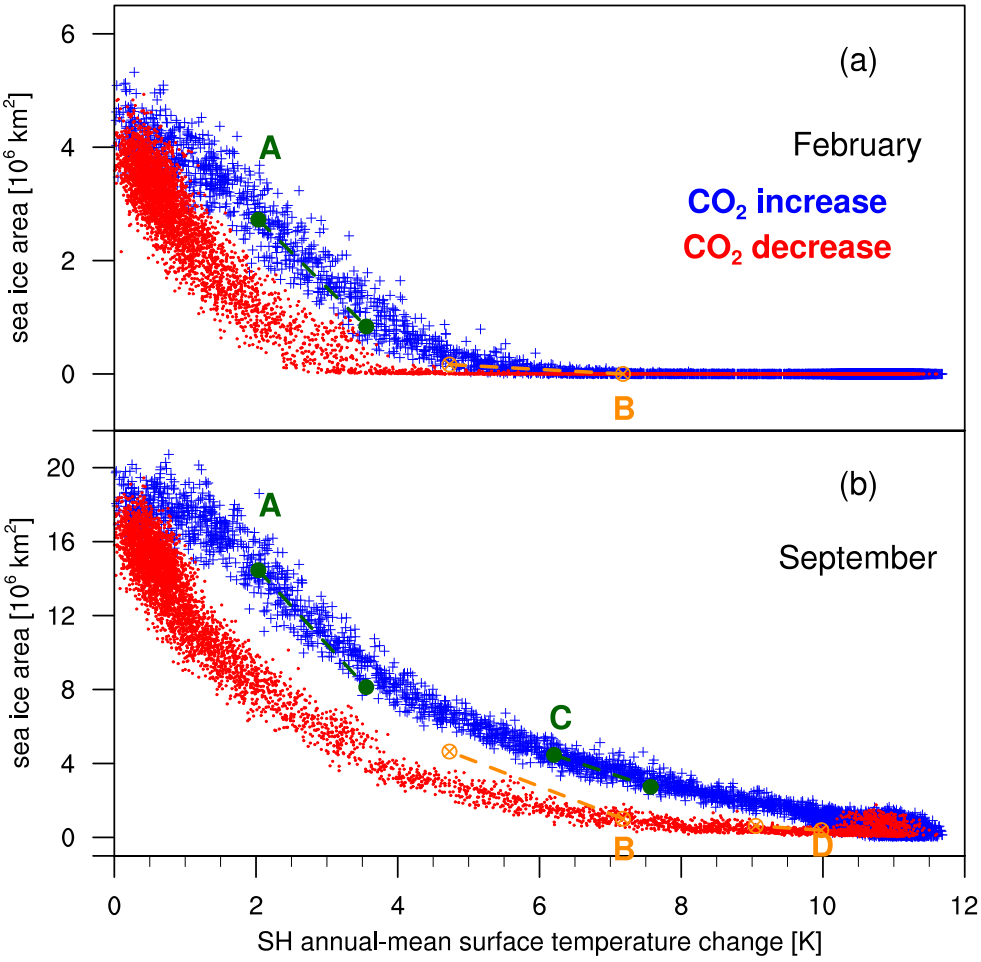

Fig. 3.10: Antarctic sea-ice area as a function of SH-averaged annual-mean surface temperature change. (a) Antarctic sea-ice area in September and (b) Antarctic sea-ice area in February. The use of blue, red, dark green and dark orange is as described in Fig. 3.2. All surface temperature changes are given relative to the simulated CNTR SH annual-mean surface temperature of 286.2 K (13.0 °C).

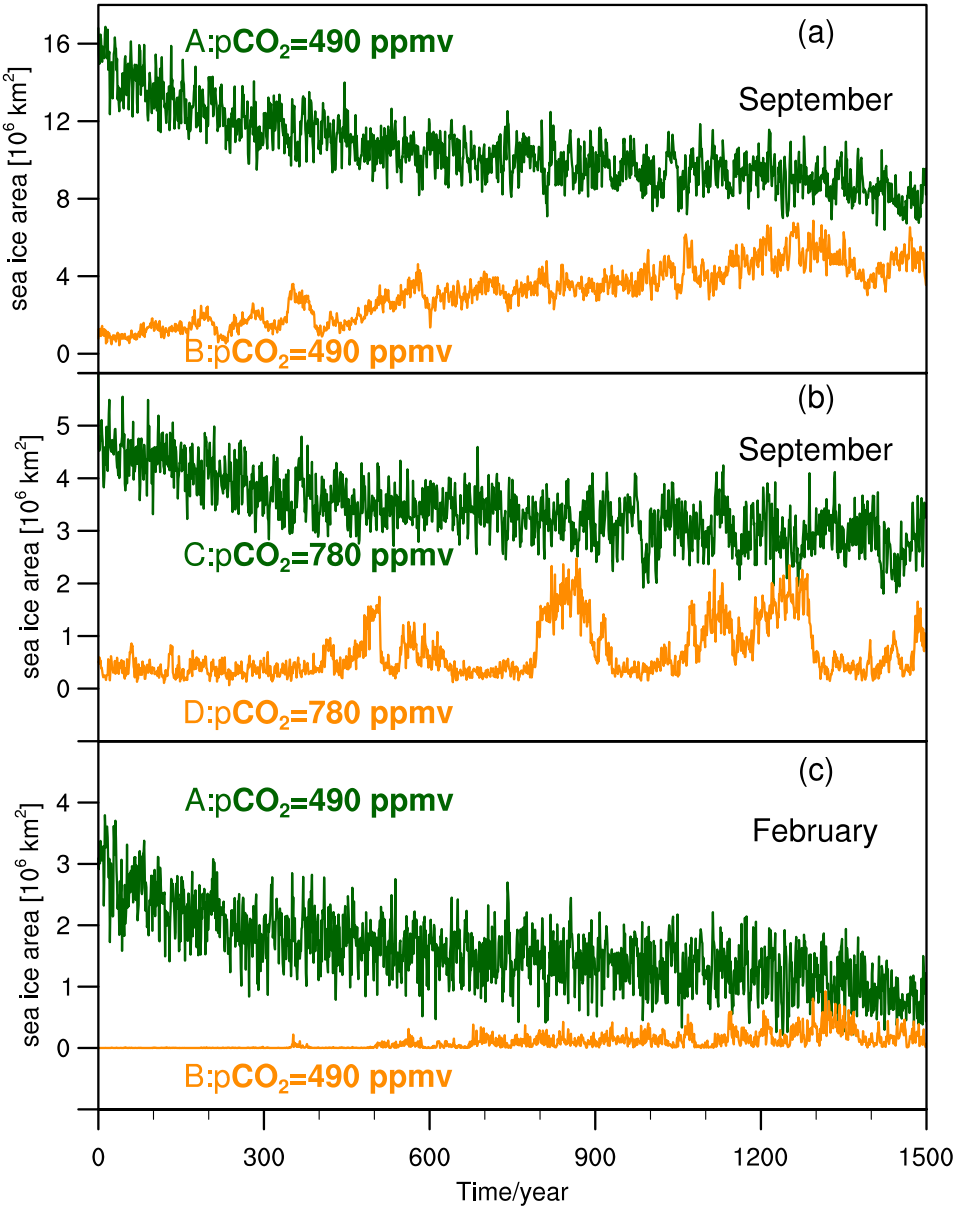

Fig. 3.11: Time series of Antarctic sea-ice area (a) in September with keeping the atmospheric CO_2 concentration fixed at 490 ppmv, (b) in September and (c) in March with keeping the atmospheric CO_2 concentration fixed at 780 ppmv. The dark green respects experiments starting from CO2_UP. The dark orange respects experiments starting from CO2_DOWN.

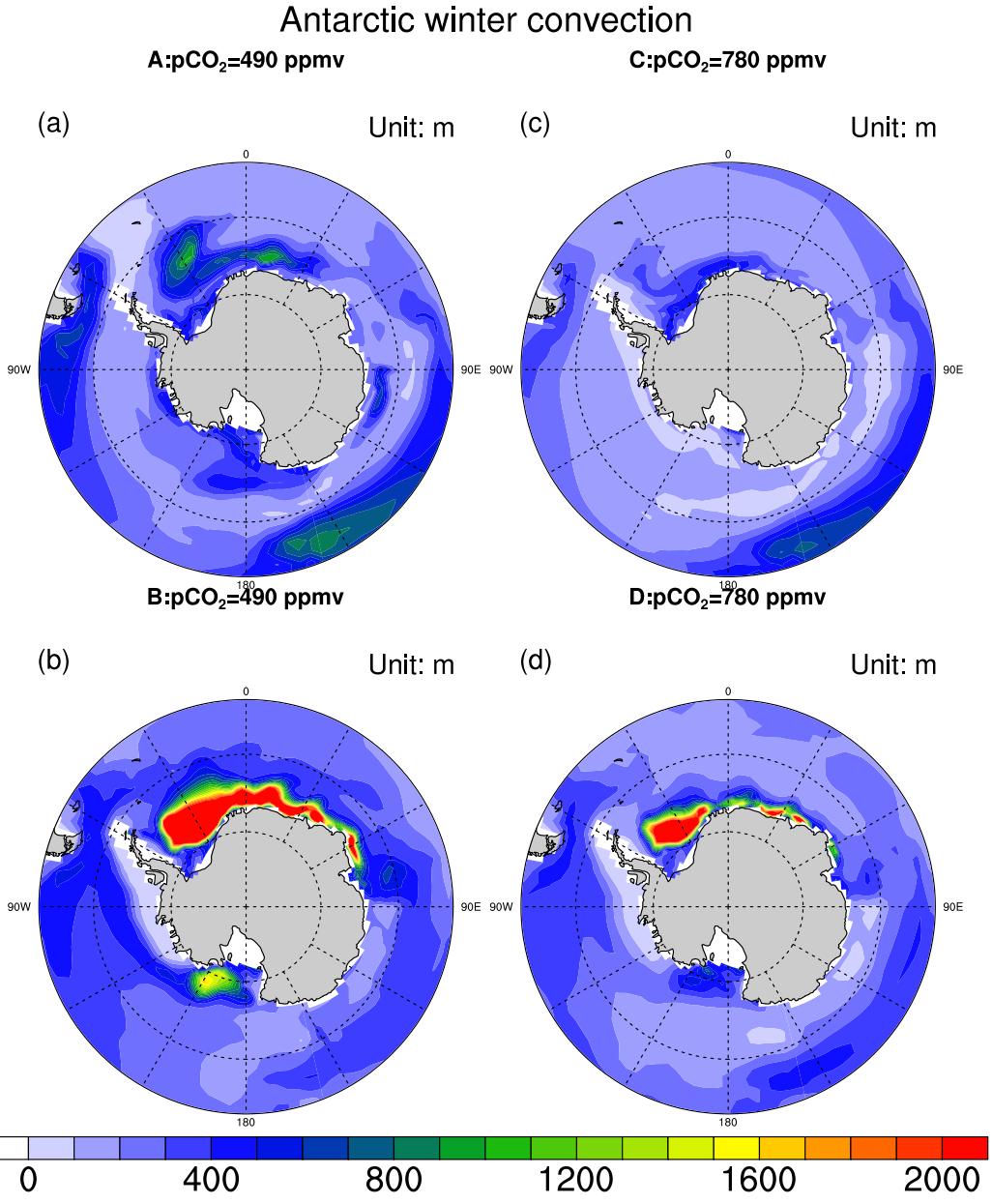

Fig. 3.12: First 100-year mean Antarctic Ocean mixed layer thickness in September from experiment (a) A: pCO_2=490 ppmv, (b) B: pCO_2=490 ppmv, (c) C: pCO_2=780 ppmv and (d) D: pCO_2=780 ppmv.

perature change is related to the oceanic stratification. Different from the Arctic Ocean, the Antarctic Ocean does not have such a strong halocline. Therefore open-ocean deep convection around Antarctic can easily be triggered by a small change of surface density (Akitomo 1999; McPhee 2003). During the CO_2 concentration increase in CO2_UP, the ocean surface is heated, which makes the water column more stable. Hence, oceanic convection and other vertical mixing processes become less frequent and less intense (Fig. 3.12a,c). The intermediate water of the Antarctic Ocean takes up heat throughout the whole period of the atmospheric CO_2 concentration increase and stabilization. However, in the CO_2 concentration decrease period in CO2_DOWN, the ocean surface is cooled, which destabilizes the water column, and frequent ocean deep convection in the Antarctic Ocean is triggered (Fig. 3.12b,d). Heat from intermediate water masses becomes entrained into the upper ocean, resulting in a higher ocean surface temperature in winter time, thus preventing sea ice formation. Hence it is the strong ocean deep convection that maintains an ice-free Antarctic Ocean throughout the CO_2 concentration decrease period. And in contrast to the Arctic, Antarctic sea ice dynamics, which are driven by surface wind patterns and currents, play an important role for the overall sea-ice area (e.g., Comiso and Nishio 2008; Stammerjohn et al. 2008; Notz and Marotzke 2012). Therefore, in contrast to the Arctic sea ice, the surface temperature change is not the only controlling factor for the Antarctic sea-ice change in a warm climate; ocean deep convection and sea ice dynamics can also play an important role. This is the reason why the Antarctic sea ice cover shows much more strongly lagged response to the atmospheric CO_2 concentration compared to the Arctic sea-ice cover. In contrast to the Arctic sea ice cover, the response of the Antarctic sea ice cover also significantly lags behind surface-temperature evolution.

3.6 Summary and Conclusions

Using the state-of-the-art AOGCM ECHAM5/MPIOM, we perform several idealized simulations to investigate the hysteresis behavior of Arctic and Antarctic sea ice in response to changing atmospheric CO_2 concentration. In contrast to previous studies with a much faster "ramp-up and ramp-down" of the atmospheric CO_2 concentration (Armour et al. 2011; Ridley et al. 2012), we very slowly change

the atmospheric CO_2 concentration over 2000 years. We investigate the impact of both the fast upper-ocean adjustment and the slow deep-ocean adjustment on the sea ice. The main findings are:

(1) We find a rapid transition during the loss of the Arctic winter sea-ice cover in a warm climate, once the NH-averaged annual-mean surface temperature has increased by about 8 K. This rapid transition is triggered by a sudden onset of strong atmospheric convection, according to the mechanism suggested by Abbot and Tziperman (2008). Consistent with previous studies with AOGCMs (Winton 2006, 2008; Tietsche et al. 2011; Armour et al. 2011; Ridley et al. 2012), we find no evidence of tipping points or rapid transitions during the loss of the Arctic summer sea ice. In contrast to the Arctic winter sea-ice loss, the summer sea-ice cover retreats linearly with increasing atmospheric CO_2 concentration.

(2) We find no evidence of multiple equilibria and true hysteresis behavior of Arctic summer or winter sea-ice cover in response to changing atmospheric CO_2 concentration. However, both the Arctic summer and winter sea-ice covers show a lagged response to changing atmospheric CO_2 concentration. There is no lagged response to the NH surface temperature change. This suggests that the lagged response of the Arctic sea-ice cover to changing CO_2 concentration is caused by the thermal inertia of the Arctic Ocean. Fixing the atmospheric CO_2 concentration at 490ppmv and 780ppmv for 1500 years, we find a slow ocean warming. This directly decreases the formation of Arctic winter sea ice and additionally causes an increase in atmospheric water vapour content, which traps more outgoing long-wave radiative flux and thus further decreases the Arctic winter sea ice. The decreased winter sea-ice formation in turn promotes further summer sea-ice loss in the following year. The corresponding positive ice–albedo feedback leads to further warming of the Arctic Ocean. Hence, it is the slowness of Arctic Ocean warming that delays the reduction of Arctic summer and winter sea-ice cover.

(3) The Antarctic sea-ice cover retreats continuously without rapid transition during the warming trajectory. Similar to the Arctic sea-ice cover, the

Antarctic sea-ice cover shows no evidence of true hysteresis behavior or multiple equilibria in response to the atmospheric CO_2 concentration. However, the Antarctic summer and winter sea-ice covers show a more strongly lagged response to the atmospheric CO_2 concentration compared to the Arctic sea-ice cover. In contrast to the Arctic sea-ice cover, the response of Antarctic winter and summer sea-ice covers lag significantly behind the surface temperature change beyond 1000 years.

(4) In the Antarctic, the response of the sea ice is greatly delayed because there is no strong halocline. Ocean deep convection can easily be triggered as we decrease the atmospheric CO_2 concentration. This causes the Antarctic ocean to remain ice-free for a very long time, and causes changes in Antarctic sea ice to lag behind the surface temperature change.

(5) Although we change the CO_2 concentration very slowly, the equilibrium area of sea ice in both hemispheres is always below the sea-ice area during the simulation with increased CO_2 concentration. Hence, the sea-ice state as simulated by any transient simulation with increasing CO_2 concentration only presents an upper bound for the amount of sea ice that can exist at any given CO_2 concentration. In particular, we find that for a CO_2 concentration of 490 ppmv the equilibrium state of the Arctic sea ice is ice free in summer; for a CO_2 concentration of 780 ppmv, the equilibrium state is ice-free all year round.

Chapter 4

AMOC in a future warm climate

— Processes governing the stability of Atlantic meridional overturning circulation in a future warm climate

We examine the hysteresis behavior of the Atlantic meridional overturning circulation (AMOC) in response to atmospheric CO_2 change by using the state-of-the-art AOGCM ECHAM5/MPIOM. The atmospheric CO_2 is increased extremely slowly from pre-industrial level to quadrupling over 2000 years, and is held constant thereafter for further 5940 years until the whole system has reached equilibrium; then the atmospheric CO_2 is decreased extremely slowly from the quadrupling to the pre-industrial level over 2000 years, and is held constant thereafter for further 3940 years until the whole system has again reached equilibrium. We find no evidence of hysteresis behavior of the AMOC in response to the CO_2 forcing and the anomalous atmospheric freshwater forcing over the North Atlantic deep water formation regions. The AMOC "recovery" trajectory is above the "weakening" trajectory, indicating that the apparent offset is a consequence of the speed of the transient change in CO_2 concentration that is not small enough to ensure an quasi-equilibrium in our experiment. The overshooting recovery of the AMOC is caused by a stronger evaporation over the tropical Atlantic, which leads to anomalously high salinity in the North Atlantic while the CO_2 decreases, resulting in a stronger deep convection and a stronger AMOC. In contrast to the previous studies with water-hosing experiments, a positive overturning freshwater transport (M_{ov}) at the southern border does not damp the freshwater forcing in

the North Atlantic and does not promote the recovery of the AMOC throughout our simulations. In a future warm climate, the long-term stability of the AMOC is not only governed by the anomalous freshwater forcing in the deep-water formation regions, but also by a stronger evaporation in the tropical Atlantic owing to the surface warming. However, such a process is not included in the water-hosing experiments. Hence, we can not use the water-hosing experiments to project the long-term stability of the AMOC in a future warm climate.

4.1 Introduction

Multiple equilibria and a rapid transition between different states of the Atlantic meridional overturning circulation (AMOC) are robust phenomena in climate models at different complexity levels due to a positive salt advection feedback (e.g. Stommel 1961; Rooth 1982; Bryan 1986; Marotzke et al. 1988; Manabe and Stouffer 1988; Stocker and Wright 1991; Marotzke and Willebrand 1991; Rahmstorf and Willebrand 1995; Ganopolski and Rahmstorf 2001; Hawkins et al. 2011). Atlantic paleoclimate records suggest that abrupt climate changes in the past were linked to rapid transitions of the AMOC due to the input of freshwater forcing in the deep water formation regions (e.g. Broecker et al. 1985; Bond et al. 1997; Marotzke 2000; Alley et al. 2003; Rahmstorf 2002; McManus et al. 2004; Ellison et al. 2006). Hence, a rapid transition and irreversible shift of the AMOC owing to the anthropogenic climate change are of particular concern in evaluating the potential societal and environmental threat posed by future climate change. The present study investigates the possibility of hysteresis behavior and processes governing the long-term stability of the AMOC in a future warm climate by using a state-of-the-art AOGCM ECHAM5/MPIOM with long-term integrations.

A warmer climate owing to the anthropogenic CO_2 emission is likely to increase the freshwater input to the North Atlantic. In turn, a gradual weakening in the strength of the AMOC is projected by AOGCMs, although there is considerable uncertainty in the magnitude of the change (Dixon et al. 1999; Mikolajewicz and Voss 2000; Gregory et al. 2005; Meehl et al. 2007). Although much work has been done to project the AMOC change in a future warm climate, the previous studies with AOGCMs mentioned here only investigated the transient behavior of the AMOC with ramping up atmospheric CO_2 forcing. To understand the hysteresis

behavior or the reversibility of the AMOC in a future warm climate, water-hosing experiments are carried out (Stouffer et al. 2006; Hawkins et al. 2011). In a water-hosing experiment, an additional freshwater flux is applied to the North Atlantic where the deep-ocean water forms. Typically the AMOC weakens by 30% in response to 0.1 Sv ($1\,\mathrm{Sv} \equiv 10^6\,\mathrm{m^3 s^{-1}}$) freshwater input and switches off rapidly in response to 1.0 Sv freshwater input (Stouffer et al. 2006). Hawkins et al. (2011) demonstrated the AMOC hysteresis behavior in a water-hosing experiment using their coarse-resolution AOGCM. They suggested that the AMOC is currently in a bistable regime.

However, the freshwater forcing in the North Atlantic is not the only influence; the direction of the freshwater transport in the South Atlantic might also be closely linked to the dynamical regime and to the stability of the AMOC (Rahmstorf 1996). Using coupled climate models of intermediate complexity, de Vries and Weber (2005) and Cimatoribus et al. (2011) further demonstrated that the sign of the overturning circulation freshwater transport (M_{ov}) in the south Atlantic border at 33 °S determines the existence of a monostable or bistable regime in their models. If M_{ov} is positive, the AMOC would import freshwater into or export salt out of the North Atlantic. In this case, a weakened AMOC would import less freshwater, causing a recovery of the AMOC (i.e., a negative salt-advection feedback), as a higher salinity tends to promote deep convection and a stronger AMOC. Hence, the AMOC exhibits a monostability in a model with a positive M_{ov} (de Vries and Weber 2005). Using data from the CMIP3 (The Coupled Model Intercomparison Project phase 3), Drijfhout et al. (2011) indicated that most modern AOGCMs have only one equilibrium state of the AMOC due to a positive M_{ov}. However, Hawkins et al. (2011) recently found bistability of the AMOC in their AOGCM, although M_{ov} is positive in their pre-industrial control run. Further analysis showed that M_{ov} becomes negative within the hysteresis regime of the AMOC in their water-hosing experiment. Therefore, Hawkins et al. (2011) concluded that the sign of M_{ov} is a useful physical indicator of the existence of a bistable regime.

In a future warm climate forced by anthropogenic CO_2 emission, how much additional freshwater will be put into the North Atlantic deep-water formation region? How do other processes like the freshwater transport across the south Atlantic border change in response to the CO_2 forcing? How do they govern the

long-term stability of the AMOC? To gain a more comprehensive understanding of these issues, we investigate the possibility of hysteresis behavior and processes governing the long-term stability of the AMOC by forcing the state-of-the-art AOGCM with an atmospheric CO_2 concentration that changes extremely slowly with time.

Starting from an equilibrated pre-industrial control run with constant atmospheric CO_2 at 278 ppmv (experiment CNTR), the atmospheric CO_2 is increased from the pre-industrial level to a quadrupling over 2000 years (experiment CO2_UP in Fig. 4.1a), and is held constant thereafter for a further 5940 years until the whole system has reached equilibrium (experiment CO2_HIGH in Fig. 4.1a). A third integration starts from the end of CO2_HIGH; the atmospheric CO_2 concentration is linearly decreased from the quadrupling to the pre-industrial level over 2000 years (experiment CO2_DOWN in Fig. 4.1a), and is held constant thereafter for a further 3940 years until the whole system has again reached equilibrium (experiment CO2_LOW in Fig. 4.1a). The extremely slow rate of change of CO_2 concentration is used to keep the system close to a quasi-equilibrium. In addition, four 1500-year simulations with constant atmospheric CO_2 at 490 ppmv and 780 ppmv are carried out to clarify the stability of the AMOC in both CO2_UP and CO2_DOWN (A, B, C, D in Fig. 4.3a,b). All the experiments are also used to study the sea ice hysteresis behavior in response to atmospheric CO_2 forcing in chapter 3. The coupled climate model used here has neither dynamic glaciers nor dynamic vegetation. As one consequence, we cannot explore the impact of ice-sheet melting on the AMOC. However, modeling studies of the impact of the Greenland ice-sheet melting on the AMOC give mixed results; some suggest a dramatic weakening of the MOC in the future warmer climate (Fichefet et al. 2003; Swingedouw et al. 2007) and others show a minor or negligible effect (e.g. Ridley et al. 2005; Jungclaus et al. 2006; Mikolajewicz et al. 2007; Vizcaíno et al. 2010).

Section 4.2 shows the AMOC in response to the change in atmospheric CO_2 concentration. In section 4.3, we perform the freshwater budget of North Atlantic throughout the simulation. Section 4.4 shows the change of atmospheric freshwater forcing over the North Atlantic. Section 4.5 gives the conclusions.

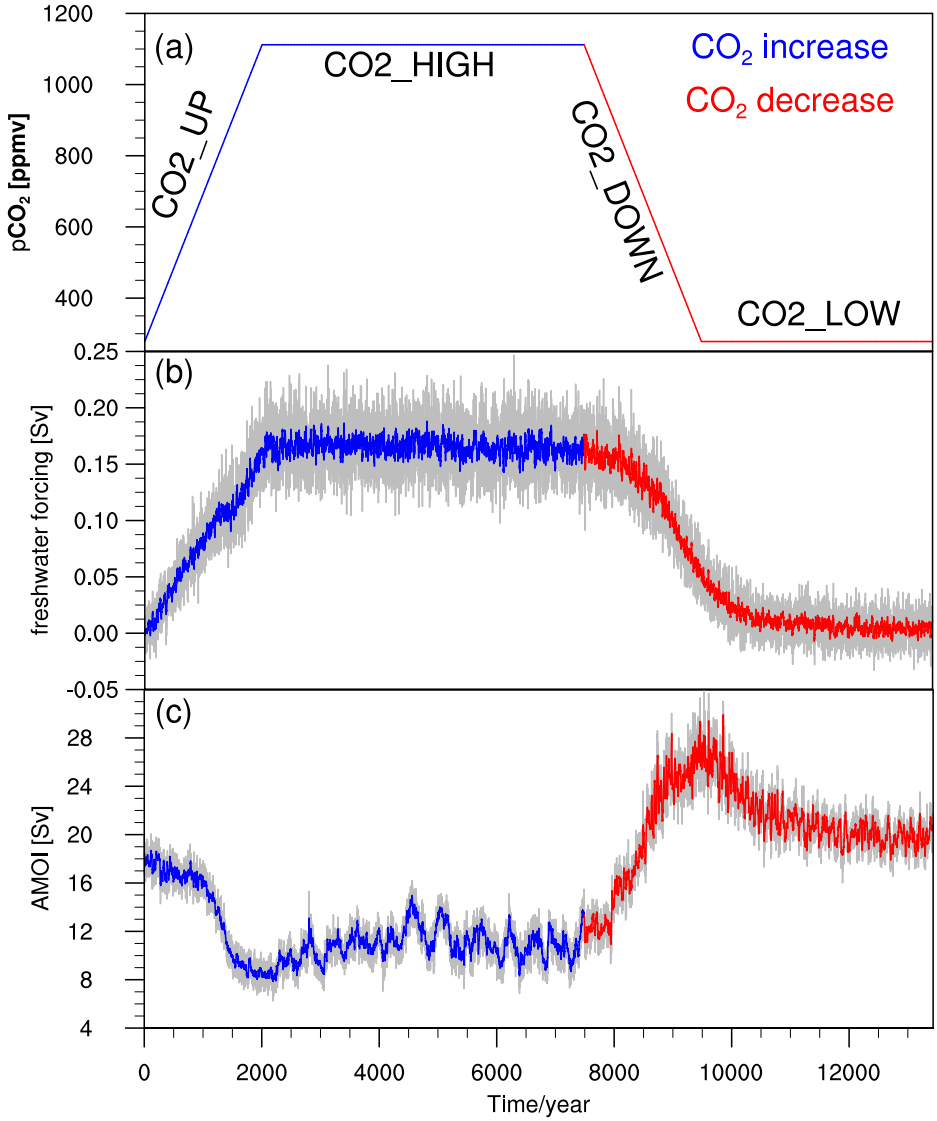

Fig. 4.1: Time series of (a) atmospheric CO_2 concentration applied throughout the simulation (Unit: ppmv), (b) atmospheric freshwater forcing anomaly (Unit: Sv) over 60−80 °N belt in North Atlantic, and (c) the AMOI (Atlantic meridional circulation index) (Unit: Sv). The anomaly in (b) is with respect to CNTR (last 100-year mean of the pre-industrial control run). The AMOI is defined as the annual-mean zonally integrated streamfunction in Sv at the depth of 1000m in the Atlantic 30 °N. Increasing CO_2 concentration (blue) results in an increasing freshwater forcing trajectory; decreasing CO_2 concentration (red) results in a decreasing freshwater forcing trajectory. The gray line in (b) and (c) represents annual-mean data for the entire simulation, other colors in (b) and (c) represent an 11-year running mean.

4.2 The AMOC response to changes in the atmospheric CO_2 concentration

4.2.1 Time evolution

As the CO_2 concentration increases in CO2_UP, the atmospheric freshwater anomaly that results from the increased precipitation and river runoff over the North Atlantic deep water (NADW) formation region relative to that in CNTR amounts to 0.16 Sv at the end of CO2_UP (Fig. 4.1b). This amount of freshwater forcing is in the AMOC bistability-regime with the water-hosing ranges of 0.1-0.5 Sv used in Earth-system Models of Intermediate Complexity (EMICS) simulations by Rahmstorf et al. (2005), and also within the ranges of 0.15-0.22 Sv used in an AOGCM simulation by Hawkins et al. (2011). The freshwater forcing is stationary while the CO_2 is held constant at 1112 ppmv in CO2_HIGH. As the CO_2 decreases in CO2_DOWN, the freshwater anomaly decreases from 0.16 Sv to 0.06 Sv at the end of CO2_DOWN and eventually goes to zero in CO2_LOW when the CO_2 is held constant at 278 ppmv(Fig. 4.1b). The freshwater input contributed from the melting of Greenland is projected to be around 0.01 Sv in 21st century by using the IPCC SRES scenario data (Gregory and Huybrechts 2006), and 0.025 Sv with CO_2 doubling and 0.1 Sv with CO_2 quadrupling by using a comprehensive earth system model with an ice-sheet model (Vizcaíno et al. 2010). Hence, the contribution of Greenland ice-sheet melting is relatively smaller than the atmospheric freshwater forcing found in ECHAM/MPIOM.

The increased atmospheric freshwater forcing could increase the ocean stratification in the North Atlantic and result in significantly weakened deep convection and a more retarded AMOC. Due to the increased freshwater forcing over the NADW formation regions, the AMOI (Atlantic meridional overturning circulation index), which is defined as the annual-mean zonally integrated streamfunction in Sv at the depth of 1000 m at 30 °N in the Atlantic, weakens from 18.5 Sv to about 8.4 Sv (decline by about 55%) as the CO_2 increases in CO2_UP (Fig. 4.1c). Thereafter, the AMOI slowly recovers and reaches a final equilibrium of 12.2 Sv, as both the CO_2 and freshwater forcing become stationary, and the AMOI shows very strong century-timescale variability in CO2_HIGH (Fig. 4.1c). As in most previous global warming studies, the AMOC weakens once CO_2 increases, but

does not collapse in our experiments. Once the CO_2 and freshwater forcing decreases again in CO2_DOWN, the AMOI recovers from 12.2 Sv to 26.5 Sv, as the CO_2 reaches 278 ppmv. After keeping the CO_2 at 278 ppmv for several millennia in CO2_LOW, the AMOI decreases to 20.3 Sv, which is still slightly stronger than that in CNTR. The AMOC upper cell becomes shallower and weaker when the freshwater forcing and the CO_2 concentration increase and remain at high levels (Fig. 4.2b,c), indicating that the NADW does not penetrate as deep as in CNTR. The AMOC upper cell becomes thicker and stronger once the freshwater forcing and the CO_2 concentration decrease and remain at low levels (Fig. 4.2d,e), indicating a stronger NADW formation.

4.2.2 Hysteresis diagram

To explore the possible hysteresis behavior of the AMOC in a future warm climate, we first discuss the hysteresis diagram of the AMOI as a function of the atmospheric CO_2 concentration (Fig. 4.3a), which is the prescribed external forcing throughout the simulation and an indirect driver of the AMOC change. In gerneral, the AMOI decreases with increasing CO_2, and the AMOI decreases from 16 Sv to 10 Sv as the CO_2 in the range of about 700-900 ppmv, and the AMOI continues decreasing slowly as the CO_2 increases further. Once the CO_2 decreases, the AMOC recovers along a trajectory above the AMOC weakening trajectory. As the CO_2 again reaches 278 ppmv, the AMOI is about 26.5 Sv, which is much stronger than that in CNTR. While keeping CO_2 at 278 ppmv for several millennia in CO2_LOW, the AMOI eventually almost recovers to the pre-industrial state. The offset between the AMOC decreasing trajectory and the recovering trajectory is suggestive of a hysteresis behavior of the AMOC in response to the CO_2 forcing. However, with fixed CO_2 forcing at 490 ppmv and 780 ppmv for 1500 years, experiments started from the AMOC weakening trajectory (A and C in Fig. 4.3a) and experiments started from the AMOC recovering trajectory (B and D in Fig. 4.3a) finally meet each other in between. For a true hysteresis, the AMOC "recovery" trajectory should be below the "weakening" trajectory, not above, and the multiple internal states for the same external forcing do not disappear as the forcing kept at a certain constant. Hence, the AMOC shows no hysteresis behavior in response to the atmospheric CO_2 forcing, and the apparent

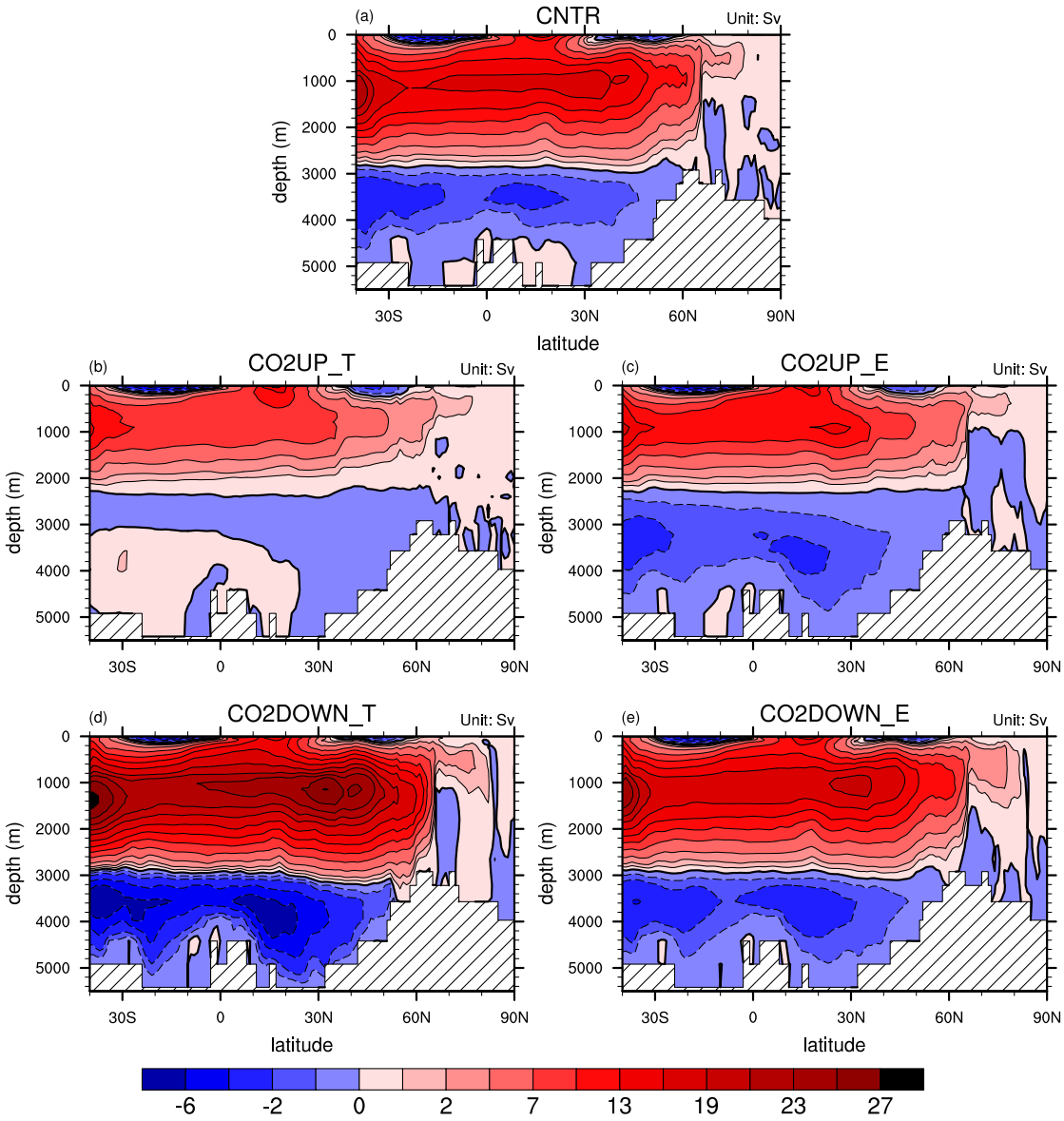

Fig. 4.2: The AMOC streamfunction (Unit: Sv, positive value corresponds to counterclockwise circulation). (a) Averaged over the last 100-year of the CNTR; (b) averaged over the first 100-year of CO2_HIGH (CO2UP_T); (c) averaged over the last 100-year of CO2_HIGH (CO2UP_E); (d) averaged over the first 100-year of CO2_LOW (CO2DOWN_T); (e) averaged over the last 100-year of CO2_LOW (CO2DOWN_E).

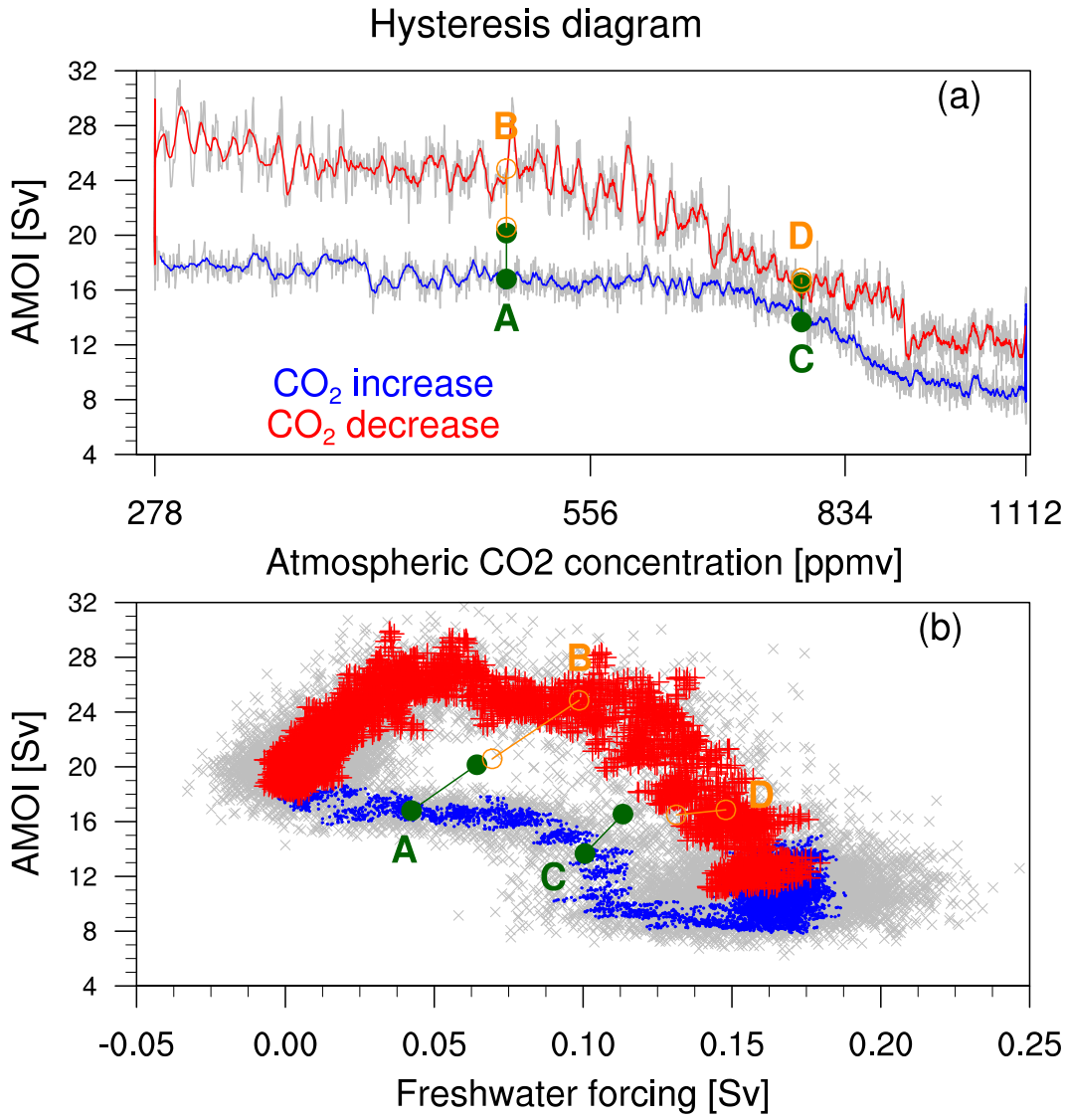

Fig. 4.3: (a) The AMOI (Unit: Sv) as a function of atmospheric CO_2 concentration (Unit: ppmv). (b) The AMOI as a function of atmospheric freshwater anomalous (Unit: Sv) over 60−80 °N belt in North Atlantic. CO_2 in (a) is plotted on a logarithmic scale, and the anomalous in (b) is with respect to the CNTR. The use of gray, blue and red is as described in Fig. 4.1. The dark green represents experiments started from CO2_UP with CO_2 fixed at 490 ppmv (A) and 780 ppmv (C) for 1500 years. The dark orange represents experiments started from CO2_DOWN with CO_2 fixed at 490 ppmv (B) and 780 ppmv (D) for 1500 years. The first 100-year and last 100-year mean of experiment A, B, C, D are plotted in (a) and (b).

hysteresis is a consequence of the speed of the transient change in CO_2 concentration that is not small enough to ensure an quasi-equilibrium in our experiments.

The freshwater forcing anomaly over the NADW formation region is one of the major direct drivers to the change in the AMOC. We also discuss the AMOI as a function of the atmospheric freshwater anomaly (Fig. 4.3b) throughout all the simulations. Gernerally, the AMOC weakens as the freshwater forcing increases, and the AMOC decreases by 6 Sv as the freshwater forcing anomaly reaches around 0.1Sv in CO2_UP. In contrast to the hysteresis diagram of the AMOC as a function of water hosing rate in the water-hosing experiment (e.g. Rahmstorf et al. 2005; Hawkins et al. 2011), the AMOI does not remain small, but recovers and becomes stronger than that in the AMOC weakening trajectory, as soon as the freshwater forcing starts to decrease. With the CO_2 concentration kept at 490 ppmv for 1500 years, the freshwater forcing and the AMOC in experiment A tend to meet those in experiment B (Fig. 4.3b), and the freshwater forcing; and with the CO_2 concentration kept at 780 ppmv for 1500 years the AMOC in experiment C tend to meet those in experiment D (Fig. 4.3b). Hence, the AMOC shows no hysteresis behavior in response to the atmospheric freshwater forcing over NADW formation regions in our experiments.

In experiment A and C, the AMOI increases while the freshwater forcing increases; and in experiment B and D, the AMOI decreases while the freshwater forcing decreases. These suggest that the changes of the AMOC in these experiments are not entirely governed by the freshwater forcing over NADW regions.

4.3 Atlantic basin freshwater budget

To gain further understanding of the processes governing the long-term stability of the AMOC in a future warm climate, we diagnose the freshwater budget of the Atlantic and Arctic ocean basin following Rahmstorf (1996), de Vries and Weber (2005) and Drijfhout et al. (2011). We consider the following equations:

$$0 = -[E - P - R] + M_{ov} + M_{az} + M_{dif} + M_{BS}, \tag{4.1}$$

$$M_{ov} = -\frac{1}{S_0}\int_{34S} \bar{v}(z)[< S(z) > -S_0]dz, \tag{4.2}$$

$$M_{az} = -\frac{1}{S_0}\int_{34S} \overline{v'(x,z)S'(x,z)}dz, \tag{4.3}$$

$$S_0 = \frac{\int_{34S} S(x,z)dxdz}{\int_{34S} dxdz}, \tag{4.4}$$

where the atmospheric freshwater contribution $[E-P-R]$ is the basin-integrated result of evaporation E, precipitation P and continental river run-off R over the Atlantic and Arctic basin. In equilibrium, $[E-P-R]$ is balanced by the meridional overturning freshwater transport (M_{ov}), the oceanic gyre circulation freshwater transport (M_{az}) at the southern border at 34 °S, the freshwater transport through Bering Strait (M_{BS}), and a diffusion term due to the ocean mixing (M_{dif}). The subscript $34S$ indicates an integration over a zonal transect near 34 °S. S_0 is a reference salinity at 34 °S which is calculated according to equation (4.4) in this study, S is the oceanic salinity, the overbar and the brackets $<>$ denote zonal integration and zonal averaging, respectively, v' and S' are deviations from zonal means. All terms in equation (4.1) can be expressed in Sv. In this study, we only consider the three major terms $[E-P-R]$, M_{ov} and M_{az}, M_{dif} and M_{BS} are not calculated because they are small. A positive sign means that the respective term carries a net freshwater flux into the Atlantic basin. In the water-hosing experiments, if M_{ov} is positive, the AMOC would export salt from Atlantic basin. In this case, a small reduction in the AMOC would export less salt, encouraging a recovery of the AMOC (i.e., a negative feedback), as higher salinity tends to promote deep mixing and a stronger AMOC (Rahmstorf 1996; de Vries and Weber 2005; Drijfhout et al. 2011; Hawkins et al. 2011). The sign of M_{ov} has been demonstrated to be a reliable indicator of a monostable or bistable regime in water-hosing experiments with OGCMs and EMICs (de Vries and Weber 2005; Dijkstra 2007; Huisman et al. 2010), but not yet in an AOGCM.

In CNTR of ECHAM5/MPIOM, the net freshwater loss (-0.4Sv) by evaporation in excess of precipitation and runoff over the whole Atlantic basin is compensated by M_{ov} (0.18 Sv) and M_{az} (0.2 Sv) (Tabel 4.1). Consistent with most AOGCMs as evaluated by Drijfhout et al. (2011), we get a positive M_{ov} in contrast to the observational result obtained using inverse modeling (Weijer et al. 1999). The positive M_{ov} indicate that the AMOC exports salt and imports fresh-

Table 4.1: Atlantic fresh water budget in CNTR of ECHAM5/MPIOM and inverse-model data (Weijer et al. 1999), unit: Sv

	M_{ov}	M_{az}	$-[E-P-R]$
Inverse-model data	-0.2	0.38	$\sim$
ECHAM5/MPIOM	0.18	0.20	-0.40

water across the Atlantic southern border. The incorrect sign of M_{ov} is caused by a precipitation bias over the Southern Atlantic which tends to freshen the ocean surface in ECHAM5/MPIOM.

Owing to the surface warming as the CO_2 increases in CO2_UP, -[E-P-R] decreases from -0.4 Sv to -1.0 Sv due to the enhanced evaporation over Atlantic. Once the CO_2 decreases and cools the surface again in CO2_DOWN, -[E-P-R] increases from -1.0 Sv to -0.57 Sv, and it eventually recovers to the pre-industrial level, when the CO_2 is held constant at 278 ppmv in CO2_LOW (Fig. 4.4a). Different from the water-hosing experiments, the enhanced evaporation in the Atlantic basin due to the surface warming may lead to anomalously high salinities in the upper ocean. This saline water can be advected into the NADW region, thereby working against the AMOC reduction and leading to a relatively stronger AMOC while it recovers.

In a warm climate, M_{ov} is not only determined by the change in the AMOC but also by the changes in salinity due to the changes in precipitation and ocean current pattern. In contrast to the water hosing-experiments (de Vries and Weber 2005; Hawkins et al. 2011), an increased M_{ov} with a weakening AMOC in CO2_UP imports more freshwater into the Atlantic, which reinforces the reduction of the AMOC (Fig. 4.4b). While the CO_2 is held constant at 1112 ppmv in CO2_HIGH, M_{ov} shows similar very strong century-timescale variability as the AMOI (Fig. 4.4b). Hence, the inter-basin freshwater exchange may play an important role in the long-term variability of the AMOC in this period as found by Weijer et al. (1999). Once the AMOC recovers in CO2_DOWN, an increased M_{ov} tends to work against the recovery of the AMOC. Hence, a positive M_{ov} does not suggest a negative salt-advection feedback and does not govern the long-term stability of the AMOC in our experiments.

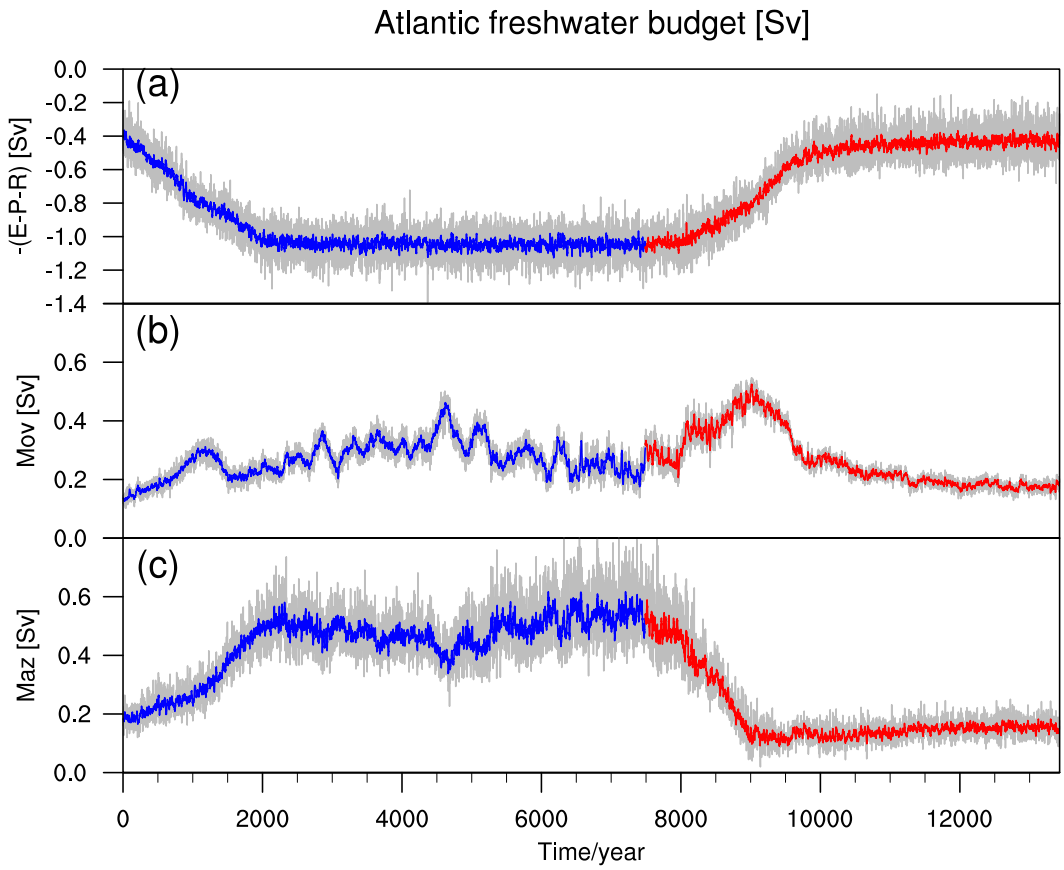

Fig. 4.4: Time series of (a) atmospheric freshwater flux (-[E-P-R]) integrated over Atlantic basin, (b) overturning freshwater transport across 34 °S (M_{ov}), and ocean gyre circulation freshwater transport across 34 °S (M_{az}), unit: Sv. Positive value means the Atlantic basin gains freshwater. The use of gray, blue and red is as described in Fig. 4.1.

To compensate the robust signal of the increased $[E-P-R]$ in CO2_UP, the subtropical gyre, M_{az} , in the South Atlantic tends to import more freshwater into the Atlantic basin, thereby reinforcing the reduction of the AMOC. While the CO_2 is decreased in CO2_DOWN, a decreased M_{az} imports less freshwater into the Atlantic, encouraging a recovery of the AMOC as a higher salinity tends to promote deep convection in North Atlantic and stronger AMOC. Hence, the change of ocean gyre freshwater transport due to the change in surface wind and precipitation may also play an important role in a future warm climate.

4.4 Evaporation changes in the subtropics and their impact on the AMOC

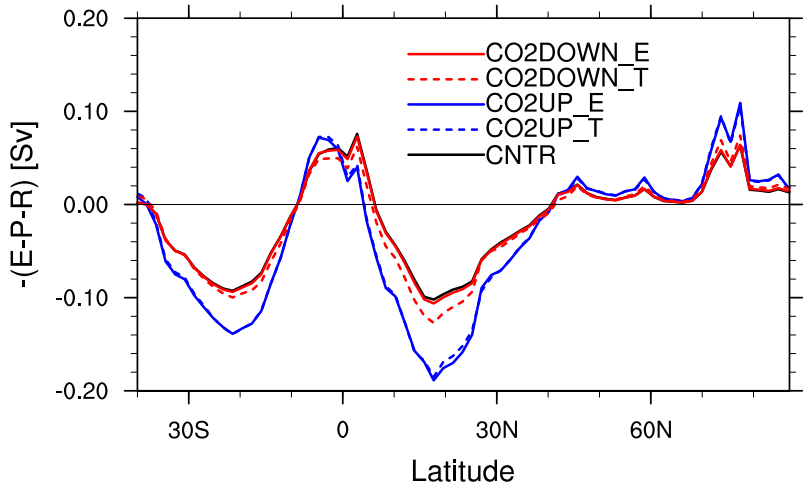

Fig. 4.5: Atlantic zonally-integrated atmospheric freshwater flux (-[E-P-R]) in different periods of the simulation, averaged over the last 100-year of CNTR (black solid line); averaged over the first 100-year of CO2_HIGH (CO2UP_T) (blue dashed line); averaged over the last 100-year of CO2_HIGH (CO2UP_E) (blue solid line); averaged over the first 100-year of CO2_LOW (CO2DOWN_T) (red dashed line); averaged over the last 100-year of CO2_LOW (CO2DOWN_E) (red solid line), unit: Sv.

As has been described in Latif et al. (2000) using an AOGCM with flux-adjustment, the large-scale tropical air-sea interaction can also influence the stability of the AMOC in a warming climate. An El Niño-like warming in the eastern equatorial Pacific and strongly enhanced precipitation in the central equatorial

Pacific lead to adiabatic warming and drying through anomalous subsidence over the tropical Atlantic, thereby increasing the evaporation in the tropical Atlantic and causing anomalously high salinities in the North Atlantic upper ocean. Such a connection could also be at work in a warm climate (Fig. 4.5 and Fig. 4.6b,c). During the CO_2 increase period in CO2_UP, an increased freshwater forcing over the NADW formation regions is the dominant process to decrease the deep ocean convection, resulting in weakening AMOC. Once the CO_2 decreases again, the freshwater forcing over the NADW formation regions decreases on the one hand, and the highly saline water is advected into the NADW formation regions on the other hand, thereby strongly increasing the surface density and causing strong deep ocean convection (Fig. 4.5 and Fig. 4.6d,e). Hence, this leads to the recovery of the AMOC, once the CO_2 concentrations is decreased.

The overshooting recovery of the AMOC obtained when we decrease the CO_2 in CO2_DOWN, is also caused by a stronger evaporation in excess of precipitation and runoff over the tropical Atlantic. As has been shown in chapter 3, for the same amount of atmospheric CO_2 concentration the surface temperature in CO2_DOWN is much higher than that in CO2_DOWN due to the thermal inertia of the ocean. This leads to a relatively stronger evaporation (Fig. 4.5) and anomalously high salinities (Fig. 4.6d) in the North Atlantic, when the CO_2 concentration is decreased, resulting in stronger deep convection and a stronger AMOC (Fig. 4.2d). Hence, in contrast to the water-hosing experiments, the large-scale tropical air-sea interaction plays an important role in the long-term stability of the AMOC in a future warm climate.

4.5 Conclusions

Using the stat-of-the-art AOGCM ECHAM5/MPIOM, we performed several idealized simulations to investigate the hysteresis behavior of the AMOC in a future warm climate. In contrast to the classical water-hosing experiments, we changed the atmospheric CO_2 concentration rather than the freshwater input in the deep-water formation regions. We conclude the following:

(1) The atmospheric freshwater forcing anomaly over the deep-water formation regions results from the increased precipitation and river runoff that

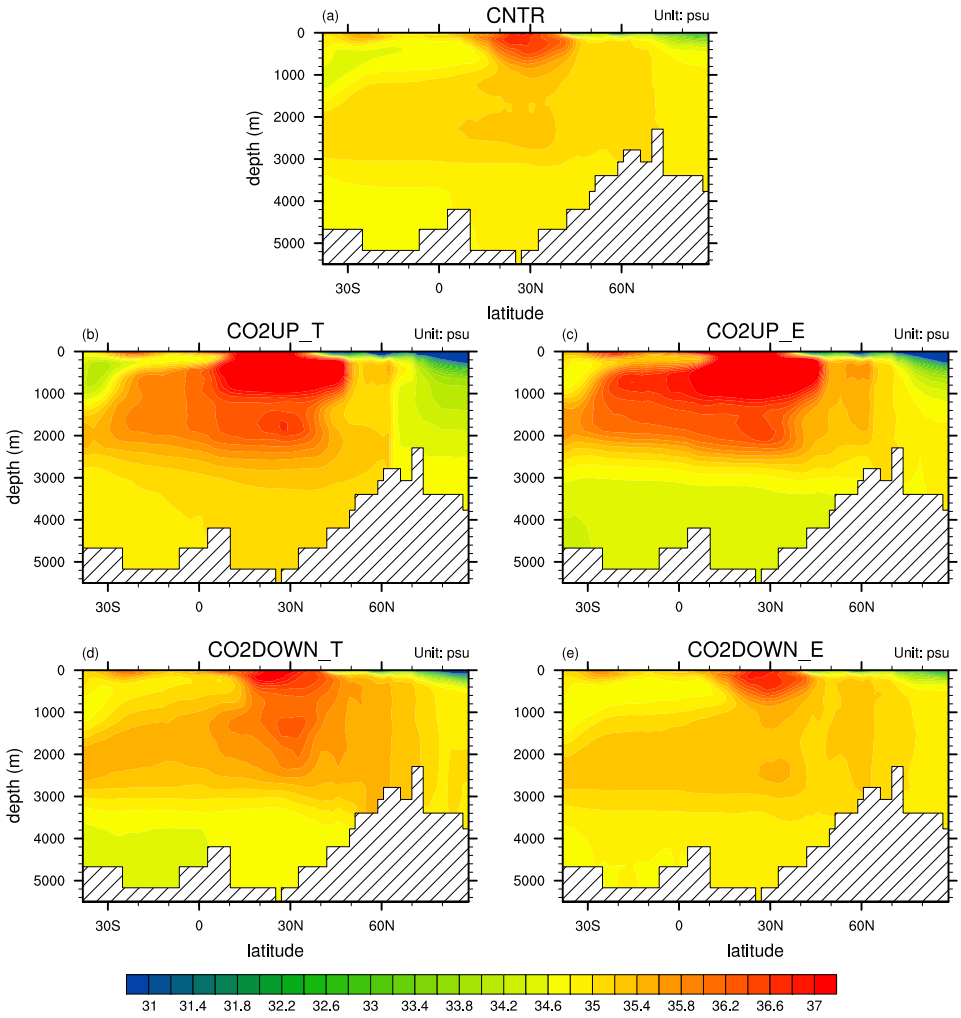

Fig. 4.6: Atlantic zonal-mean salinity (unit: psu), (a) averaged over the 100-year of the CNTR; (b) averaged over the first 100-year of CO2_HIGH (CO2UP_T); (c) averaged over the last 100-year of CO2_HIGH (CO2UP_E); (d) averaged over the first 100-year of CO2_LOW (CO2DOWN_T); (e) averaged over the last 100-year of CO2_LOW (CO2DOWN_E).

amounts to 0.16 Sv after a CO_2 quadrupling. This amount of freshwater forcing is within the AMOC bistability-regime with the water-hosing range of 0.1-0.5 Sv input into the North Atlantic. The freshwater input contributed from the melting of Greenland is projected to be around 0.01 Sv in the 21st century by using the IPCC SRES scenario data (Gregory and Huybrechts 2006), and 0.025 Sv with CO_2 doubling and 0.1 Sv with CO_2 quadrupling by using a comprehensive earth system model with an ice-sheet model (Vizcaíno et al. 2010). Hence, the contribution of Greenland ice-sheet melting is smaller than the atmospheric freshwater forcing found in our experiments.

(2) As in most of previous global warming studies, the AMOC weakens once the CO_2 increases, but does not collapse in our experiments. The AMOC weakens from 18.5 Sv in CNTR to 12.2 Sv (decline by 34.5%) after a CO_2 quadrupling in the final equilibrium.

(3) We find no evidence of hysteresis behavior of the AMOC in response to the CO_2 forcing and the anomalous atmospheric freshwater forcing over the NADW formation regions. The AMOC recovers once the CO_2 decreases in CO2_DOWN and becomes stronger than that in CO2_UP. This overshooting recovery in CO2_DOWN is caused by a stronger evaporation over the tropical Atlantic. With the same amount of atmospheric CO_2 concentration the surface temperature in CO2_DOWN is much higher than that in CO2_DOWN due to the thermal inertia of the ocean. This leads to a stronger evaporation and higher salinities in the North Atlantic while CO_2 decreases, resulting in stronger deep convection and a stronger AMOC.

(4) Consistent with other AOGCMs (Drijfhout et al. 2011), ECHAM5/MPIOM shows a positive value of M_{ov} in its pre-industrial control run, which is opposite to the observations. In a warm climate, M_{ov} is not only determined by the change in the AMOC but also by the changes in salinity due to the changes in precipitation and ocean current pattern. In the CO_2 increasing period in CO2_UP, an increased M_{ov} tends to import more freshwater into the Atlantic, which reinforces the reduction of the AMOC. And once the CO_2 increases, a further increase in M_{ov} tends to import even more fresh-

water into the Atlantic, which works against the recovery of the AMOC. Hence, in our experiment, M_{ov} does not dampen the freshwater forcing in the North Atlantic and does not promote the deep convection and recovery of the AMOC. We do not find multiple equilibria and hysteresis behavior of the AMOC in our experiments, not because of the a wrong sign of M_{ov} in pre-industrial control climate of ECHAM5/MPIOM, but because of the enhanced evaporation over the tropical Atlantic in a warm climate. The enhanced evaporation leads anomalously high salinities in the North Atlantic upper ocean, thereby strongly increasing the surface density and leading strong deep ocean convection.

(5) We cannot use the water-hosing experiments to project the long-term stability of the AMOC in a future warm climate. In water-hosing experiments, we only consider the impact of anomalous atmospheric freshwater forcing on the stability of the AMOC. However, in a future warm climate, a stronger evaporation in the tropical Atlantic owing to the surface warming also plays an important role in governing the long-term stability of the AMOC; such a process cannot be considered in the water-hosing experiments.

Chapter 5

Conclusions and Outlook

5.1 Conclusions

I conclude my thesis by revisiting the research questions posed in the Chapter 1.

1. Deep-ocean heat uptake and equilibrium climate response

- What is the equilibrium surface-temperature response to atmospheric CO_2 quadrupling in ECHAM5/MPIOM? Does the equilibrium surface-temperature response in ECHAM/MPIOM confirm of results in ECHAM5/SOM?

The equilibrium global-mean surface-temperature change in ECHAM5/MPIOM is 10.8K. ECHAM5/SOM slightly overestimate the equilibrium global-mean surface-temperature change by 0.3K. This suggests that the change in AMOC and the reduced northward ocean heat transport have very limited effect on the global-mean surface temperature change, although the AMOC weakens in equilibrium by 46%. However, ECHAM5/MPIOM shows less warming over the northern-hemisphere mid and high latitudes, but larger warming over the tropical ocean and especially over the southern-hemisphere high latitudes. ECHAM5/MPIOM shows similar polar amplification in both the Arctic and the Antarctic, in contrast to ECHAM5/SOM, which shows stronger polar amplification in the northern hemisphere. The southern polar warming in ECHAM5/MPIOM is greatly delayed by Antarctic deep-ocean warming due to convective and isopycnal mixing. Hence, the change in deep-ocean circulation and its corresponding heat transport play a very important role in determining the geographic pattern of equilibrium surface temperature response and its time evolution.

- What is the final equilibrium of the ocean temperature in response to atmospheric CO_2 quadrupling in ECHAM5/MPIOM? Does the ocean warming in ECHAM5/MPIOM confirm of resluts in an upwelling-diffusion model or a multi-box ocean model?

The ocean temperature shows a near-uniform warming of around 8.0K at almost all levels of the ocean; this result confirms globally averaged multi-box ocean model simulation (e.g. Harvey and Schneider 1985), but does not support the globally averaged upwelling-diffusion ocean model simulations because of their incorrect application of a constant ocean bottom temperature (e.g. Harvey and Schneider 1985; Raper et al. 2001; Marčelja 2010).

- Does the effective climate response method described in Gregory et al. (2004) give an accurate estimation of the equilibrium climate response?

We evaluate the effective climate response method described in Gregory et al. (2004) with our simulation, and we show that their method to estimate equilibrium climate response is accurate to within 10%, despite some non-linearity where the changes in the deep ocean circulation influence the pattern of the surface warming and atmospheric feedback.

2. Sea ice in a future warm climate

- Does the Arctic sea ice show hysteresis behavior in a future warm climate? Which processes govern the long-term stability of Arctic sea ice?

In our simulation, we find no evidence of multiple equilibria and hysteresis behavior of Arctic summer and winter sea ice cover in response to atmospheric CO_2 forcing. However, both the Arctic summer and winter sea ice covers show a lagged response to the change in atmospheric CO_2 forcing. There is no lagged response to the Northern Hemisphere surface temperature change. A strong halocline in the Arctic ocean is responsible for maintaining water column stability, thus isolating the surface water from the deep water in the Arctic. In addition, the thermodynamic forcing is more relevant for the change in Arctic sea ice cover because the sea ice movement in the Arctic is constrained by the surrounding land masses (e.g. Eisenman 2010; Notz and Marotzke 2012). Consequently, the

change in the Arctic sea ice is governed by the surface warming. The Arctic sea-ice area shows a lagged response to the atmospheric CO_2 forcing, because the surface temperature change lags to the atmospheric CO_2 forcing due to the ocean thermal inertia.

- Is there any rapid transition during the retreat of Arctic sea ice?

We find a rapid transition associated with the sudden loss of the Arctic winter sea ice cover in a warm climate once the NH-averaged annual-mean surface temperature has increased by about 8.0 K. This rapid transition may be triggered by atmospheric convection, which can warm the Arctic by trapping the outgoing long-wave radiation and keep the Arctic ice-free in winter time. Consistent with previous studies, the Arctic summer sea ice cover retreats linearly with CO_2 increase in a warm climate.

- Does the Antarctic sea ice show hysteresis behavior in a future warm climate? Which processes govern the long-term stability of Antarctic sea ice?

The Antarctic sea ice cover retreats continuously without any rapid transition during the warming trajectories, and it also shows no evidence of hysteresis behavior and multiple equilibria in response to the atmospheric CO_2 forcing. However, the Antarctic sea ice cover shows much more strongly lagged response to the atmospheric CO_2 forcing compared to the Arctic sea ice. In contrast to Arctic sea ice, the response of Antarctic sea ice cover significantly lags behind the Southern Hemisphere surface air temperature change. Different from the Arctic ocean, the Antarctic ocean does not have such a strong halocline, thus open-ocean deep convection in Antarctic can be triggered by the change of the surface density (Akitomo 1999; McPhee 2003). Heat from the intermediate water becomes entrained into the upper ocean, resulting in warmer winter and a higher sea surface temperature, thus preventing the Antarctic sea ice formaion in winter time. Hence it is the strong deep ocean convection that maintains an ice-free Antarctic ocean throughout once the atmospheric CO_2 is decreased. And in contrast to the Arctic, Antarctic sea ice dynamics driven by surface wind pattern and currents also play a far more important role for the overall sea ice area (e.g. Comiso and Nishio 2008; Stammerjohn et al. 2008; Notz and Marotzke 2012). Therefore, in contrast to the Arctic sea ice change, the surface temperature change is not the

controlling factor for the Antarctic sea ice change in a warm climate; the deep ocean convection and sea ice dynamics can also play an important role. This is the reason why the Antarctic sea ice covers show much more strongly lagged response to the atmospheric CO_2 forcing compared to the Arctic sea ice cover; and in contrast to the Arctic sea ice cover, the response of the Antarctic sea ice cover also lags significantly behind the local surface air temperature.

3. AMOC in a future warm climate

- Does the AMOC show hysteresis behavior in response the atmospheric CO_2 forcing?

We find no evidence of hysteresis behavior of AMOC in response to the CO_2 forcing and to the consequent anomalous atmospheric freshwater forcing over the NADW formation regions. The AMOC "recovery" trajectory is above the "weakening" trajectory, not below as would be the case in experiments with hysteresis behavior, indicating that the apparent offset is a consequence of the speed of the transient change in CO_2 concentration that is not small enough to ensure a quasi-equilibrium in our experiment.

- Which processes govern the long-term stability and reversibility of AMOC in a future warm climate?

The overshooting recovery of the AMOC is caused by a stronger evaporation over the tropical Atlantic, which leads to anomalously high salinities in the North Atlantic while the CO_2 decreases, resulting in a stronger deep convection and a stronger AMOC. In contrast to previous studies with water-hosing experiments, a positive overturning freshwater transport (M_{ov}) at the southern border does not damp the freshwater forcing in the North Atlantic and does not promote the recovery of the AMOC throughout our simulations. In a future warm climate, the long-term stability of the AMOC is not only governed by the anomalous freshwater forcing in the deep-water formation regions, but also by a stronger evaporation in the tropical Atlantic caused by the surface warming. However, such a process is not represented in the water-hosing experiments. Hence, we cannot use the water-hosing experiments to project the long-term stability of the AMOC in a future warm climate.

Bibliography

Aagaard, K., L. K. Coachman, and E. Carmack, 1981: On the halocline of the Arctic Ocean. *Deep-Sea Research Part A*, **28**, 529–545.

Abbot, D. S. and E. Tziperman, 2008: Sea ice, high latitude convection, and equable climates. *Geophys. Res. Lett.*, **35**, L03 702, doi:10.1029/2007GL032 286.

Abbot, D. S., C. C. Walker, and E. Tziperman, 2009: Can a convective cloud feedback help to eliminate winter and spring sea ice at high CO_2 concentrations? *Journal of Climate*, **22**, 5719–5731.

Akitomo, K., 1999: Open-ocean deep convection due to thermobaricity. 1.Scaling argument. *Journal of Geophysical Research*, **104**, 5225–5234.

Alley, R. B., et al., 2003: Abrupt Climate Change. *Science*, **299**, 2005–2010.

Arakawa, A. and V. R. Lamb, 1977: Computational design of the basic dynamical processes of the UCLA general circulation model. *Methods in Computational Physics*, **17**, 173–265.

Armour, K., I. Eisenman, E. Blanchard-Wrigglesworth, K. McCusker, and C. M. Bitz, 2011: The reversibility of sea ice loss in a state-of-the-art climate model. *Geophys. Res. Lett.*, **38**, L16 705, doi:10.1029/2011GL048 739.

Boer, G. J. and B. Yu, 2003: Climate sensitivity and climate state. *Climate Dyn.*, **21**, 167–176.

Bond, G. C., et al., 1997: A pervasive millennial-scale cycle in north atlantic holocene and glacial climates. *Science*, **278**, 1257–1266.

Broecker, W. S., D. M. Peteet, and D. Rind, 1985: Does the ocean-atmosphere system have more than one stable mode of operation? *Nature*, **315**, 21–26.

Bryan, F., 1986: High-latitude salinity effects and interhemispheric thermohaline circulations. *Nature*, **323**, 301–304.

Budyko, M. I., 1969: The effect of solar radiation variations on the climate of the earth. *Tellus*, **21**, 611–619.

Cimatoribus, A. A., M. den Toom, S. S. Drijfhout, and H. Dijkstra, 2011: Sensitivity of the atlantic meridional overturning circulation to south atlantic freshwater anomalies. *Climate Dyn.*, doi:10.1007/s00 382–012–1292–5.

Comiso, J. C. and F. Nishio, 2008: Trends in the sea ice cover using enhanced and compatible AMSR-E, SSM/I, and SMMR data. *J. Geophys. Res.*, **113**, doi:10.1029/2007JC004 257.

Cubasch, U., et al., 2001: Projections of future climate change. In Houthton et al. (eds.): Climate Change 2001: The Physical Science Basis. Contribution of Working Group I to The IPCC Third Assessment Report of the Intergovernmental Panel on Climate Change. Cambridge University, Cambridge, U.K., 526–582.

Danabasoglu, G. and P. R. Gent, 2009: Equilibrium climate sensitivity: Is it accurate to use a slab ocean model? *J. Climate*, **22**, 2494–2499.

de Vries, P. and S. L. Weber, 2005: The Atlantic freshwater budget as a diagnostic for the existence of a stable shut down of the meridional overturning circulation. *Geophys. Res. Lett.*, **32**, L09 606, doi:10.1029/2004GL021 450.

Dijkstra, H., 2007: Characterization of the multiple equilibria regime in a global ocean model. *Tellus*, **59**, 695–705.

Dixon, K. W., T. L. Delworth, M. J. Spelman, and R. J. Stouffer, 1999: The influence of transient surface fluxes on North Atlantic overturning in a coupled GCM Climate Change Experiment. *Geophys. Res. Lett.*, **32**, doi:10.1029/1999GL900 571.

Drijfhout, S. S., S. L. Weber, and E. van der Swaluw, 2011: The stability of the moc as diagnosed from model projections for pre-industrial, present and future climates. *Climate Dyn.*, doi:10.1007/s00 382–010–0930–z.

Eisenman, I., 2010: Geographic muting of changes in the arctic sea ice cover. *Geophys. Res. Lett.*, **37**, L16 501, doi:10.1029/2010GL043 741.

Eisenman, I., 2012: Factors controlling the bifurcation structure of sea ice retreat. *J. Geophys. Res.*, **117**, D01 111, doi:10.1029/2011JD016 164.

Eisenman, I. and J. S. Wettlaufer, 2009: Nonlinear threshold behavior during the loss of Arctic sea ice. *Proc. Natl. Acad. Sci.*, **106**, 28–32.

Ellison, C. R. W., M. R. Chapman, and I. R. Hall, 2006: Surface and deep ocean interactions during the cold climate event 8200 years ago. *Science*, **312**, 1929–1932.

Fichefet, T., C. Poncin, H. Goosse, P. Huybrechts, I. Janssens, and H. L. Treut, 2003: Implications of changes in freshwater flux from the Greenland Ice Sheet for the climate of the 21st century. *Geophys. Res. Lett.*, **30**, doi:10.1029/2003GL017 826.

Ganopolski, A. and S. Rahmstorf, 2001: Rapid changes of glacial climate simulated in a coupled climate model. *Nature*, **409**, 153–158.

Gent, P. R., J. Willebrand, T. J. McDougall, and J. C. McWilliams, 1995: Parameterizing eddy-induced tracer transports in ocean circulation models. *J. Phy. Oceanogr.*, **25**, 463–474.

Gill, A. E., 1982: *Atmosphere-Ocean Dynamics*, 599–602. International Geophysics Series, Academic Press.

Gornitz, V., S. Lebedeff, and J. Hansen, 1982: Global sea level trend in the past century. *Science*, **215**, 1611–1614.

Gregory, J. M., 2000: Vertical heat transport in the ocean and their effect on time-dependent climate change. *Climate Dyn.*, **16**, 501–515.

Gregory, J. M. and P. Huybrechts, 2006: Ice-sheet contributions to future sea-level change. *Philos. Trans. R. Soc. A.*, doi:10.1098/rsta.2006.1796.

Gregory, J. M. and M. Webb, 2008: Tropospheric adjustment induces a cloud component in CO_2 forcing. *J. Climate*, **21**, 58–71.

Gregory, J. M., et al., 2004: A new method for diagnosing radiative forcing and climate sensitivity. *Geophys. Res. Lett.*, **31**, doi:10.1029/2003GL018 747.

Gregory, J. M., et al., 2005: A model intercomparison of changes in the Atlantic thermohaline circulation in response to increasing atmospheric CO_2 concentration. *Geophys. Res. Lett.*, **32**, L12 703, doi:10.1029/2005GL023 209.

Griffies, S. M., 1998: The Gent-McWilliams skew-flux. *J. Phy. Oceanogr.*, **28**, 831–841.

Hansen, J., et al., 2007: Dangerous human-made interference with climate: A GISS modelE study. *Atmos. Chem. Phys.*, **7**, 2287–2312.

Harvey, L. D. D. and S. H. Schneider, 1985: Transient climate response to external forcing on $10^0 - 10^4$ year time scales part 1: experiments with globally averaged, coupled, atmosphere and ocean energy balance models. *J. Geophys. Res.*, **90**, 2191–2205.

Hawkins, E., R. S. Smith, L. C. Allison, J. M. Gregory, T. J. Woollings, H. Pohlmann, and B. de Cuevas, 2011: Bistability of the Atlantic overturning circulation in a global climate model and links to ocean freshwater transport. *Geophys. Res. Lett.*, **38**, L10 605, doi:10.1029/2011GL047 208.

Heinemann, M., J. H. Jungclaus, C. Li, H. Schmidt, S. Rast, and J. Marotzke, 2012: Paleocene-Eocene Thermal Maximum warming does not require large CO_2 forcing. **In preparation.**

Held, I., M. Winton, K. Takahashi, T. L. Delworth, F. Zeng, and G. K. Vallis, 2010: Probing the fast and slow components of global warming by returning abruptly to pre-industrial forcing. *J. Climate*, **23**, 2418–2427.

Hibler, W. D., 1979: A dynamic thermodynamic sea ice model. *J. Phy. Oceanogr.*, **9**, 815–846.

Hoffert, M. I., A. J. Callegari, and C.-T. Hsieh, 1980: The role of deep sea heat storage in the secular response to climatic forcing. *J. Geophys. Res.*, **85**, 6667–6679.

Holland, M., C. Bitz, L. B. Tremblay, and D. Bailey, 2008: The role of natural versus forced change in future rapid summer arctic ice loss. *Arctic Sea Ice Decline: Observations, Projections, Mechanisms,and Implications*, E. DeWeaver, C. Bitz, and B. Tremblay, Eds., AGU, Washington, D. C., Geophys. Monogr. Ser., Vol. 180, 133–150.

Holland, M. M. and C. M. Bitz, 2003: Polar amplification of climate change in coupled models. *Climate Dyn.*, **21**, 221–232.

Holland, M. M., C. M. Bitz, and B. Tremblay, 2006: Future abrupt reductions in the summer Arctic sea ice. *Geophys. Res. Lett.*, **33**, L23 503, doi:10.1029/2006GL028 024.

Huisman, S. E., M. den Toom, H. A. Dijkstra, and S. Drijfhout, 2010: An indicator of the multiple equilibria regime of the Atlantic meridional overturning circulation. *J. Phys. Oceanogr.*, **40**, 551–567.

Jungclaus, J. H., et al., 2006: Ocean circulation and tropical variability in the coupled model ECHAM5/MPI-OM. *J. Climate*, **19**, 3952–3972.

Knutti, R. and G. C. Hegerl, 2008: The equilibrium sensitivity of the earth's temperature to radiation changes. *Nature Geoscience*, **1**, 735–743.

Landerer, F. W., J. H. Jungclaus, and J. Marotzke, 2007: Regional dynamic and steric sea level change in response to the IPCC-A1B scenario. *J. Phys. Oceanogr.*, **37**, 296–312.

Latif, M., E. Roeckner, U. Mikolajewicz, and R. Voss, 2000: Tropical stabilization of the Thermohaline Circulation in a greenhouse warming simulation. *J. Climate*, **13**, 1809–1813.

Levitus, S., J. I. Antonov, and T. Boyer, 2005: Warming of the world ocean, 1955-2003. *Geophys. Res. Lett.*, **32**, doi:10.1029/2004GL021 592.

Levitus, S., J. I. Antonov, T. Boyer, R. A. Locarnini, H. E. Garcia, and A. V. Mishonov, 2009: Global ocean heat content 1955-2008 in light of recently revealed instrumentation problems. *Geophys. Res. Lett.*, **36**, doi:10.1029/2008GL037 155.

Levitus, S., J. I. Antonov, T. P. Boyer, and C. Stephens, 2000: Warming of the world ocean. *Science*, **287**, 2225–2229.

Li, C., J.-S. v. Storch, and J. Marotzke, 2012: Deep-ocean heat uptake and equilibrium climate response. *Clim. Dyn*, doi: 10.1007/s00 382–012–1350–z.

Lindsay, R. W. and J. Zhang, 2005: The thinning of the Arctic sea ice 1988–2003: Have we passed a tipping point? *J. Climate*, **18**, 4879–4894.

Lyman, J. M., S. A. Good, V. V. Gouretski, M. Ishii, G. C. Johnson, M. D. Palmer, D. M. Smith, and J. K. Willis, 2010: Robust warming of the global upper ocean. *Nature*, **465**, 334–337.

Manabe, S. and R. J. Stouffer, 1980: Sensitivity of a global climate model to an increase of CO_2 concentration in the atmosphere. *J. Geophys. Res.*, **85**, 5529–5554.

Manabe, S. and R. J. Stouffer, 1988: Two stable equilibria of a coupled ocean-atmosphere model. *J. Climate*, **1**, 841–866.

Marotzke, J., 2000: Abrupt climate change and thermohaline circulation: Mechanisms and predictability. *Proc. Natl. Acad. Sci.*, **97**, 1347–1350.

Marotzke, J., P. Welander, and J. Willebrand, 1988: Instability and multiple steady states in a meridional-plane model of the thermohaline circulation. *Tellus*, **40**.

Marotzke, J. and J. Willebrand, 1991: Multiple equilibria of the global thermohaline circulation. *J. Phys. Oceanogr.*, **21**, 1372–1385.

Marsland, S. J., H. Haak, J. H. Jungclaus, M. Latif, and F. Roeske, 2003: The Max- Planck-Institute global ocean/sea ice model with orthogonal curvilinear coordinates. *Ocean Modelling*, **5**, 91–127.

Marčelja, S., 2010: The timescale and extent of thermal expansion of the global ocean due to climate change. *Ocean Science*, **6 (1)**, 179–184,doi:10.5194/os–6–179–2010.

McManus, J. F., R. Francois, J. M. Gherardi, L. D. Keigwin, and S. Brown-Leger, 2004: Collapse and rapid resumption of atlantic meridional circulation linked to deglacial climate changes. *Nature*, **428**, 834–837.

McPhee, M. G., 2003: Is thermobaricity a major factor in Southern Ocean ventilation? *Antarctic Science*, **15**, 153–160.

Meehl, G., et al., 2007: Global climate projections. In Solomon et al. (eds.): Climate Change 2007: The Physical Science Basis. Contribution of Working Group I to the Fourth Assessment Report of the Intergovernmental Panel on Climate Change. Cambridge University, Cambridge, U.K. and New York, USA, 747–845.

Mikolajewicz, U., M. Vizcaíno, J. H. Jungclaus, and G. Schurgers, 2007: Effect of ice sheet interactions in anthropogenic climate change simulations. *Geophys. Res. Lett.*, **34**, L18 706. doi:10.1029/2007GL031 173.

Mikolajewicz, U. and R. Voss, 2000: The role of the individual air-sea flux components in co2-induced changes of the ocean's circulation and climate. *Climate Dyn.*, **16**, 627–642.

North, G. R., 1990: Multiple solutions in energy balance climate models. *Global Planet. Change*, **82**, 225–235.

Notz, D., 2009: The future of ice sheets and sea ice: Between reversible retreat and unstoppable loss. *Proc. Natl. Acad. Sci.*, **106**, 20 590–20 595.

Notz, D., F. A. Haumann, H. Haak, J. H. Jungclaus, and J. Marotzke, 2012: Sea-ice evolution in the Arctic as modeled by MPI-ESM. *Journal of Advances in Modelling Earth Systems*, Submitted manuscript.

Notz, D. and J. Marotzke, 2012: Observations reveal external driver for Arctic sea-ice retreat. *Geophys. Res. Lett.*, **39**, L08 502, doi:10.1029/2012GL051 094.

Pacanowski, R. C. and S. Philander, 1981: Parameterization of vertical mixing in numerical models of the tropical oceans. *J. Phy. Oceanogr.*, **11**, 1443–1451.

Parker, D., C. Folland, A. Scaife, J. Knight, A. Colman, P. Baines, and B. Dong, 2007: Decadal to multidecadal variability and the climate change background. *J. Geophys. Res.*, **112**, doi:10.1029/2007JD008 411.

Rahmstorf, S., 1996: On the freshwater forcing and transport of the atlantic thermohaline circulation. *Climate Dyn.*, **12**, 799–811.

Rahmstorf, S., 2002: Ocean circulation and climate during the past 120,000 years. *Nature*, **419**, 207–214.

Rahmstorf, S., 2007: A semi-empirical approach to projecting future sea-level rise. *Science*, **315**, 368–370.

Rahmstorf, S. and J. Willebrand, 1995: The role of temperature feedback in stabilizing the thermohaline circulation. *J. Phys. Oceanogr.*, **25**, 787–805.

Rahmstorf, S., et al., 2005: Thermohaline circulation hysteresis: a model intercomparison. *Geophys. Res. Lett.*, **32**, L23 605, doi:10.1029/2005GL023 655.

Ramanathan, V. and Y. Feng, 2008: On avoiding dangerous anthropogenic interference with the climate system: Formidable challenges ahead. *Proc. Natl. Acad. Sci.*, **105**, 14 245–14 250,doi: 10.1073/pnas.0803838 105.

Randall, D., et al., 2007: Climate models and their evaluation. In Solomon et al. (eds.): Climate Change 2007: The Physical Science Basis. Contribution of Working Group I to The IPCC Fourth Assessment Report of the Intergovernmental Panel on Climate Change. Cambridge University, Cambridge, U.K. and New York, USA, 589–662.

Raper, S. C. B., J. M. Gregory, and T. J. Osborn, 2001: Use of an upwelling-diffusion energy balance climate model to simulate and diagnose AOGCM results. *Climate Dyn.*, **17**, 601–613.

Redi, M. H., 1982: Oceanic isopycanal mixing by coordinate rotation. *J. Phy. Oceanogr.*, **12**, 1154–1158.

Ridley, J., J. Lowe, and D. Simonin, 2008: The demise of arctic sea ice during stabilisation at high greenhouse gas concentrations. *Clim. Dyn*, **30**, 333–341.

Ridley, J. K., P. Huyberechts, J. M. Gregory, and J. A. Lowe, 2005: Elimination of the Greenland Ice Sheet in a high CO2 climate. *J. Climate*, **18**, 3409–3427.

Ridley, J. K., J. A. Lowe, and H. T. Hewitt, 2012: How reversible is sea ice loss? *The Cryosphere*, **6**, 193–198.

Roeckner, E., et al., 2003: The atmospheric general circulation model ECHAM5, Part I: Model description. *Max-Planck-Institut für Meteorologie, Rep. 349*, 127pp.

Roeckner, E., et al., 2006: Sensitivity of simulated climate to horizontal and vertical resolution in the ECHAM5 atmosphere model. *J. Climate*, **19**, 3771–3791.

Rooth, C., 1982: Hydrology and ocean circulation. Progress in Oceanography. *Progress in Oceanography*, **11**, 131–149.

Sellers, W. D., 1969: A global climate model based on the energy balance of the earth-atmosphere system. *J. Appl. Meteor.*, **8**, 392–400.

Semtner, A. J., 1976: A model for the thermodynamic growth of sea ice in numerical investigations of climate. *J. Phy. Oceanogr.*, **6**, 379–389.

Senior, C. A. and J. F. B. Mitchell, 2000: The time dependence of climate sensitivity. *Geophys. Res. Lett.*, **27**, 2685–2688.

Serreze, M. C. and J. A. Francis, 2006: The arctic amplification debate. *Clim. Change*, **76**, 241–264.

Stammerjohn, S. E., D. G. Martinson, R. C. Smith, X. Yuan, and D. Rind., 2008: Trends in Antarctica annual sea ice retreat and advance and their relation to El Nino-Southern Oscillation and Southern Annular Mode Variability. *J. Geophys. Res.*, **113**, doi:10.1029/2007JC004 269.

Stocker, T. and D. Wright, 1991: Rapid transitions of the oceanâs deep circulation induced by changes in surface water flux. *Nature*, **351**, 729–732.

Stommel, H., 1961: Thermohaline convection with two stable regimes of flow. *Tellus*, **13**, 224–230.

Stouffer, R. J. and S. Manabe, 1999: Response of a coupled ocean-atmosphere model to increasing atmospheric carbon dioxide: Sensitivity to the rate of increase. *J. Climate*, **12**, 2224–2237.

Stouffer, R. J. and S. Manabe, 2003: Equilibrium response of thermohaline circulation to large changes in atmospheric CO_2 concentration. *Climate Dyn.*, **20**, 759–773.

Stouffer, R. J., et al., 2006: Investigating the causes of the response of the Thermohaline Circulation to past and future climate changes. *J. Climate*, **19**, 1365–1387.

Swingedouw, D., P. Braconnot, P. Delecluse, E. Guilyardi, and O. Marti, 2007: Quantifying the amoc feedbacks during a 2x co2 stabilization experiment with land-ice melting. *Climate Dyn.*, doi:10.1007/s00 382–007–0250–0.

Tietsche, S., D. Notz, J. H. Jungclaus, and J. Marotzke, 2011: Recovery mechanisms of Arctic summer sea ice. *Geophys. Res. Lett.*, **38**, L02 707, doi:10.1029/2010GL045 698.

Valcke, S., D. Caubel, and L. Terray, 2003: OASIS3 Ocean Atmosphere Sea Ice Soil user's guide. Tech. rep., CERFACS Tech Rep TR/CMGC/03/69, 85 pp., Toulouse, France.

Vermeer, M. and S. Rahmstorf, 2009: Global sea level linked to global temperature. *Proc. Natl. Acad. Sci.*, **106**, 21 527–21 532,doi:10.1073/pnas.0907765 106.

Vinnikov, K. Y., et al., 1999: Global warming and Northern Hemisphere sea ice extent. *Science*, **286**, 1934–1937.

Vizcaíno, M., U. Mikolajewicz, J. H. Jungclaus, and G. Schurgers, 2010: Quantifying the amoc feedbacks during a 2x co2 stabilization experiment with land-ice melting. *Climate Dyn.*, doi:10.1007/s00 382–009–0591–y.

von Schuckmann, K. and P. Y. L. Traon, 2011: How well can we derive global ocean indicators from Argo data? *Ocean Science*, **7**, 783–791, doi:10.5194/os–7–783–2011.

Voss, R. and U. Mikolajewicz, 2001: Long-term climate changes due to increased CO_2 concentration in the coupled atmosphere-ocean general circulation model ECHAM3/LSG. *Clim. Dyn.*, **17**, 45–60.

Weijer, W., W. P. M. D. Ruijter, H. A. Dijkstra, and P. J. van Leeuwen, 1999: Impact of interbasin exchange on the Atlantic overturning circulation. *J. Phys. Oceanogr.*, **29**, 2266–2284.

Wigley, T. M. L. and S. C. B. Raper, 1987: The thermal expansion of sea water associated with global warming. *Nature*, **330**, 127–131.

Wigley, T. M. L. and S. C. B. Raper, 1992: Implications for climate and sea level of revised IPCC emission scenarios. *Nature*, **357**, 293–300.

Williams, K. D., W. J. Ingram, and J. M. Gregory, 2008: Time variation of effective climate sensitivity in GCMs. *J. Climate*, **21**, 5076–5090.

Winton, M., 2006: Does the Arctic sea ice have a tipping point? *Geophys. Res. Lett.*, **33**, L23 504, doi:10.1029/2006GL028 017.

Winton, M., 2008: Sea ice-albedo feedback and nonlinear arctic climate change. *Arctic Sea Ice Decline: Observations, Projections, Mechanisms,and Implications*, E. DeWeaver, C. Bitz, and B. Tremblay, Eds., AGU, Washington, D. C., Geophys. Monogr. Ser., Vol. 180, 111–131.

Winton, M., K. Takahashi, and I. M. Held., 2010: Importance of ocean heat uptake efficacy to transient climate change. *J. Climate*, **23**, 2333–2344.

Acknowledgements

Foremost, I would like to express my sincere gratitude to my advisor Prof. Dr. Jochem Marotzke for the continuous support of my Ph.D study and research, for his patience, motivation and immense knowledge. His guidance helped me in all the time of research and writing of this thesis. I would like to thank my co-advisor Dr. Jin-Song von Storch for taking the time to discuss whatever issues when I knocked on her door. Thanks to Prof. Dr. Hartmut Graßl for chairing my panel and for guidance throughout my panel meeting.

I would like to thank the IMPRS-ESM and the ocean group at the MPI-M. It has been a pleasure to meet so many fellow students and colleagues, some of them became my friends. Special thanks to Dr. Antje Weitz and Cornelia Kampmann for their organisational and mental support. Thanks to the German Climate Computation Center and to the Central IT services for their technical support.

My sincere thanks also goes to Dr. Dirk Notz for first-hand insight into the world of sea ice and for reading the manuscript of chapter 3 carefully and for many helpful suggestions and comments. I am grateful to Dr. Johann H. Jungclaus for reading the manuscript of chapter 2 carefully during the internal review process and for pieces of helpful comments. I would like to thank Dr. Malte Heinemann, Dr. Aiko Voigt, Dr. Erich Roeckner, Dr. Steffen Tietsche and Dr. Peter Düben for many discussions and suggestions. I would like to thank Dr. Helmuth Haak and Michael Botzet for their supports and interests in my work. I would like to thank Dr. Iris Ehlert for all the helpful conversation in the kitchen during the last months before my submission. Sepecial thanks goes to Dr. Eleftheria Exarchou, Laura Niederdrenk, Max Popp and Dr. Kenji Shimizu for proof-reading and providing pieces of suggestions.

Also, thanks especially to Peter Düben, Eleftheria Exarchou and Nina Wilkens- for sharing office with me and for making me feel comfortable in the office.

Acknowledgements

My grateful goes to my friends, Rongyu, Yan, Weiqiang, Xiuhua, Chuanyu, Yuexin, Shiqiang for all the fun we had here in Hamburg and making me feel comfortable in Hamburg.

Last but not the least, I would like to thank my wife Hongmei for reading the manuscript and many suggestions, for tolerating my moodiness during the entire process, for bringing me food to keep me going, for taking care of most household duties while I lived in my office, for heading off our kid from interrupting me, for juggling her hectic schedule so I could meet my advisor on short notice and for her understanding and love during the past few years. I would also like to thank my little daughter Yizhen for giving me a lot of fun with painting on my manuscript. I would like to thank my parents, parents-in-law, brother, sister, sister-in-law, brother-in-law for their support throughout my studies.



ISSN 1614-1199